DEVELOPMENT OF LEAD-FREE ELECTROLESS NICKEL PLATING SYSTEMS AND METAL THIN FILMS ON SILICONE AND NAFION MEMBRANES

WANG KE

NATIONAL UNIVERSITY OF SINGAPORE

2008

DEVELOPMENT OF LEAD-FREE ELECTROLESS NICKEL PLATING SYSTEMS AND METAL THIN FILMS ON SILICONE AND NAFION MEMBRANES

WANG KE
(M.Sc., CUGB; M.Eng., CUGW)

A THESIS SUBMITTED

FOR THE DEGREE OF DOCTOR OF PHILOSOPHY

DEPARTMENT OF CHEMICAL AND BIOMOLECULAR ENGINEERING

NATIONAL UNIVERSITY OF SINGAPORE

2008

ACKNOWLEDGEMENTS

I would like to express my sincere gratitude to my supervisor, A/Prof. Hong Liang, and my co-supervisor, Dr. Liu Zhao-Lin, for their invaluable guidance and suggestions, continual encouragement, great patience and support throughout the course of my study.

I would like to specially thank all the technical and clerical staff in the Department of Chemical & Biomolecular Engineering for their assistance in the set-up of experimental systems and in the use of materials characterization equipments. Thanks are also extended to Mr. Yin Xiong, Ms. Zhang Xinhui and Ms. Tay Siok Wei for their supportive comments and cheerful assistance.

I am extremely grateful to my beloved family members for their love and support throughout the course of this program.

Finally, I would like to thank to National University of Singapore for granting me a research scholarship throughout this study period.

TABLE OF CONTENTS

SUMMARY

Electroless metal deposition/plating, as a versatile surface finishing technology, has been successfully applied in many industries to date. Among the established electroless plating systems, the electroless nickel plating (ENP) system is of the most importance due to its significant industrial value. ENP generally produces an integrity Ni-P alloy film on the target substrate with very strong adhesion strength and unique physical and chemical properties, such as, hardness, corrosion resistance, wear resistance and so on.

Being an autocatalytic reaction at the plating frontier, the ENP process is vulnerable to decompose at any time due to the presence of insoluble colloidal particles in the plating solution as the plating proceeds. In most of commercial ENP applications, lead is introduced in the ppm level as the stabilizer to ensure a stable plating process that consists of several metal-turnover (MTO) rounds. But the co-deposition of Pb(0) atom in the EN deposition layer and the presence of Pb^{2+} ion in the spent solution cause harmful effects to the human beings and high cost for the waste-solution treatment. Hence, it has been an urgent issue to explore a less toxic or environmental friendly stabilizer in place of Pb^{2+} ion in ENP solutions.

Another challenge to the development electroless metal plating is how to apply this technique in the arena of Hi-tech, i.e., biomedical and new energy industries, in which the metallization of polymer materials is an essential step.

Poly(dimethylsiloxane) (PDMS) is an important polymeric material that has broad applications because of its excellent thermal and chemical stability. The surface metallized PDMS is expected to find applications in the medical/health industry. However, electroless metallization on PDMS is seldom reported due to its high hydrophobicity.

Proton exchange membrane fuel cell (PEMFC) is regarded as an alternative power generator to the combustion engine for PEMFC uses hydrogen fuel and has a higher efficiency, higher power density and zero pollutant emissions. The performance of PEMFCs greatly depends on the membrane electrode assembly (MEA), in which an electrolyte membrane is sandwiched between two electrodes. Among different electrolyte membranes, Nafion® is the most commonly used because of its good mechanical and chemical stability and high proton conductivity. The enhancement of Pt utility and improvement of the endurance of Pt catalyst to carbon monoxide and other oxidative intermediates are the key issues which will affect the market acceptance of PEMFC. Electroless Pt and Au plating approaches were attempted in this thesis work with the aim to deposit Pt or Pt-Au bimetallic catalyst directly on the surface of Nafion® membrane. Here the built Pt-Au bimetallic nanoparticle is anticipated to improve the resistance of the Pt catalyst to poisoning adsorbates.

The interest of this PhD research is to investigate solutions to the above problems, namely exploring effective substitutes for lead salt stabilizer in ENP system and advancing electroless plating technology for the fabrication of special devices. In the first part of this thesis, three kinds of environment friendly and effective bath stabilizers are presented. They are sulfur-containing amino acids (cysteine and

methionine), Bi^{3+}-complex ions and phosphines. Among them, cysteine, methionine and Bi^{3+}-complex ions stabilize the ENP bath by controlling the oxidation rate of hypophosphite ions at the plating surface. Each of them exhibited a wide effective stabilizing range from 10^{-9} to 10^{-5} mol/L before the critical concentration, above which the EN plating becomes idle. Below the critical concentration, the concentrations of stabilizers did not show significantly effects on the characteristics of ENP process and EN deposit. Although the sulfur-containing amino acid type and Bi^{3+}-complex ion type are anodic type stabilizers, they are associated with different stabilization chemical mechanisms.

Unlike sulfur-containing amino acids and Bi^{3+}-complex ions, phosphines are a type of cathodic stabilizer that prevents the ENP process from decomposition through suppressing the rapid reduction of Ni^{2+} ions at highly reactive Ni surface sites. And consequently, there is no a critical concentration for them. It is unique for phosphines that the phosphorus-content in the Ni-P deposition layer gradually increases by increasing the concentration of phosphines in the solution, which results in the improvement of anti-corrosion property of as-deposited Ni-P plating layer. In addition, thermal annealing of the Ni-P layer could largely promotes its corrosion resistance by almost 20 times due to the formation of diffusion layer between the brass substrate and crystalline layer.

In the second part, methods for metallization of PDMS and Nafion® membrane are reported. Firstly, a method to electroless plate a well-adhered Ni/P alloy thin film on the surface of modified PDMS was successfully developed. At the first, PDMS was modified by including an appropriate surfactant in the PDMS matrix and partially

embedding TiO_2 nonoparticles on its surface to make a hydrophilic and rough surface; and then, ENP was carried out on the surface of modified PDMS substrate after activated in a $Pd/SnCl_2$ suspension. The deposited Ni-P alloy film is rough and irregular in structure and shows high electrical conductivity and an electromagnetic interference (EMI) shielding property.

Secondly, methods to deposit PEMFC anode catalyst directly to Nafion® membrane by means of electroless plating, in which Pt or Pt-Au bimetallic thin layer consisted of highly dispersed particles with size smaller than 100 nm, were successfully developed. The size of deposited metal particles and the surface morphology of deposition layer were found to strongly depend upon the plating time. According to the assessment in a single stack PEMFC, both of Pt and Pt-Au catalysts displayed better electrode reactivity than the normally used carbon black supported PtRu catalyst; whereas Pt/Nafion® anode showed better cell performance than Pt-Au/ Nafion® anode when the current density was above 1.4 A/cm^2.

Keywords: electroless nickel plating (ENP), stabilizer, sulfur-containing amnio acids, Bi^{3+}-comples ions, phosphines, stabilization mechanism, surface metallization, poly(dimethylsiloxane) (PDMS), electromagnetic interference (EMI); Nafion® membrane, polymer electrolyte membrane fuel cell (PEMFC), Pt-based catalyst

NOMENCLATURE

Symbol	Description	Unit
A	plating area in Eq. (3.1)	cm^2
a	a constant in Eq. (4.1)	--
CPE	constant phase element	F
C_s	stabilizer concentration	mol/L
C_S^c	critical stabilizer concentration in Eq. (4.1)	mol/L
D	length of the wires Eq. (6.2)	cm
E_f^0	Fermi energy level in Eq. (4.1)	eV
I_s	current Eq. (6.2)	A
k	Boltzmann constant in Eq. (4.1)	eV/K
L	distance between two wires Eq. (6.2)	cm
L_{Pt}	platinum loading in Eq. (7.1)	mg/cm^2
p	dipole moment	D
Rc/	corrosion resistance of the coating	Ω
R_{Ni}	deposition rate of nickel in Eq. (4.1)	mg/cm^2hr
R_{Ni}^0	nickel deposition rate without stabilizer in Eq. (4.1)	mg/cm^2hr
R_P	deposition rate of phosphorus in Eq. (4.1)	mg/cm^2hr
R_P^0	phosphorus deposition rate without stabilizer in Eq. (4.1)	mg/cm^2hr
Rs	resistance of the solution	Ω
t	plating time in Eq. (3.1)	hr
T	temperature	K
U	DC voltage in Eq. (6.2)	V
V_d	decomposition volume	ml
W	weight of plating layer in Eq. (3.1)	g

Greek symbols

Symbol	Description	Unit
r	deposition rate in Eq. (3.1)	μm/hr
ρ_s	surface resistivity	Ω/sq

LIST OF FIGURES

LIST OF TABLES

Chapter 1 Introduction

1.1 Background

Electroless metal deposition/plating is a surface finishing technology in which a single or several metallic atom layer film(s) is/are plated on a material surface which is generally known as a substrate. Metals that can be deposited by electroless plating include nickel, copper, platinum, gold and so on. Among them, electroless nickel plating (ENP) is undoubtedly of the most importance, which has been widely employed in industries such as aerospace, automobile, gas and oil and electronics due to its unique physical and chemical properties (Mallory, 1990; Riedel, 1991; Jiang, 2000).

ENP is a chemical reduction-oxidation process in which the driving force for the reduction of Ni^{2+} ions is supplied from a reducing agent in solution. This process is autocatalytic in nature because the redox reaction is catalyzed by the nickel being deposited itself (Sadeghi, 1983; Schlesinger, 2000). This autocatalytic nature leads to the inherent instability of ENP bath. With the proceeding of plating, colloidal particles of insoluble nickel phosphite can act as highly efficient catalytic sites, and trigger overwhelming deposition of nickel black, known as a “self-accelerating chain reaction” or the plating-out process, and result in failure of plating bath (Mallory, 1990; Riedel, 1991; Schlesinger, 2000). Traditionally Pb^{2+} ion is employed in ppm as stabilizer in commercial ENP baths to prolong their service life which not only

improve the overall efficiency of the ENP, but also minimize the waste solution; however, the use of Pb has been restricted worldwide due to its harmful effects to human being through chronic contact (Castellino, 1995). Development of lead-free ENP baths has consequently become obligatory (Chen, 2006). Therefore, it is necessary to explore some non-toxic chemicals to replace lead as the stabilizer in ENP solution and understand the stabilizing mechanisms of these substitutes in ENP process.

Polydimethylsiloxane (PDMS) is a very useful material that has broaden applications in automotive, electric and electronics industries, food packaging, composite membranes and medical/biomedical devices (Jershow, 2002; Iwasaki, 2007; Qi, 2007). Metallization of polymer substrate has major applications in the microelectronics industry such as magnetic storage devices and printed circuit boards (Yan, 2004; Azzaroni, 2006). In addition suitably metallized polymers have potential applications in medical/biomedical industry (Metz, 2001; Gray, 2005). Different methods have been developed to metallize many polymers, for example, physical vapor deposition (PVD), chemical vapor deposition (CVD), and electroless plating (Mittal, 1998 & 2001; Kim, 2001; Carlo, 2002; Sipaut; 2007). However, reports have seldom been published for metallizing PDMS, especially for ENP, likely because of its highly hydrophobic nature. Consequently it is essential to develop a simple and inexpensive method to modify PDMS surface to make it suitable for metallization by ENP.

Nowadays, proton exchange membrane fuel cell (PEMFC) has been expected to be an alternative power source for automobiles and portable applications due to

cleanliness, security and sustainability (Alkire, 1997; Wei, 2007). Among different available membranes used in PEMFCs, Nafion® and its derivatives have received considerable attention due to their strong chemical resistance and high proton conductivity (Kundu, 2007). Besides the membrane, another key material for PEMFCs is the catalyst. In general, platinum and its alloy are employed as the catalyst in the electrodes of PEMFCs, due to their excellent catalytic activity and stability under fuel cell operation conditions (Koh, 2007; Liu, 2007; Mani, 2008; Ramaswamy, 2008). It is well known that the performance of PEMFCs greatly depends on the membrane electrode assembly (MEA). There are two approaches for fabrication of MEAs: (1) catalyst powder or powder type and (2) in situ catalyst formation on the surface of the gas diffusion layer (GDL) or the membrane. And generally, the latter method has higher Pt utilization than the former. The in situ formation of catalyst primarily includes impregnation and deposition methods. Among them, deposition is very attractive due to the formation of high-purity Pt and ease of control catalyst loading (Ayyadurai, 2007). Physical vapor deposition (PVD), chemical vapor deposition (CVD), sputter deposition and electrodeposition have been reported to deposit catalyst on the surface of GDL or the membrane (Debe, 2000 & 2003; Hampden-Smith, 2002; Wu, 2007). Electroless platinum plating (EPP), however, a much cheaper technique, is still seldom employed for the in situ Pt deposition. Therefore it is reasonable to develop a process for the fabrication of MEA with EPP.

1.2 Objectives of this thesis work

The two main purposes of this thesis work are (i) replacement of lead by other environment-friendly organic and inorganic compounds as the stabilizer in acidic ENP solutions and investigation of the reaction mechanisms of these substitutes at the plating surface during ENP process, and (ii) developing electroless plating methods to modify the surface of polymers and consequently broaden the potential applications of these modified polymers in biomedical and new energy industries. The details of research execution are highlighted as follows:

1. Identifications of three groups of environmental-friendly stabilizers those are sulfur-containing amino-acids, Bi^{3+}-complex ion and phosphines, to replace Pb in the ENP solution, and proposal of suitable ligands to introduce indissoluble Bi^{3+} ion and phosphines into the weak acidic ENP solution.

2. Mechanism study of the stabilizing effect of each substitute stabilizers in ENP process, which includes (i) exploring the reactions between the stabilizers and the deposited Ni^{0} atom at the plating surface and the Ni^{2+} ion in the bulk solution, (ii) investigating the effect of stabilizers on the anodic oxidation of hypophosphite at the plating surface, the rate determining step of ENP process, (iii) comparing the stabilizing capability of different stabilizers, and (iv) simulating the relationship between stabilizer concentration and nickel deposition rate for Bi^{3+}-complex ion.

3. Investigation of the effects of substitute stabilizers on ENP process and EN deposit, such as plating rate, deposit composition, surface morphology et al. and their performances in long-time ENP operation.

4. Development of a reverse surface roughness approach to surface metallize the hydrophobic PDMS substrate by ENP and investigation of the unique properties of Ni-P deposit on PDMS to highlight its potential application in biomedical industry.

5. Development of an electroless plating method to directly deposit Pt or Pt-Au bimetallic thin layer on the surface of Nafion® membrane as the catalyst for PEMFC and characterization of its cell performance.

1.3 Thesis organization

Chapter 2 gives a detailed review about the general knowledge of electrochemical metal deposition methods, the basic components of ENP solution and their role in ENP process, detailed process of ENP, the reaction mechanisms having been proposed to explain the phenomena in ENP process and the limitations of them, physical and chemical properties of the EN deposit and its broad applications, substitute stabilizers for lead investigated to date and their influences on ENP process and EN deposit, methods developed for surface metallization of hydrophobic polymers and approaches for fabrication of MEAs for PEMFC.

In Chapter 3 the topic of interest is the roles of two sulfur-containing amino acids, cysteine and methionine, as the stabilizer in ENP bath. The relationship between nickel deposition rate and concentration of two amino acids was set up and the critical concentrations for cysteine and methionine were determined as well. Two stabilizing mechanisms were come up with to explain the different experimental phenomena observed for cysteine and methione in ENP process. The influences of these two amino acids on the EN deposits such as P-content and surface morphology were investigated. The bath stabilizing capability of cysteine and methionine was assessed through a continuous operation comprising 4 metal-turn-over (MTO) runs and the properties of EN deposits from each MTO run were evaluated.

Chapter 4 presents the role of Bi^{3+}-complex ion as the stabilizer in ENP process. Asymmetric derivatives of EDTA (ethylene diamine tetraacetic acid) were introduced into the ENP solution as a unique type of ligand to form soluble Bi^{3+}-complex in the weak acidic environment. The relation of ENP deposition rate with the stabilizer concentration was investigated and a modified kinetic model was established which successfully simulate the effect of the stabilizer concentration (C_s) on the deposition rates of nickel (R_{Ni}) and the phosphorus (R_P) respectively on the basis of the electric double layer theory. A series of experiments were carried out to clarify how the coordinated Bi^{3+} ion participates the ENP process and the result shows that Bi^{3+} ion stabilizes ENP bath through the disproportionational reaction with Ni atom at plating surface which controls the oxidation of hypophosphite. In addition, the effects of Bi^{3+}-complex ion concentration on the performance of ENP process and properties of EN deposit were studied in detail as well.

In Chapter 5 the effects of phosphine ligands as the stabilizer on the formation and characteristics of EN deposit were investigated. Here the hydrophobic phosphines were introduced into ENP solution by firstly forming complexes with high-concentrated lactic acid. It was noteworthy that phosphine compounds did not significantly retard the anodic oxidation of hypophosphite at the plating surface as other stabilizers did, because they are a specially cathodic-type stabilizer. The P-content of the EN deposit increased with the increasing concentration of phosphines in the ENP solution which improved of corrosion resistance of EN deposit. After annealing at 500 ^{o}C for 1 hr, the corrosion resistance of EN deposit was greatly enhanced due to the formation of a three-layer structure. Finally the stabilizing capability of phosphines was evaluated by a continuous 4-MTO test and stabilizing mechanisms were established for each phosphine.

In Chapter 6 a success method to electroless plate a well-adhered Ni/P alloy thin film on the surface of modified PDMS was developed. This methods involved hydrophilization of hydrophobic PDMS, coating TiO_2 nanoparticles on the surface of hydrophilic PDMS, activation of modified PDMS surface and ENP. The surface metalized PDMS substrate showed electromagnetic shielding property which is attractive in biomedical industry. There were two novel developments in this Chapter: firstly, the development of a reverse surface roughness approach for modification of hydrophobic PDMS which increased the wettability of the PDMS surface and created a half-exposed TiO_2 layer at the top of PDMS substrate, this measure was essential for the following ENP; secondly, the development of an irregular and rough Ni-P thin film on the modified PDMS surface by ENP, this

alloyed metal layer brought unique electromagnetic shielding (EMI) property to PDMS substrate. Compare with other polymer surface metallization methods, the great advantages of this method come from its low operation cost and simple equipment requirement.

Chapter 7 reports an electroless plating method to directly deposit Pt or Pt-Au bimetallic thin layer on the surface of Nafion substrate as the catalyst for PEMFC. Firstly, a stable electroless Pt or Au plating system containing several stabilizers was developed, in which Pt or Au could be electroless deposited on activated Nafion® substrate at a reasonable plating rate. The relation of particle size and distribution with the metal loading or plating time was studied and the optimum plating conditions were determined. Finally, the cell performance was tested in which electroless deposited Pt or Pt-Au Nafion membrane was used as the anode for reduction of hydrogen, and both of them showed a higher output power than the traditional PtRu anode.

Finally, conclusions of this thesis and recommendations for future work are given in Chapter 8.

Chapter 2 Literature Review

2.1 Electrochemical metal deposition methods

In general, the electrochemical metal deposition methods can be classified as electrolytic metal deposition/plating and electroless metal deposition/plating, in which metals are deposited from a liquid medium, generally aqueous, by electrolysis or electroless (autocatalytic) means. The former may be defined as a process in which the item to be coated with metal is made the cathode in an electrical circuit. The electroless process, as its name suggests, uses no external current source, in which the reduction of metal ions to the metal atoms is due to the presence of chemical reducing agents in solution (Gawrilov, 1974; Riedel, 1991; Paunovic, 2006).

It is well known that the electrochemical metal deposition that will be discussed in detail in the following parts has numerous industrial applications. The study on the electrolytic and electroless metal plating is, hence, of great significance to current research in metal deposition.

2.1.1 Electrolytic metal deposition/plating

Electrolytic metal deposition/plating is defined as a process in which the item to be coated with metal is made the cathode in an electrical circuit. In this process, the

electron that derives from the dissolving metal (the same element as the deposited metal) worked as the anode plays an integral role in the reaction.

For electrolytic plating, the electrochemical nature of the metal deposition process can be just simplified written as a chemical reduction-oxidation reaction as the Equation 2.1 (Raub, 1980; Riedel, 1991):

$$Me^{Z+}_{solution} + ze^{-} \xleftrightarrow{Reduction/Oxidation} Me_{lattice} \qquad (2.1)$$

Where Me is metal atom; z is valence of the metal ion and e^{-} is electron.

Typically, an aqueous metal solution is used as the electrolyte because of their excellently electrical conductivity and the high solubility of most metallic salts in water. Other advantages include its low cost and operation safety (Raub, 1980; Riedel, 1991). The schematic drawing of electrolytic metal plating is shown in Figure 2.1, in which the cathode and the anode are connected via an external electrical source, to produce an electric cycle (Raub, 1980; Riedel, 1991).

In the case of electrolytic metal deposition from an aqueous solution, the metal is generally not present as a simple ion, but rather as a hydrated complex. It is believed that the hydrated metal ions are discharged when moving from bulk solution to the substrate surface. As the hydrated ion comes close to the diffusion layer, the surrounding water molecules have to re-orientate themselves due to the electrostatic expelling force from the substrate surface. Finally, at the inner Helmholtz layer, the metal ion becomes naked due to the very high electrostatic potential. Hence it is the

pure metal ion, instead of hydrated ion, that is involved in the actual electrochemical process at the cathode surface (Gerischer, 1957; Riedel, 1991). The reduced atom is initially adsorbed on the cathode surface, then migrates along the surface to a growth point and is incorporated into the metal lattice (Raub, 1980; Riedel, 1991).

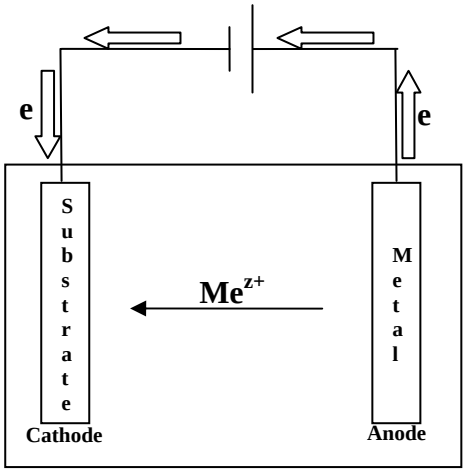

Figure 2.1 Schematic Representation of Electrolytic Metal Deposition

2.1.2 Electroless metal deposition/plating

Electroless metal plating is a chemical deposition process, in which the deposition of a metal from its electrolyte solution relies on chemical reduction rather than external electrical source to supply the necessary electrons. In other words, the chemical plating process involves the transfer of electrons between reacting chemical species.

All chemical deposition processes can be classified into following two groups according to their reaction mechanisms (Riedel, 1991):

- Deposition by ion exchange or charge exchange (immersion deposition or displacement reaction):

When a metal substrate is immersed in a metal salt solution of a second (deposition) metal, the simultaneously spontaneous oxidation of the substrate and deposition of the second metal occur at the surface of metal substrate. Here the substrate atoms loss electrons, become cations and diffuse into the solution. The deposition metal ions accept electrons from the substrate and deposit on it. The reaction equations for this process can be expressed as:

$$\boldsymbol{Me_s - ne^- \rightarrow Me_s^{n+}} \qquad (2.2)$$

$$\boldsymbol{Me_d^{z+} + ze^- \rightarrow Me_d} \qquad (2.3)$$

Where $\boldsymbol{Me_s}$ is the substrate metal; $\boldsymbol{Me_d}$ is the deposition metal; $\boldsymbol{n}$ and $\boldsymbol{z}$ are valence for the two metal; $\boldsymbol{e}$ is the electron.

This plating proceeds at the expense of consumption of substrate metal. Because the reaction involves the ions of substrate metal and ions in solution, the reaction come to stop when the substrate metal is covered with deposited metal. Therefore, chemical plating by displacement yields deposits limited to only a few microns in thickness, usually 1 to 3μm; and the deposit quality is poor that causes the application of this method is extremely limited. So the applications of chemical plating via displacement process are rare.

- Deposition of metal from a solution containing reducing agents (electroless plating):

This process is a continuous metal deposition and a thick deposit is often obtained. Such deposition occurs only at certain catalytically active surface, which means the deposition reaction initially occurs at the surface of catalytic metal substrate exclusively and subsequently continues on the initial deposit. In this case electrons first transfer from the reducing agent to the surface of metal substrate, and then from the surface to the deposition metal ions. The reaction equations for this process can be expressed as:

$$\boldsymbol{R_{Solution} \rightarrow R^{n+}_{Solution} + ne^-} \qquad (2.4)$$

$$\boldsymbol{Me^{z+}_{Solution} + ze^- \rightarrow Me_{lattice}} \qquad (2.5)$$

Where $\boldsymbol{R}$ is the reducing agent; $\boldsymbol{Me}$ is the deposition metal; $\boldsymbol{n}$ and $\boldsymbol{z}$ are valence; $\boldsymbol{e}$ is the electron.

Electroless plating is characterized by the selective reduction of deposition metal ions only at the surface of a catalytic substrate immersed into the plating solution. The deposition metal ions continue depositing on the substrate through the catalytic action of the deposit itself. Therefore, the term autocatalytic is often used to describe the electroless plating process for the deposit that itself catalyzes the reduction reaction. Other than immersion deposition, in electroless plating the substrate metal atom does not loss electron. So the substrate is not consumed during the plating process.

2.1.3 Advantages of electroless deposition

Electrolytic deposition process is technically more straightforward and less expansive than electroless deposition. However, electroless deposition provides the following advantages over electrolytic deposition:

- More uniform and less porous deposits are produced on complex parts.
- Powder supplies and electrical contacts are unnecessary.
- Deposits can be produced directly on non-conductor.
- Deposits have unique chemical, mechanical or magnetic properties.

For above reasons, electroless deposition of metals has been developed to be a surface coating technology of great importance. The metals those can be deposited by electroless plating include nickel, copper, platinum, gold, silver and cobalt which are autocatalytic in nature. Among them, electroless nickel plating (ENP) is undoubtedly the most important one in use today. The widespread applications of ENP are contributed to its uniquely physical and chemical properties (Mallory, 1990).

2.2 History overview of ENP

As early as 1844, Wurtz discovered that metallic nickel could be deposited from its aqueous salt solution by reduction with hypophosphite. However, Wurtz only obtained a black power. It was Breteau who first obtained the bright metallic deposits of nickel-phosphorus alloys in 1911, almost 70 years after Wurtz's

discovery. The first patent on an ENP bath was issued to Roux in 1916. These baths, nevertheless, decomposed spontaneously and formed deposits on any surface that was in contact with the solution (Mallory, 1990; Riedel, 1991).

Interest in ENP was really triggered off after Brenner and Riddell (1946) developed a practical ENP system for achieving continuous ENP. The technology used in their ENP system has been the main scientific basis for that used today. The first commercially available ENP solution was produced by General American Transportation Cooperation (G.A.T.C.) under the trade name “Kanigen” in 1955. Apart from “KANIGEN” process, in the mid end of 1970’s, the “Durnicoat” process based on sodium hypophosphite reduction and “Nibodur” process using sodium borohydride as the reducing agent were developed (Mallory, 1990; Riedel, 1991). From then on, the ENP process has been investigated further and expanded by many workers to its present state of development.

2.3 Basic composition of ENP

The uniquely physical and chemical properties of an ENP deposit depend on its composition that, in turn, mainly depends on the formula of the ENP bath. It is noteworthy that the ENP bath has undergone modifications without changing the basic components since the inception of this technology. The essential components for an ENP bath are a nickel source, a reducing agent, suitable complexing agents, stabilizers and surfactants.

2.3.1 Nickel source

The nickel source in ENP solution can be provided by nickel sulfate, nickel chloride, or nickel acetate (Chen, 1997). Among them nickel sulfate is preferred, especially for acid ENP solutions. Nickel chloride was used as the nickel source in the early stage of ENP development. But the chloride anion not only brought tensile stress in ENP deposit, but also brought a deleterious effect on corrosion resistance when the ENP bath is used to plate aluminum, or when the plated ENP film was used to work as a protective coating in corrosion applications (Mallory, 1990; Jiang, 2000). Consequently, nickel chloride is only used in very limited applications today (Delaunois, 2001; Haque, 2005; Zhong, 2006). When use nickel acetate as the nickel source, there is not significant difference in bath performance or deposit quality compared with nickel sulfate. Because nickel acetate is more expensive than nickel sulfate, it is seldom used in industrial sectors either. Nickel hypophosphite is an ideal nickel source. By using it the accumulation of sulfate anions will be eliminated and the buildup of alkali metal ions will be kept to minimum when the ENP bath is in long-time operation. Unfortunately these advantages gained by nickel hypophosphite are offset by its high price (Mallory, 1990; Jiang, 2000).

For most industrial applications, the nickel concentration of an ENP solution is about 6.5 ± 1.0g (0.09-0.13 mol/L). The nickel concentration shows no or little influence on the plating rate, if it is equal to or greater than approximately 5g/L (0.085mol/L). In another word, the plating reaction is zero order with respect to the nickel ion concentration (Baldwin, 1968).

2.3.2 Reducing agents

Apart from the nickel source, the most important bath component is the reducing agent. The common used reducing agents, in order of popularity, are sodium hypophosphite, sodium borohydride, dimethylamine borane (DMAB) and hydrazine, which are structurally similar in that each contains two or more reactive hydrogens (Taheri, 2001). In each case hydrogen is evolved during the ENP process and the nickel reduction is said to result from the catalytic dehydrogenation of the reducing agent. Table 2.1 summaries the four reducing agents with some of their properties.

Table 2.1 Reducing agents for ENP (Mallory, 1990; Jiang, 2000)

Reducing agent	Formula	Free electrons	pH range of ENP solution	Redox Potential (V)
Sodium hypophosphite	$NaH_2PO_2 \cdot H_2O$	2	4-6; 7-10	-1.4
Sodium borohydride	$NaBH_4$	8	12-14	-1.2
Dimethylamine borane	$(CH_3)_2NH \cdot BH_4$	6	6-10	-1.2
Hydrazine	H_2NNH_2	4	8-11	-1.2

Unlike the electrolytic nickel plating, the EN deposit is not pure nickel but alloy contains phosphorus, boron or nitrogen, which depends on the reducing agent used.

Among these different ENP processes, the Ni-P based alloy process is predominant, due to the low price of sodium hypophosphite and the unique physical and chemical properties of Ni-P alloy. The overall reaction in the hypophosphite reduction of nickel ion may be simply written as:

$$2H_2PO_2^- + Ni^{2+} + 2H_2O \rightarrow 2H_2PO_3^- + H_2 + 2H^+ + Ni^0 \quad (2.6)$$

Equation 2.6 completely fails to account for the phosphorus component of Ni-P alloy and relationship between the nickel deposition and the reactants. The co-deposition of phosphorus involves a secondary reaction that will be discussed in the following. In addition, Gutzeit (1959) has shown that the plating rate is dependent on hypophosphite concentration, but independent on the nickel concentration when it is above 0.02 mol/L.

Lee (1963) reported the influence of the concentration of hypophosphite on the phosphorus-content (P-content) of Ni-P alloy. He pointed out that the increase of hypophophite concentration in the ENP solution resulted in increasing P-content in the Ni-P deposit. The P-content, typically 7-13 wt.%, in the deposit determines crystal structure of deposit, which in turn influences its properties (Ma, 1986; Tulsi, 1986). Low phosphorus EN deposits (P-content < 7% wt) are microcrystalline, that is, they consist of many very small grains. Deposits have higher P-content can be considered amorphous (Yamasaki, 1981).

Borohydride is used to reduce nickel ion in basic ENP solution. Among the borohydride reducing agents, sodium borohydride is the most widely used because of its availability (Singh, 1989; Mallory, 1990). The borohydride ion is a powerful reducing agent, the decomposition of which yields eight electrons for the reduction reactions in ENP process. Generally the electroless deposition of nickel using borohydride as the reducing agent can be written as follows:

$$BH_4^- + 4Ni^{2+} + 8OH^- \rightarrow B(OH)_4^- + 4H_2O + 4Ni^0 \qquad (2.7)$$

The deposits obtained from ENP solution using boron-containing reducing agents are Ni-B alloys. These deposits exhibit many of the same characteristics as Ni-P deposits, but they are especially suitable for certain uses, primarily in electronic devices. Similar to Ni-P alloy coating, the characteristics of Ni-B deposit change with boron content (Baudrand, 1995). Usually the boron content in Ni-B alloy ranges from 1 to 10 wt.% (Mallory, 1990). Similar to Ni-P alloy, the quantity of amorphous phase in the Ni-B deposit is proportion to the boron content of such deposit (Gawrilov, 1979; Kumar PS, 1994; Kumar A, 1998).

Besides borohydride, amine borones are used to reduce nickel ion in basic ENP as well. Amine borones are covalent compounds that generally have three active hydrogens boned to the boron atom. The commercial use of amine boranes in ENP is limited to dimethylamine borane (DMAB). The reaction of DMAB with nickel can be described as follows (Mallory, 1990; Riedel, 1991):

$$(CH_3)_2NHBH_3 + 3Ni^{2+} + 3H_2O \rightarrow 3Ni^0 + (CH_3)_2NH_2^+ + H_3BO_3 + 5H^+ \quad (2.8)$$

$$2[(CH_3)_2NHBH_3] + 4Ni^{2+} + 3H_2O \rightarrow 2Ni^0 + Ni_2B + 2[(CH_3)_2NH_2^+] + H_3BO_3 + 6H^+ + 1/2\,H_2O \quad (2.9)$$

Hydrazine is a powerful reducing agent in aqueous alkaline solutions. Although using hydrazine nickel deposits of 99.9% purity can be obtained, this process has found little industrial usage. ENP solutions base on hydrazine are not very stable and the as-deposited Ni films lack many of the attributes of Ni-P or Ni-B alloy that formed from hypophosphite or boron-containing reducing agent respectively. The deposit of hydrazine system is brittle and has poor corrosion resistance (Mallory,

1990; Riedel, 1991; Jiang, 2000). It was reported that hydrazine can be catalytically decomposed to hydrogen and nitrogen gases by the resultant nickel nanoparticles (Wu, 2003). In its simplest form, the nickel reduction by hydrazine in ENP process can be written as:

$$Ni^{2+} + H_2H_4 \xrightarrow{H_2O} Ni^0 + N_2 + H_2 + 2H^+ \qquad (2.10)$$

2.3.3 Complexing agents

In ENP solution, the solvated nickel ions interact with and are weakly bound to a specific number of water molecules. This kind of complexed nickel ion is called "free" nickel ion. During the ENP process of acidic hypophosphite bath, these free nickel ions may precipitate as nickel phosphate or nickel hydroxide. The precipitate interferes with the chemical balance of the solution by removing nickel ions, has a detrimental effect on the quality of deposits, and may trigger spontaneous bath decomposition. Therefore, complexing agents, usually organic acids or their salts, are usually added into ENP solution to control the availability of the free nickel ions (Martyak, 1996 & 1997). When the free nickel ions are combined with complexing agents, their chemical properties in aqueous solution such as colour, reduction potential and solubility, can be altered. The complexing agents commonly used in ENP solutions are ammonia, alkanolamines, monocarboxylic acids, dicarboxylic acids, hydrocarboxilic acids and their salts, etc (Mallory, 1990; Jiang, 2000; Wang, 2003).

The three principal functions that complexing agents perform in the ENP bath are:

1. exert a buffering action to prevent the rapid pH change of ENP solution;

2. retard the tendency for the precipitation of nickel salts, e.g. basic salts or phosphites;
3. reduce the concentration of free nickel ion in ENP bulk solution.

In addition, complexing agents can also affect the nickel deposition rate and nickel deposit. In ENP solution, the reduction of nickel is said to take place at "free" coordination sites, that is, those sites that are weakly bound to coordinated water molecules, so that the rate of nickel deposition is proportional to the rate at which the nickel complex dissociates to form free nickel ion. Consequently, the electroless nickel complex with a smaller stability constant usually shows a higher deposition rate than that with numerically a larger stability constant. Lactic acid and citric acid are examples of complexing agents that form weak and strong nickel complex respectively in ENP solutions (Mallory, 1990; Jiang, 2000; Wang, 2003).

2.3.4 Surfactants

Micropitting on the as-deposited Ni-P surface is one of the problems usually met in ENP. The adsorption of tiny hydrogen bubbles at the surface of a plated Ni-P deposit is regarded as the root cause of micropitting. The formation of such pinholes on the Ni-P surface decreases the corrosion resistance of the Ni-P plating, especially in the acidic corrosive environments (Chen, 2002). Fortunately, incorporation of some surfactants with suitable structure in the ENP solution can significantly lessen micropitting on Ni-P deposit and then improve the corresponding corrosion resistance (Karuppusamy, 1992; Chen, 2002). Furthermore, the addition of some surfactants in ENP solution can preserve the bath temperature and reduce the

evaporation of plating solution. This is because the surfactant in ENP solution is also a vesicant that forms a white foam layer at the solution surface (Jiang, 2000).

The surfactants used in ENP solution can be classified according to their different kinds of charges, namely nonionic (e.g. Tween 80), cationic (e.g. dodecyltimethylammonium chloride) and anionic (e.g. sodium dodecylbenzenesulfonate) (Jiang, 2000). The effects of different surfactants on the nickel deposition rate and the resulting electroless Ni-P deposits, in the acidic hypophosphite ENP bath, were examined by Chen (2002). It was reported that an addition of small amounts of surfactants to the ENP bath could increase the nickel deposition rate by 25% compared to that from the surfactant-free bath. However, an excessive addition of nonionic surfactants to the ENP bath would yield the Ni-P deposits with inferior surface quality and slow the nickel deposition rate. In contrast, the surface properties of the Ni-P deposits were less influenced by the amount of ionic surfactants present in the ENP bath. The surfactants were found to have not effect on the composition of Ni-P deposit. No matter which surfactant was chosen, the P-content of the Ni-P deposits was stabilized (Chen, 2002).

2.4 Reaction mechanisms of ENP in acidic hypophosphite bath

ENP is a quite complicated redox process. Problems, for instance how to increase plating rate, enhance hypophosphite efficiency and regulate the P-content of the deposit, can hardly be solved if its reaction mechanisms are not understood. Therefore it is necessary to have an explicit understanding of the ENP reaction

mechanisms from both theoretical and practical viewpoints. By now, several reaction mechanisms have been proposed to explain the ENP process, such as hydrogen atomic model, metal oxide model, hydride ion mechanism, classical electrochemical mechanism and mixed potential theory (van der Meerakker, 1981; Mallory, 1990; Abrantes, 1994; Hwang, 1995; Malecki, 2000). However, none of them can provide a satisfactory explanation for all the experimental phenomena in ENP process.

2.4.1 Atomic hydrogen mechanism

The atomic hydrogen mechanism was first porposed by Brenner and Riddell. According to this mechanism, the actual nickel reductant in ENP process is the atomic hydrogen that acts by heterogeneous catalysis at the catalytic nickel surface (Mallory, 1990; Abrantes, 1994). The atomic hydrogen, generated by the reaction of water with hypophosphite, is absorbed at the catalytic nickel surface:

$$H_2PO_2^- + H_2O \longrightarrow H_2PO_3^- + 2H_{ad} \qquad (2.11)$$

The absorbed atomic hydrogen reduces nickel ions at the catalytic surface:

$$Ni^{2+} + 2H_{ad} \rightarrow (Ni^{2+} + 2H^+ + 2e) \rightarrow Ni^0 + 2H^+ \qquad (2.12)$$

Two atomic hydrogen atoms also combine together and form hydrogen, which always accompanies catalytic nickel reduction:

$$2H_{ad} \rightarrow (H + H) \rightarrow H_2 \qquad (2.13)$$

Atomic hydrogen mechanism was further modified by Gutzeit (1959). He attributed the formation of atomic hydrogen to the dehydrogenation of the hypophosphite ion during formation of the metaphosphite ion (Equation 2.14) that subsequently formed an orthophosphate molecule and a hydrogen ion with water (Equation 2.15). In addition the formation of elemental phosphorus in ENP deposit was attributed to a secondary reaction between hypophosphite and atomic hydrogen (Equation 2.16):

$$H_2PO_2^- \xrightarrow{cat} PO_2^- + 2H \qquad (2.14)$$

$$PO_2^- + H_2O \longrightarrow HPO_3^- + H^+ \qquad (2.15)$$

$$H_2PO_2^- + H \longrightarrow P + OH^- + H_2O \qquad (2.16)$$

Atomic hydrogen mechanism is consistent with some observed results of ENP process; however, it fails to explain why the stoichiometric utilization of hypophosphite is always less than 50%, and does not account for the simultaneous reduction of nickel and hydrogen.

2.4.2 Hydride transfer mechanism

Hydride transfer mechanism was first suggested by Hersch (1955) and then modified by Lukes (1964), in which the hypophosphite ion was assumed to act as the donor of hydride ions (H^-) (Mallory, 1990).

In hydride transfer mechanism, the reaction of hypophosphite to provide hydride ion is different due to the pH of solution. In acid solution hypophosphite reacts with water at the catalytic surface, which may be expressed as the following equation:

$$2H_2PO_2^- + 2H_2O \rightarrow 2H_2PO_3^- + 2H^- + 2H^+ \qquad (2.17)$$

The corresponding reaction in alkaline solution is given by:

$$2H_2PO_2^- + 6HO^- \rightarrow 2H_2PO_3^- + 2H^- + 2H_2O \qquad (2.18)$$

The reduction of nickel ion proceeds as follows:

$$Ni^{2+} + 2H^- \rightarrow (Ni^{2+} + 2H^+ + 2e) \rightarrow Ni^0 + H_2 \qquad (2.19)$$

The hydride ion can also react with a hydrogen ion in acid solution or water in alkaline solution:

Acid:

$$H^+ + H^- \rightarrow H_2 \qquad (2.20)$$

Alkaline:

$$H_2O + H^- \rightarrow H_2 + OH^- \qquad (2.21)$$

According to Lukes (1964), the hydrogen that appeared as hydride ion was originally bonded to phosphorus in the hypophosphite. The codeposition of phosphorus was also accounted for, if Equation 2.16 is included in this mechanism (Mallory, 1990). The hydride mechanism presents a satisfactory explanation for the

coupled reduction of nickel and hydrogen. But according to this mechanism, hydrogen evolution should be at least equivalent to metal deposition; however, it was contrary to the observations of some authors (van den Meerakker, 1981).

2.4.3 Electrochemcial mechanism

Electrochemical mechanism was originally proposed by Brenner and Riddell, and later modified by other researchers. In this mechanism the whole ENP process can be divided into two parts, namely, the anodic (oxidation) reaction and the cathodic (reduction) reactions. The anodic reaction between hypophosphite and water generates the electrons for cathodic reactions (Mallory, 1990; van den Meerakker, 1981):

$$H_2PO_2^- + H_2O \rightarrow H_2PO_3^- + 2H^+ + 2e, \quad E^0 = 0.50\ \text{V} \qquad (2.22)$$

The nickel, hydrogen and elemental phosphorus are formed in cathodic reactions:

$$Ni^{2+} + 2e \rightarrow Ni, \quad E^0 = -0.25\ \text{V} \qquad (2.23)$$

$$2H^+ + 2e \rightarrow H_2, \quad E^0 = 0.00\ \text{V} \qquad (2.24)$$

$$H_2PO_2^- + 2H^+ + e \rightarrow P + 2H_2O, \quad E^0 = 0.50\ \text{V} \qquad (2.25)$$

According to the electrochemical mechanism, the ENP process is a primary cell reaction, in which several competing redox reactions synchronously take place at the catalytic surface and form a multi-electrode system. In this system the hydrogen gas and the elemental phosphorus are the by product during nickel deposition. This

mechanism implies that the nickel ion concentration ought to have significant effect on the rate of nickel deposition; but the converse is true (Mallory, 1990; Jiang, 2000).

2.4.4 Metal Hydroxide Mechanism

The metal hydroxide mechanism that involves the coordination of hydroxyl ions with hexaquonickel ion was first proposed by Cavallotti and Salvago (1968), and then supported by the calorimetric study of Randin and Hintermann (1970). In this mechanism, the chemical reduction of nickel at a catalytic surface can be represented by the following reactions:

Ionization of water at catalytic nickel surface:

$$2H_2O \rightarrow 2H^+ + 2OH^- \qquad (2.26)$$

Coordination of hydroxyl ions to solvated nickel ion:

$$Ni^{2+} + 2HO^- \rightarrow Ni(OH)_2 \qquad (2.27)$$

Reaction of hydrolyzed nickel species with hypophosphite:

$$H_2PO_2^- + Ni(OH)_2 \rightarrow Ni + H_2PO_3^- + H \qquad (2.28)$$

The direct interaction of the catalytic nickel surface with hypophosphite gives phosphorus co-deposition:

$$H_2PO_2^- + Ni \rightarrow NiOH^+ + P + OH^- \qquad (2.29)$$

$$NiOH^{+} + H_2O \rightarrow Ni(OH)_2 + H \qquad (2.30)$$

Two hydrogen atoms can combine and form hydrogen gas:

$$H + H \rightarrow H_2 \qquad (2.31)$$

The metal hydroxide mechanism successfully explains the lamellar structure of the Ni-P deposit, as well as the different behavior of electroless copper, silver and palladium plating in which the metal ions are reduced by hypophosphite without P codeposition. This mechanism, however, can not explain the experiments in which the anodic and cathodic reactions take place in a cell with two compartments separated by a glass frit (Mallory, 1990; Riedel, 1991; Jiang, 2000).

2.4.5 Mixed potential theory

It is Paunovic who first identified electroless metal plating in terms of mixed potential theory in 1968. Since then, this theory has been used to explain the ENP results by different researchers (Bindra, 1987; Hessami, 1989; Kim, 1996). According to mixed potential theory, mechanisms of electroless plating can be interpreted in terms of the electromechanical parameters of the partial anodic and cathodic reactions. Here the electroless plating can be considered as the superposition of anodic and cathodic reaction at the mixed (deposition) potential. In the opinion of this theory, the anodic reactions are independent of the cathodic reactions occurring simultaneously at the catalytic surface, and the rates of these separate partial reactions depend only on the electrode potential, the mixed potential.

Consequently, the polarization curves for independent anodic and cathodic processes may be added to predict the overall rates and the mixed potential (Gafin, 1993; Stevanovic, 1999). However, in the actual circumstances the two partial reactions are not independent of each other (Bindra, 1987). And the mixed potential theory can not explain the fully ENP process (Tzeng, 1996).

Although all of these mechanisms can explain most characteristics of the ENP systems for which they were originally proposed, there is experimental evidence that none of them can explain completely the phenomena observed in ENP process. This is due to the fact that ENP is a quite complicate heterogeneous autocatalytic system. In this system there is a three-way correlation between deposit properties, deposit structure and deposition conditions, for example, bath composition, concentration of different components, pH, temperature, agitation, etc. Therefore there is still much hard work needed to be done in order to understand the reaction mechanism of ENP.

2.5 Process of ENP

2.5.1 Pretreatment of substrate

The condition of the substrate prior to plating has significant effects on the results of ENP. Basically, the surface to be plated must be capable of initiating the deposition reaction. In terms of their catalytic activity for the electroless deposition process, substrates can be classified as intrinsically active materials and extrinsically catalytic materials (Xiang, 2001).

2.5.1.1 Intrinsically active materials

All intrinsically active materials are metals that are capable of sustaining electroless plating without any aid. For hypophosphite-based ENP bath, these materials are the dehydrogenation catalyst metals from Group VII of the Periodic Table, i.e. cobalt (in alkali only), nickel, ruthenium, rhodium, palladium (Baudrand, 1995), osmium, iridium and platinum, on which nickel can be directly electroless deposited.

2.5.1.2 Extrinsically catalytic materials

Extrinsically catalytic materials are not catalytically active in nature. Therefore, nuclei of an intrinsically active metal are needed to be deposited on their surface to induce the self-catalytic ENP process (Mallory, 1990). Generally these materials can be divided into:

a) Metallic materials, such as aluminum and beryllium (Court, 2000), which are less noble than nickel. When they are immersed into a nickel solution before ENP, nickel nuclei deposit on them by a displacement exchange process (not an ENP process). These nickel nuclei in turn induce ENP to take place.
b) Metallic materials, such as copper (Lin, 1999), silver and gold (Jiang, 2000), which are nobler than nickel. For these materials it is necessary either to apply a short time cathodic current pulse to deposit nickel nuclei electrolytically on their surface or to form a thinly galvanic nickel layer on surface via contacting them with a piece of nickel or metal less noble than nickel. Once these materials with catalytically metal nuclei on the surface are immersed into the ENP bath, the ENP process is activated.

c) Non-metallic materials, such as graphite (Caturla, 1995), diamond (Laptev, 1994), PTFE (Zhang, 2001), and PI (Sawai, 1990; Homma, 1991; Seita, 1999), which are insulators. For them the seeds of an intrinsically active metal, usually Pd, must be deposited on their surface prior to ENP (Brandow, 1995, 1997; Schilling, 1996). This pretreatment is called activation that consists of either a two-step or a one-step process (Charbonnier, 2001). In the two-step process, the substrate is immersed into aqueous $SnCl_2$ (sensitization) and $PdCl_2$ (activation) solutions successively. In the one-step process, the substrate is immersed in a mixed $SnCl_2$-$PdCl_2$ colloidal solution. Here the Sn^{2+} ions are oxidized to provide electrons for Pd^{2+} reduction. And the reduced Pd atoms act as the catalyst to provide nucleation sites for the subsequent nickel deposition.

2.5.2 Effects of variables on the ENP process

2.5.2.1 Effect of temperature

The temperature at which the ENP reaction occurs is the principle variable that determines the rate of the reaction (Mallory, 1990). It's well known that the plating rate is very slow, if any, plating occurs at temperatures below about 60 ^{o}C. The optimization temperatures for acidic hypophosphite ENP baths are between 80-90 ^{o}C. As the temperature is increased, the plating rate increases exponentially. But if the temperature is allowed to increase much above 90 ^{o}C, the possibility of ENP solution plate-out or even solution decomposition increases.

Generally the operation temperature for alkaline ENP solutions is lower than acidic solutions, which can be operated between 60-70 ^{o}C. For ENP solutions in which dimethylaminoborane (DMAB), diethylaminoborane (DEAB) or hydrazineborane is used as the reducing agent, the plating can be even carried out at an ambient temperature (Jiang, 2000).

It is noteworthy that the P-content of EN deposits is decreased with the increase of operation temperature, and thus influences the properties of EN deposits, with all other variables held constant (Baldwin, 1968).

2.5.2.2 Influence of pH

For acidic ENP solutions hydrogen ion (H^+) accumulates during nickel reduction, which lowers the pH of the solutions. When the pH decreases, the most noticeable change in the ENP process is a concurrent decrease in the deposition rate. Because the oxidation rate of hypophosphite was decelerated with the increase of H^+ ions in the plating solution. In addition, lowering of pH results in the increase of P-content in the EN deposit and consequently affects the properties of EN deposit.

2.5.2.3 Influence of nickel and hypophosphite ion concentration

The nickel concentration of ENP solutions for most industrial application usually lies in the range 5.5-7.5 g/L (0.09-0.13 M). If the nickel concentration is equal to or greater than approximately 5g/L (0.085M), it has little or no effect on the plating rate (Baldwin, 1968). In other words, the plating rate is to be zero order with respect

to the nickel ion concentration. If the nickel concentration is less than 5.8g/L (0.1 mol/L), the P-content decreases with its increase, whereas if the nickel concentration is above 0.1 mol/L, it has little effect on the composition of Ni-P deposit.

The effect of hypophosphite concentration on the plating rate and deposit composition is more significant compared with nickel concentration. In general, increase of the hypophosphite concentration in the ENP solution results in an increase in the nickel deposition rate and P-content in EN deposit (Malecki, 2000).

2.5.2.4 Influence of phosphite anion

The phosphite anion is generated by the oxidation of hypophosphite during the ENP process. For continuous operation of an ENP bath, the depleted hypophosphite and nickel must be replenished. As a result, phosphite anion accumulates in the plating bath. When its concentration reaches 30 g/L, phosphite begins to compete with the complexing agent for nickel ions. Because nickel phosphite is relatively insoluble, it may precipitate from the ENP solution and then induce the bath decomposition. Therefore, it is necessary to add excess complexing agents to prevent precipitation of nickel phosphite with the extension of bath operation time (Mallory, 1990). Another serious consequence of phosphite presence in the ENP solution is its effect on the internal stress of Ni-P deposit. As the phosphite concentration increases, the internal stress becomes more tensile. The tensile stress is harmful to many applications such as corrosion and memory disk (Baldwin, 1968).

The tolerance of ENP bath to the phosphite anion depends on the recipe of the bath and the nature of the complexing agent (Mallory, 1990).

2.5.2.5 Influence of complexing agents

As mentioned previously, complexing agents can reduce the concentration of free nickel ions and prevent the precipitation of nickel phosphite and basic nickel salts. They, consequently, can exert influence on both plating rate and deposit composition. In summary, electroless nickel complexes with low-value (weak) stability constants, i.e. nickel-lactic acid complex, will show higher plating rates and yield deposits with lower P-content than those with numerically higher (strong) stability constants, i.e. nickel-citric acid complex (Mallory, 1990; Jin, 1999).

2.5.2.6 Influence of agitation

Agitation of ENP solution is usually brought about by air injection, pumped circulation or stirring. Although agitation is not necessary for ENP, it is always useful for the plating process. Proper agitation increases the rate of reactants transported to and the rate of spent reaction products removed from the surface of work to be plated. This is especially true for heavily profiled sections or those with larger depressions or blind holes as well as for plating the interior walls of tubes. Because the reduction of nickel is under diffusion control, agitation improves the nickel deposition rate and reduces the P-content of the deposited films (Sevugan, 1993; Jiang, 2000).

2.5.2.7 Influence of bath loading

Bath loading is defined as the ratio of the total plated area of substrates immersed in the solution to the bath volume, which is expressed as cm^2/dm^3. Usually the bath loading for ENP is controlled at 0.5-1.5 cm^2/dm^3 for most industrial applications. Bath loading affects the plating rate and P-content in the deposit. The lower the bath loading, the higher of the plating rate and the lower of the P-content in the deposit (Kalantary, 1992; Jiang, 2000).

2.6 Structure and properties of electroless nickel (EN) deposits

2.6.1 Structure of EN deposits

As-deposited electroless nickel (EN) is a metastable, supersaturated alloy. Under equilibrium conditions, the alloys consist of essentially pure nickel and the intermetallic Ni_3P compound. In the light of the P-content, EN deposits are classified into three types, viz., low (1-3 wt.% P), medium (4-7 wt.% P) and high (7 wt.% and above) phosphorus EN coatings (Keong, 2002). The co-deposition of phosphorus with nickel greatly affects physical and chemical properties of EN plating, such as density, structure and corrosion resistance, etc. In general, EN deposits having phosphorus >7 wt.% are amorphous in nature and show good solderability and corrosion resistance; while EN deposits with phosphorus < 7 wt.% in structure are crystalline, or microcrystalline, or mixtures of both and exhibit good hardness and wear resistance. The structural change occurs when amorphous EN

deposits are annealed above 300^{o}C, giving rise to formation of Ni and Ni_3P phases (Mai, 1988; Lambert, 1989; Martyak, 1994; Kumar, 1996).

2.6.2 Properties of EN deposits

2.6.2.1 Mechanical properties of EN deposit

EN is a relatively strong but brittle material, similar to glass. The high tensile strength and low ductility of Ni-P alloy is due to the microcrystalline and amorphous structures that essentially preclude plastic deformation. The deformation is hence mostly elastic until fracture occurs (Mallory, 1990; Jiang, 2000).

The hardness of EN is much higher than electrodeposited nickel. It means EN has the great resistance to permanent deformation by indentation. The heat treatment and P-content have significant effects on the hardness of Ni-P alloy (Marshall, 1992). It was reported that the hardness of EN decreases with increasing P-content (Parker, 1986) or heat-treatment temperature (Yu, 1993).

2.6.2.2 Internal stresses in EN deposit

Internal stresses that develop with deposits can be classified as extrinsic stresses and intrinsic stresses. Extrinsic stresses are primarily owing to differences in the thermal expansion coefficients of electroless nickel and the substrates to be plated. Tensile stress develops in EN deposits if substrate materials have larger expansion coefficients than Ni-P alloy; while compressive stress develops if substrate materials

have smaller coefficients (Mallory, 1990). The internal stresses affect the fatigue properties of the substrate. Compressive stresses enhance the fatigue life of substrates; whereas tensile stresses lead to a decrease in the fatigue life. Generally a higher P-content in EN deposits results in a lower tensile or a higher compressive stress (Mallory, 1990). Annealing of EN deposit increases tensile stresses and decreases compressive ones, leading to a significant decrease in the fatigue life (Berrios, 1998).

2.6.2.3 Electric and magnetic properties of EN deposit

The electrical resistivity of EN is higher than that of electroplated nickel due to the alloying element such as phosphorus and boron. Furthermore, the amorphous EN deposits exhibit larger values of electrical resistivity than the crystalline ones. Heat treatment of amorphous EN deposits leads to their crystallization and thus substantially reduces the electrical resistivity (Loos, 1990).

The magnetic properties of EN deposits depend on their structure. Crystalline deposits are ferromagnetic, while amorphous deposits are essentially non-magnetic (Sugita, 1984).

2.6.2.4 Corrosion resistance of EN deposits

One of the primary industrial applications of ENP is to provide protection for common metal surfaces exposed to corrosion. Generally, EN deposits provide better

corrosion protection than the equivalent electroplated nickel, due to the lower porosity as well as the more uniform thickness of EN deposits.

The P-content of EN deposits is nearly correlative with the corrosion resistance of deposits. It is generally believed that the excellent corrosion resistance of high phosphorus EN deposits is due to their amorphous structure (Lo, P. H., 1994; Lo, Y. L., 1995).

Tensile internal stresses render EN deposits more susceptible to corrosive attack, because the internal stresses increase the potential differences between deposits and substrates which results in lower breakdown potential and higher corrosion current (Mallory, 1983).

The influence of heat treatment on corrosion resistance of EN deposits is different due to the annealing temperature. At lower temperatures (in 150-200 ^{o}C range), heat treatment has little effect on corrosion resistance. In the temperature range of 300 to 400 ^{o}C, heat treatment lowers the corrosion resistance, probably as a result of microcracking. After annealing at 600-700 ^{o}C, the corrosion resistance improves because of improved bonding EN deposit to the substrate and improved integrity of deposit (Parker, 1981).

Expect factors mentioned above, many other factors, such as, pretreatment of substrates, deposit thickness and formulation of EN solutions, have significant effects on the corrosion resistance of EN deposits (Mallory, 1990; Mimani, 1996; DiBari, 1997; 1998; 1999)

2.6.2.5 Wear properties of EN deposits

In addition to corrosion protection, another primary reason for using EN is to protect substrates from wear. Wear consists of adhesive wear, resulting from the welding of the mating surfaces, and abrasive wear, coming from the abrading between particles and the surfaces. Adhesive and abrasive wear are related to, though not directly, to the hardness of a surface. The greater the hardness, the less deformation, and consequently, there is less intimate contact and less welding and friction (Palaniappa, 2008).

It is well known that the hardness of EN deposits is close correlative with the P-content and heat treatment. Generally speaking, the low phosphorus EN deposits have greater wear protection than the high ones. The abrasion resistance of EN deposits enhances with increasing heat treatment temperature. Such treatment, nevertheless, may lower their corrosion resistance. This improvement may be due to the precipitation of Ni_3P that increases the deposit hardness and the larger grain size of the deposits (Mallory, 1990; Yu, 1993; Jiang, 2000).

Because good adhesion of EN deposit to the substrate is essential for satisfactory wear performance, a hard substrate should be selected to provide better support for EN deposits. In order to obtain the optimal wear performance, the contacting surface of EN deposits is needed to be polished and lubricated. However, it is worthy of note that EN deposits are not suitable for use under high shear and load conditions for they are brittle in nature especially after heat treatment (Mallory, 1990; Jiang, 2000).

2.7 Applications of ENP

2.7.1 Engineering applications

Engineering applications of ENP can be found in virtually every industry due to its unique physical properties, for instance hardness, corrosion resistance, wear resistance and uniform plating, as well as the ability to plate non-conductor surfaces. In addition to its engineering features, the unique ability to plate non-conductors such as glass, ceramics, polymers and graphite has made EN a very useful material that offers a cost-effective alternative with equivalent performance to more expensive metal alloys.

At present the major industrial fields for engineering applications of ENP are aerospace, automotive, petroleum, chemical processing, food processing industries and so on (Mallory, 1990).

2.7.2 Magnetic applications

ENP is a well-known wet process to produce magnetic film, because of its uniform deposit and low cost (Saito, 1999). As the demand for devices of higher recording density and smaller volume increases, electroless Ni-P based alloys, such as Ni-Fe-P, Ni-Co-P and Ni-Co-Re-P, have been used to fabricate soft magnetic thin films with high saturation magnetization and high permeability (Matsubara, 1989; Osaka, 1991).

The magnetic properties of electroless deposited magnetic films are influenced by various parameters, such as the composition of ENP bath and heat treatment (Osaka, 1991). Matsubara (1994) pointed out that the magnetic properties of Ni-Co-P film are affected by the concentrations of $CoSO_4$ and $NiSO_4$ in the solution. The saturation magnetization (Ms) increases as the increase of $CoSO_4$ concentration. Kim (1995) further pointed that the magnetic properties of Ni-Co-P alloy film can be controlled by the plating conditions, deposited film thickness and heat treatment.

2.8 Stabilizers for ENP

An ENP solution can be operated under normal operation conditions over extended periods without adding stabilizers; however it may decompose spontaneously at any time due to the auto-catalytic nature of ENP process. When the ENP bath begins to decompose, two important phenomena appear: one is an increase in the volume of hydrogen gas evolved; the other is the appearance of finely-divided black particles throughout the bulk of the solution. Here, the particles consist of nickel particle, and either nickel phosphide or nickel boride, depending on the reducing agent used.

Two reasons cause the decomposition of EN plating bath:

1. The detaching of reduced Ni atoms at the plating surface of the substrate. Not all reduced Ni atoms in ENP process deposit at the substrate surface. A small portion of them reenter the bulk solution as the agglomeration form (tiny Ni colloids). These Ni colloids possess highly reactive surfaces and thus become

parent nuclei for ENP. They arouse localized nickel reduction in the bulk and consequently cause the decomposition of the ENP bath.

2. The formation of insoluble nickel phosphide or nickel boride in plating solution. It was discovered that the existence of hydroxyl ions at the surface of these solid particles of colloidal or near-colloidal dimensions are able to cause the localized reduction of nickel ions to the metal by the homogeneous reaction (Gutzeit, 1959):

$$Ni^{2+} + 2H_2PO_2^- + 2OH^- \rightarrow 2HPO_3^{2-} + Ni + 2H^+ + H_2 \quad (2.32)$$

The finely divided nickel precipitate, in turn, acts as a highly efficient catalyst because of its large surface area, thus triggering a “self-accelerating chain reaction”.

In order to avoid the decomposition of ENP bath, trace amount of stabilizers is added into the plating bath to prolong the bath-life and improve the economic benefit. Stabilizers are chemicals that deliberately added in ENP solutions to avert the nickel reduction in the bulk solution that triggers the subsequent random decomposition of the entire plating bath (Riedel, 1991; Schlesinger, 2000). It must be pointed out that the amount of stabilizer in the plating bath (expressed as mg/L or mol/L) is very critical to its stabilization effect. Insufficient addition can not prevent the bath decomposition; while excessive addition will make the ENP reactions completely ceased.

Several methods have been developed to assess the effectiveness of stabilizers and determine their optimum concentration in the plating solution, which generally can

be divided into two types. One is to study the effect of stabilizer concentrations on the plating rate or deposition (mixed) potential (Kivel, 1965; Das, 1996). The other is to test the endurance of an ENP bath to the presence of catalytically reactive metal colloidal particles by adding $PdCl_2$ solution (El-Rehim, 1996).

The stabilizer systems vary greatly in different EN formulations. The most effective stabilizers, in general, can be divided into the four classes:

I. Compounds of Group VI elements: ***S***, ***Se***, ***Te***
II. Compounds containing oxygen: $\boldsymbol{AsO_2^-}$, $\boldsymbol{IO_3^-}$, $\boldsymbol{MoO_4^{2-}}$
III. Heavy metal cations: $\boldsymbol{Sn^{2+}}$, $\boldsymbol{Pb^{2+}}$, $\boldsymbol{Cd^{2+}}$, $\boldsymbol{Sb^{3+}}$
IV. Unsaturated organic acids: ***maleic***, ***thiourea***

Among these stabilizers, only lead and cadmium are widely used in industrial sectors at present, especially for lead. The addition of Pb^{2+} ions to ENP solutions slightly affects the composition and structure of the deposits and leads to the deposition of Ni-P alloys with a smooth surface and uniform thickness (Chu, 1999). Anisotropic deposition of nickel has been obtained by adding an appropriate amount Pb^{2+} ion to an acidic ENP bath (van der Putten, 1993). Because the edges of a given pattern experience an additional contribution from nonlinear diffusion, mass transport to these hedges is enhanced compared to the bulk of a substrate. As a result the adsorption of lead at the hedges is faster than other parts. Therefore these edges can be selectively poisoned by choosing proper Pb^{2+} concentration, which leads to growth of bevels with an angle. However the toxicity of it is not desirable. Lead may cause many diseases such as neuropsychological and behavioral disturbances, acute

or chronic lead nephropathy and hypertensive crises (Nicolo, 1995). Therefore a lead-free ENP has been encouraged; for instance, the European Union has imposed the Restriction of the Use of Certain Hazardous Substances in Electrical & Electronic Equipment Directive (RoHS Directive) to restrict the use of lead.

To date, several inorganic and organic substitutes have been proposed to replace lead in ENP solutions.

2.8.1 Inorganic substitute stabilizers

Some heavy metal and transition metal cations, such as Tl^{+}, Hg^{+}, Ti^{4+}, Cu^{+} and Cu^{2+}, have been reported to replace Pb as the stabilizer in ENP solution.

$TlNO_3$ and organic mercury [PhHgOAc, mersalyl, meroxyl (Na 2,4-dihydroxy-3,5-di(hydroxymercuri)benzophenone-2'-sulfonate] were reported to stabilize the ENP bath due to their inhibiting effect on the ENP process (Gulla, 1971; Nihei, 1975). However, due to their high toxicity, they are potentially harmful to the environment (Goyer, 1991; Tabandeh, 1994) and thus, their use has been strictly controlled (EPA, 1995; EPA, 2000; EPA, 2005).

An ENP solution stabilized by $Ti(SO_4)_2$ was proposed in which borohydride (KBH_4) was used as reducing agent, complemented by complexing agent ethylene diamine (Guo, 1996). Desirable properties of the deposited nickel film included hardness, corrosion resistance, porosity and superior adhesion. However, $Ti(SO_4)_2$ is very

costly and hence this method has limited industrial applications due to economical considerations.

Among the inorganic stabilizers, monovalent cuprous (Cu^{+}) and the cupric (Cu^{2+}) ion have been most widely studied by researchers (Gulla, 1972; Tarozaite, 1981, 1986; Bielinski, 1983). It was found that the Cu^{+} ions improved the solution stability without significantly retarding the deposition rate while Cu^{2+} ion increased reaction rate and hypophosphite utilization efficiency. The improvement of solution stability was proposed to be due to the formation of randomly dispersed copper particles (approximately one-third of the added Cu) (Armyanov, 1999). The enhancement of the deposition rate by Cu^{2+} was attributed to the improved activity of plated electroless Ni-Cu alloy (Lelental, 1975). This increased catalytic activity was primarily due to the weaker chemisorption of hydrogen on the Ni-Cu alloy deposit surface, unlike that of the pure nickel surface (Armyanov, 1999). In addition to improving the thermal stability, the Ni-Cu-P ternary system is also known to improve the brightness and smoothness of the deposit.

2.8.2 Organic substitute stabilizers

At present, the most accepted organic stabilizers are sulfur-containing compounds. In addition, there are also some non-sulfur containing stabilizers such as arsenazo and pyrimidine which have been reported to have exceptional performance in ENP bath.

It was found that the stability of ENP bath was increased by adding 0.00001-0.0002 M arsenazo compound to the solution containing nickel salt 0.01-0.3 M, sodium hypophosphite 0.02-0.5 M, Na acetate 0.05-0.3 M, and glycine 0.05-0.5 M (Tarozaite, 1980). Similar to $TlNO_3$ and organic mercury, the usage of the arsenazo compound in ENP bath has been stringently regulated by Environmental Protection Agency Regulations (EPA, 2001) due to its hazardous effects on the environment.

In another study, pyrimidine was added as the stabilizer in a basic ENP solution with borohydride as the reducing agent. It was reported that the anodic oxidation of BH^{4-} was not electrochemically related to the cathodic reduction of Ni^{2+} in the initial reaction stages (Gaevskaya, 1992).

More importantly, different kinds of sulfur-containing compounds have been used to replace Pb^{2+} ion in the ENP solution as the stabilizer.

A small amount of sodium thiosulfate in basic ENP baths, in which borohydrides or boranes acted as the reducing agent, was reported to stabilize the bath, increase the yield of Ni, and reduce the nickel particles in the bulk solution (Prokopcikas, 1971). Tracer studies with ^{35}S showed that all deposits formed in the baths contained S. It was highlighted by Prokopcikas that the S was probably incorporated in the coating as a sulfide and occupied catalytically active centers on the surface of the deposit responsible for the decomposition of the reducing agents. Therefore, the stabilizing effect of the $S_2O_3^{2-}$ ion was attributed to the deposition of that sulfide on the plated nickel surface. Sodium thiosulfate was also reported to stabilize the plating bath for

plastic substrates, in which boron hydride hydrazine was used as reducing agent (Reksc, 1990).

Triazolium thiolate and sodium thiocyanate, in the concentration about 0.05-10 mg/L, were proved to increase the nickel deposition rate and stabilize the plating bath (Egli, 2003). Moreover, triazolium thiolate enhances the plating rate more than sodium thiocyanate does where equivalent quantities are used. So, use of mesoionic compounds therefore makes it easier to maintain (or control) the plating solution

It was reported that 3-amino-5-mercapto- I ,2,4-triazole (AMTA) can be used as an effective stabilizer for ENP (Liu, 2008). During plating AMTA can be adsorbed at the surface active site, increase reaction activation energy, reduce plating rate and enhance bath stability. In addition, AMTA could interact with Ni^{2+} ion to form an intermediate compound and increase the reduction rate of Ni^{2+} ion which explains the increase nickel deposition rate at low AMTA concentration.

Sotskaya[a] et al. (2003) studied the effects of organic stabilizers containing –S-S- fragments such as disodium salt of 4,4'-dithiobenzenedisulfoacid and 2,2'-diaminodithiobenzene on ENP. Both of them can substantially control the random nickel deposition in bulk solution, except that the former accelerates the nickel deposition rate at the substrate surface while the latter decelerates it.

Among the sulfur-containing stabilizers, thiourea ($\boldsymbol{NH_2CSNH_2}$) is the one of that has been most widely investigated by different researchers, which, like other sulfur-containing stabililzers, was reported to exert both an accelerating and an inhibiting

effect on the plating rate, depending on its concentration (Baskaran, 2006; Cheong, 2004; Xu, 2003; Sotskaya[b], 2003; Lin, 2002; Ryabinina, 1999; Han, 1997). It was first reported by Han that thiourea accelerated the nickel deposition rate at low concentrations. But the nickel deposition rate was dramatically reduced over the range of thiourea concentrations from 3 to 9mg/L. In fact, the deposition rate was close to zero when the thiourea concentration was above 9 mg/L (Han, 1997). It was also pointed out that thiourea merely inhibited the nickel deposition reaction, but had no impact on hydrogen evolution, i.e. hydrogen evolution was independent of the nickel concentrations.

The distinctly different behavior of Pb^{2+} ion and thiourea in the ENP process was studied by Lin et al (2002). It was found that when its concentration was less than 3 mg/L, thiourea enhanced the deposition rate. In contrast, for the same concentration, Pb^{2+} ion decreased the deposition rate. In addition to this apparent difference, thiourea enhanced the crystallization of deposit, while Pb^{2+} ion gave rise to amorphous structure. Generally a smoother and finer textured deposit was obtained when Pb^{2+} ion was used as a stabilizer instead of thiourea.

2.9 Metallization of hydrophobic silicone elastomer

2.9.1 Metallization of polymers by different methods

Polymers have been widely used in different industrial sectors due to their numerous advantages such as easy processing for low price mass products, the possibility of

precise shaping by injection moulding, low weight, etc. However, nowadays a large number of industrial applications require the deposition of thin metallic films to provide functional properties of the surface like electric conduction, electromagnetic shielding, wear protection, gas diffusion barrier properties or decorative purposes. Therefore, the interest in the metallization of polymers has been gradually increasing (Yan, 2004; Azzaroni, 2006). A number of possible routes to metal deposition on polymers have been attempted including ion beam assisted deposition (Kupfer, 2000), plasma assisted deposition (Kim, 2001), chemical vapour deposition (Park, 2007) and physical vapour deposition (Wang, 2006). These techniques require specialized equipment and must be performed in vacuum that result in the huge equipment and operation cost. In comparison with the aforementioned deposition methods, ENP is relatively inexpensive. However the metallization of polymers by ENP is limited due to its complex protocols of surface pretreatment.

Although different methods have been developed for metallization of polymers, the study on metallization of Poly(dimethylsiloxane) (PDMS), one of the most popularly used silicone rubber in industries, is still limited, to date. This is likely because of its high hydrophobicity that makes the surface modification of PDMS is difficult and complicated.

In the next section, the properties of PDMS, currently available techniques for PDMS metallization and problems need to be resolved before ENP can proceed on PDMS surface will be discussed in detail.

2.9.2 Metallization of Poly(dimethylsiloxane) (PDMS)

PDMS is the most widely used silicon-based organic polymer, and is particularly known for its unusual rheological (or flow) properties. The applications of PDMS range from contact lenses and medical devices to additives, in shampoos, food, adhesives and so on. The extensive applications of PDMS as a structural material extends from advantages such as optically transparent, non-toxic, non-flammable, gas-permeable, chemically inert and easily sealing with other materials (Makamba, 2003; Roman, 2006).

In spite of these advantages, metallization of PDMS is difficult because of its inert and hydrophobic nature. Several methods have recently been reported to modify the surface of PDMS to make it suitable for metallization.

Nickel has been successfully deposited on modified PDMS surface with assistance of plasma and UV (Yan, 2004). In this method, PDMS was first treated by Ar-plasma for 30 sec to improve its wettability. Ar-plasma-pretreated PDMS was then coated with a thin layer of 1-vinylimidazole through UV graft copolymerization. After pretreatment, modified PDMS was activated via a one-step process in an acidic $PdCl_2$ solution and followed by ENP.

A reliable fabrication method of transferable micron scale metal pattern for PDMS metallization has been reported (Lee, 2005; Lim, 2006). They utilized a bonding agent, 3-mercaptopropyl trimethoxysilane (MPT), to maintain adhesion between PDMS and embedded thin-film structure (micrometer-scale gold). Here the thiol

terminal group of MPT can interact with an Au surface, allowing selective assembly, while the silane-terminal alkoxy groups remain available to interact with the silicone of PDMS. The MPT was first organized on gold surface to form a self-assembled monolayer (SAM) on a silicon wafer. PDMS was then poured onto the wafer and cured. Finally the cured PDMS with embedded thin gold film was peeled away from the wafer and the Au patterned PDMS was obtained.

Polyelectrolyte brushes were used as an efficient adhesion layers for site-selective metallization of different polymeric substrates, for example metallizing PDMS by electroless copper plating (Azzaroni, 2006).

Here the microcontact-printed initiator domains were first created on the PDMS. Then cationic brushes of 2-(methacryloyloxy) ethyl-trimethylammonium chloride (METAC) were grown from the substrate using aqueous atom transfer radical polymerization (ATRP). The patterned METAC modified substrate was followed by immersing in a $PdCl_4^{2-}$ solution to anchor catalyst and subsequently electroless plating. It must be noted that this method not only provides excellent adhesion between the deposited metal and substrate, but also can be applied to electrolessly metallize a large variety of polymeric substrates of different metal for example Cu and Ni by controlling the catalyst.

2.10 Development of Pt-based electrocatalysts for proton exchange membrane fuel cells (PEMFCs)

Proton exchange membrane fuel cells (PEMFCs) are a kind of clean, secure and sustainable power source of high energy density and simple structure (Wang, 2005). Nowadays, PEMFCs have been expected to be an alternative power source for automobiles and portable applications, to reduce the dependence on fossil fuel (Alkire, 1997; Wei, 2007).

The standard material used as the proton exchange membrane in PEMFCs is the perfluorinated copolymers containing sulfonic acid groups. Among different available membranes Nafion® and its derivatives have received considerable attention due to their strong chemical resistance and high proton conductivity (Kundu, 2007).

Besides the membrane, another key material for PEMFC is the catalyst. Generally, platinum and its alloy, such as PtRu, PtCu, PtCo, are employed for fuel oxidation and oxygen reduction in PEMFC due to their excellent catalytic activity and stability under fuel cell operation conditions (Koh, 2007; Liu, 2007; Mani, 2008; Ramaswamy, 2008).

It is well known that CO, a poisoning agent, has negative effect on PEMFC electrodes made of Pt. Unfortunately regardless of whether produced by the steam reforming, partial oxidation of hydrocarbon or liquid fuels followed by water-gas

shift reaction, H_2 generally contains about 1 vol.% CO (Monyanon, 2006). In practice, the preferential oxidation (PROX) of CO may be the simplest and the least expensive method for CO removing during fuel cell operation (Marino, 2004). Metals like Ru, Ru, Au, are effective for the PROX of CO. But among them, only Au is proven has high catalytic activity for CO oxidation at low temperature (Monyanon, 2006; Russo, 2006). Moreover, the Pt covered Au nanoparticles or nanoporous gold leaf was reported to enhance the Pt utility in PEMFC (Zhao, 2006; Zeis, 2007).

The most important component part of a PEMFC is the membrane electrode assembly (MEA). Generally the fabrication of MEAs falls mainly into two approaches, namely, (i) electrocatlyst powder or power type and (ii) in situ electrocatalyst powder or non-powder type. The former method involves the precipitation of the metal catalyst from aqueous solution by chemical reduction. The latter method involves the directly depositing catalyst on the surface of the gas diffusion layer (GDL) or membrane surface (Ayyadurai, 2007; Farhat, 2008). The catalyst formation in the non-powder type primarily includes impregnation and deposition, in which deposition is more attractive due to its high purity of product and ease of control. The deposition methods include physical vapor deposition, chemical vapor deposition, sputter deposition and electrodeposition (Lee, 2007; Kim, 2008; Spataru, 2008).

Although ENP has been widely used, the application of electroless platinum plating (EPP) or electroless gold plating (EGP) is still limited, especially for fuel cell. Fujii and Ito (2006) reported high performance Pt catalysts for PEMFC in which Pt were

deposited on carbon black (CB) by electroless plating. In addition, they pointed out that catalysts consisted of larger Pt particles showed poor power density and, hence, were not suitable as fuel cell catalyst. Pt-based electrocatalysts were also prepared on carbon nantubes (CNTs) for PEMFC by electroless plating (Liu, 2002). The Pt/CNT electrodes showed high electrocatalytic activity for oxygen reduction as tested by a single stack PEM fuel cell. In addition, Pt was directly deposited on polypyrrole modified Nafion composite membranes for direct methanol fuel cell (DMFC) as well (Li, 2007). But EPP was seldom used to deposit catalyst directly on pristine Nafion® membrane, because the electron cannot be transported inside the poorly electron-conductive Nafion® membrane.

2.11 Problem definition

It is known that the co-depositon of Cu or S deteriorates the corrosion resistance of ENP film which is an important desired characteristic for many materials. There is therefore a need to find new stabilizers that have negligible effects on not only the ENP deposit but also the environment.

As mentioned previously, the study on the substitute stabilizers for Pb in ENP solution is far from maturity. Most of the research did not involve the study of ENP bath life by metal-turnover (MTO) and their stabilization mechanism; the former is a typical way to evaluate the stability of an ENP bath while the latter is important for future applications of stabilizers industrially. Hence it is necessary to carry out

systematic research to investigate the effect of stabilizers on the ENP bath life and understand the stabilization mechanisms of different stabilizers.

Besides improving the environmental friendliness of stabilizers, the applications of ENP can be significantly boosted if they are also able to metallize hydrophobic polymers. To metallize hydrophobic polymers, such as PDMS, by ENP, three major problems have to be resolved. Firstly, a hydrophilic substrate surface has to be created. Secondly, initiating sites have to be implanted on the polymer surface. Last but not least, coherence between deposited nickel and polymer substrate has to be improved.

In order to reduce the high cost of precious metals and equipments used in MEAs and enhance the chemical resistance of Pt to carbon monoxide, the method that directly deposits Pt or its alloy onto Nafion membrane by electroless plating may be a solution of great potential. Although Nafion® is hydrophilic, it is still a challenge to develop an effective activation solution that not only initiates the plating but also increases the adhesion between metal and membrane. Another challenge is to prepare Pt-Au bimetallic particle in nano-scale that has great resistance to carbon monoxide. Furthermore, the investigation about the effects of the plating conditions on catalyst size and distribution is necessary to improve the cell performance.

Chapter 3 Roles of Sulfur-Containing Amino Acids in Electroless Nickel Plating Bath

In this chapter two typical sulfur-containing amino acids, cysteine and methionine, were employed as stabilizers in place of lead(II) acetate in electroless nickel plating (ENP) system. Each of these compounds presents a critical stabilizing concentration of ca.10^{-5} mol/L, below which the ENP rate is promoted with increasing concentration but above which it is significantly suppressed. Their role in stabilizing the ENP bath was found to involve inhabitation of anodic reaction of hypophosphite. The chemical adsorption of these two amino acids on active nickel sites at the plating surface was studied via their adsorption on an in-situ generated Ni powder. The stabilization mechanism was investigated by using potentiometry, X-ray photoelectron spectroscopy (XPS), and Vis-UV / infrared spectroscopy. In addition, the bath stabilizing capabilities of these two amino acids and the change of ENP properties with time were assessed through a continuous operation comprising four metal-turnover (MTO) runs.

3.1 Introduction

As introduced in Chapter 2, Electroless nickel plating (ENP) has achieved a broad spectrum of industrial applications since the development of the first practical plating system by Brenner and Riddell in 1946 (Section 2.7 of Chapter 2). And the low bath stability has been a key issue for an ENP system, due to the autocatalytic nature of Ni-P alloy deposit. As plating proceeds, insoluble particles consisting of nickel and nickel phosphite are produced in the plating bath, and deposition of nickel takes place overwhelmingly on these finely dispersed particles driven by the autocatalytic nature, and this plating-out process would quickly lead to failure of the plating bath (Section 2.8 of Chapter 2).

To date, most commercial EN baths contain Pb^{2+} ions in parts per million quantities as the stabilizer to ensure a smooth plating rate throughout a continuous process that consists of several MTO rounds. MTO is a method to evaluate the long-term performance of a stabilizer. One MTO is defined as the completion of reduction of the nickel salt initially present in the fresh plating solution. However, lead is a harmful substance that causes several severe diseases in humans through chronic contact (Castellino, 1995). Lead in the EN bath pollutes the environment through two channels: the lead(0) atoms codeposit in Ni plating layers and the lead(II) ions remaining in spent ENP solution. The replacement of lead with low-environment-impact stabilizers has become reinforced by law (Chen, 2006). In principle, an ENP stabilizer behaves to deactivate the autocatalysis that sustains plating. Sulfur-containing organic compounds have been proposed as substitutes for lead (Han,

1997; Reda, 2001; Lin, 2002; Sotskaya[a,b], 2003; Cheong, 2004), because they are Lewis bases. Nevertheless, previous studies primarily examined their effects on the EN deposition rate but provided inadequate information on the chemistry of stabilization as well as effects on MTO and corrosion resistance of the Ni-P plating layer.

Investigating reaction mechanism of ENP (Malory, 1990; Riedel, 1991; Jiang, 2000; Yin, 2004) has practical significance for improving performance of ENP systems. Among theose mechanisms discussed in Section 2.4, the electrochemical mechanism originally proposed by Brenner and Riddell (1946) has been widely cited. It splits ENP into anodic and cathodic processes. On the basis of this model, the role of the stabilizer is considered to be passivation of the anodic reaction through either disprotionational deposition ($Pb^{2+} + 2e^- \rightarrow Pb$) or adsorption of the Lewis base to the Ni surface. Sulfur-containing organic compounds are soft coordination ligands and could form surface complexes with Ni(0) atoms. The surface-adsorbed sulfur-containing compounds would consequently retard the anodic reaction ($H_2PO_2^- + H_2O \rightarrow H_2PO_3^- + 2H^+ + 2e^-$). This chapter reports an investigation of the involvement of two sulfur-containing amino acids in the anodic process in the acidic ENP system. This is because the oxidation rate of hypophosphite ions affects the nickel deposition rate. We also investigated whether the type of amino acid has an effect on the composition and surface morphology of the resultant nickel plating layer and, in turn, on its corrosion resistance in strongly acidic environments. In addition, the study also covered the influence of the two amino acids on the continuous Ni deposition rate of their respective ENP baths. The new insight of this

work is the founding that variations in the sulfur group, such as thiol in cysteine and sulfide in methionine, give rise to rather different ENP stabilization chemistries.

3.2 Experimental

3.2.1 Materials

All chemicals used in this work were analytical-grade. Nickel sulfate hexahydrate, sodium hypophosphite monohydrate, ammonium hydroxide, sodium acetate, thiourea, L-cysteine and methionine were purchased from Merck, lactic acid and acetone from Fisher, and DL-malic acid from Acros.

Deionized (DI) water with a resistivity of greater than 15 MΩ cm, generated by a Millipore Elix10 purification system, was used for solution preparation and the rinsing of glassware and samples.

Brass hull cell test panels used as the substrate in this work was purchased from Hiap Guan Electroplating Material (Singapore).

3.2.2 Plating rate vs stabilizer concentration

The plating solution was formulated in house, and its main components are listed in Table 3.1. In this investigation, each data point of a curve was collected from a small plating bath containing 80mL of plating solution, the starting pH of which was

adjusted to 5.00 ± 0.03 by the addition of 25% ammonium hydroxide solution at room temperature before plating. The temperature of the plating solution was maintained at 90 °C by using a water bath (Haake DC30/W13) as the heating source. The change in the thickness of Ni plating layer on a brass plate (0.25×50×37 mm^3) within 30 min with the variation of stabilizer concentration was investigated. The brass substrate was carefully cleaned via the following two steps before use: it was first subjected to ultrasonication in an alkaline-based detergent solution for 5 min and then rinsed with acetone and DI water alternatively a few times. The plating was initiated by touching the substrate with a clean pure nickel coil in the ENP bath, and after that the plating was maintained for 30 min. The plated sample was cleaned with DI water and dried in the air. The mass gained (*W*) was obtained from an analytical balance (A&D GR-200 Goldbell, Singapore) with a precision to 10 μg and the deposition rate *r* was determined by the equation:

$$r = \frac{W \times 10^4}{\rho A t} \qquad (3.1)$$

where *r* is the deposition rate in micrometers per hour, *W* the weight of plating layer in grams, *A* the plating area in square centimeters; *t* the plating time in hours, and ρ = 7.8g/ cm^2 is taken as the density of Ni-P alloy by assuming a P-content of approximately 13%. All data presented in this experiment were the mean values of 5-time repeated measurements.

Table 3.1 Composition of acidic hypophosphite plating bath

Components	Concentration
Nickel (II) sulfate hexahydrate	22.4 g/L
Sodium hypophosphite monohydrate	25 g/L
DL-Malic Acid	4 g/L
Sodium Acetate	8.5 g/L
Lactic Acid	21 ml/L
Stabilizers	variable

3.2.3 Electrochemical analysis of the oxidation rate of hypophosphite

The anodic reaction of hypophosphite in the presence of cysteine or methionine was evaluated using the potentiostat/galvanostat technique on an electrochemical analyzer (Autolab, model JP202). The experiments were carried out in an electrochemical cell equipped three-electrodes (CFC-13 Coating Flat Cell, Scriber Associate, Southern Pines, NC, USA). The working electrode was plated brass (13 cm^2), the counter-electrode was a spent platinum mesh with a surface area of 25 cm^2, and the reference electrode was a standard silver/silver-chloride electrode (Metrohm 6.0726.100, Herisau, Switzerland). The solution charged into the cell contained sodium hypophosphite and a sulfur-containing stabilizer whose concentration was varied, and the pH of the solution was maintained at 5.00 ± 0.03. This solution was kept still, and its temperature was held at 70 °C during potential scanning unless otherwise noted. Then, the current-potential curves were obtained from a potential scan at a rate of 10 mV/s. For each concentration, the anodic potentiodynamic scanning (PDS) was repeated 5 times to reduce the accidental error.

3.2.4 Assessment of ENP bath stability

The starting conditions of ENP bath and the pretreatment of substrate were the same as described in section 3.2.2, except that the pH (5.00 ± 0.05) of the plating bath was controlled by frequently addting 25% ammonium hydroxide solution and mild air agitation was introduced throughout the entire plating process. The stabilizer concentration in MTO experiments was fixed at 10^{-5}M. The plating solution volume of 1.2 L and the plating load (defined as the plated area in decimeters divided by the volume of plating solution in liters) of 2.5 dm^2/L were fixed throughout the MTO tests. The plating bath was filled after about each 30-min interval of plating by controlled amounts of the two concentrated replenishing solutions (~ 40 mL each), which are main nickel sulfate hexahydrate, sodium hypophosphite monohydrate, DL-malic acid, sodium acetate and lactic acid, to supplement the components consumed. The stabilizer in the plating bath was replenished at the beginning of each MTO, and the brass substrate was changed after the completion of each MTO. For each stabilizer, all data reported in MTO evaluation were the mean value of 3 repeated experiments.

3.2.5 Evaluation of corrosion resistance

The corrosion resistance of the plating layer generated from each MTO was assessed by potentiodynamic polarization technique. The measurements were conducted in the three-electrode electrochemical system, which was the same setup as used to measure the anodic oxidation rate (Section 3.2.3), and the liquid medium was HCl solution (1M, 100 mL). A scan rate of 1 mV/sec was used.

3.2.6 In situ adsorption of the two amino acids on fresh nickel powders

Four aqueous solutions (20 mL of each): 0.05M $NiSO_4$, 0.05M $NiSO_4$ + 0.05M thiourea, 0.05M $NiSO_4$ + 0.05M cysteine and 0.05M $NiSO_4$ + 0.05M methionine were prepared, and an excess of sodium boron hydride ($NaBH_4$, 0.1g) was added to each of the solutions under vigorous stirring. The resultant black suspensions were centrifuged after the reduction had completed (bubbling had eased). The precipitates were washed with DI water, centrifuged five times, and then dried at 60 °C. The powders obtained were investigated by X-ray photoelectron spectroscopy (XPS, Kratos Axis HiS System) to examine whether sulfur adsorbed species were present on the nickel metal particles. The binding energies of the XPS peaks were calibrated using the carbon 1s peak that was corrected to 284.6 eV. The Ni 2p XPS signal presents two peaks, $2p_{1/2}$ and $2p_{3/2}$, with the former being 17 eV higher than the latter. In addition, the intensity of the Ni $2p_{3/2}$ peak is double of that of the Ni $2p_{1/2}$ peak. Therefore, only the position of the lower-binding-energy $2p_{3/2}$ peak is quoted. The curve fitting was carried out with XPS PEAK (version 4.1). Because nickel is a transition element, the background used here was of the Shirley type. An X-ray satellite peak (around 861.5 eV) appeared at the higher bonding-energy (BE) side of the Ni $2p_{3/2}$ peak.

3.2.7 Other instrumental analyses

The surface morphology and composition of the Ni-P plating layer was recorded on a field-emission scanning electron microscope/energy-dispersive X-ray (FE-SEM/EDX) instrument (JEOL, JSM-6700F, Tokyo, Japan), in which data about

deposit composition were collected from the three locations on each sample and the mean value was reported. UV-visible spectrophotometer (UV-3101PC, Shimadzu, Kyoto, Japan) was employed to examine the UV-visible adsorption spectra of the seven aqueous solutions with the solute, namely, pure nickel sulfate, pure thiourea, pure cysteine, pure methionine, nickel sulfate/thiourea, nickel sulfate/cysteine, and nickel sulfate/methionine, in which the concentrations of nickel sulfate and the sulfur-containing compounds were all set at 0.05 mol/L.

3.3 Results and Discussion

3.3.1 An investigation of the dual effects of the two S-containing amino-acids on ENP rate

To benchmark the performance of these two amino acids, thiourea, a commonly used organic stabilizer (Section 2.8.2 of Chapter 2), was employed to undertake equivalent studies. The curves of ENP rate versus the concentration of stabilizer revealed the effects of the three S-containing amino acids on ENP (Figure 3.1). Both cysteine and methionine display almost the same a gentle accelerating role in the concentration range from 10^{-9} to 10^{-5} mol/L. However, they function slightly different in inhibiting the plating rate at the higher concentration (>10^{-5} mol/L). Cysteine causes a rapid decrease in the plating rate at a concentration of 3×10^{-4} mol/L, whereas methionine brings about a more slowly decreasing slope. These two amino acids behave rather similarly with thiourea (Han, 1997) in terms of showing opposite roles in the two concentration ranges. Previously the role of S-containing

compounds was deemed to impede the oxidation of hypophosphite (Feldstein, 1971; Ohno, 1985; Gyanutene, 1996; Han, 1996 & 1997; Sotskaya[a,b], 2003), which is known as the anodic reaction.

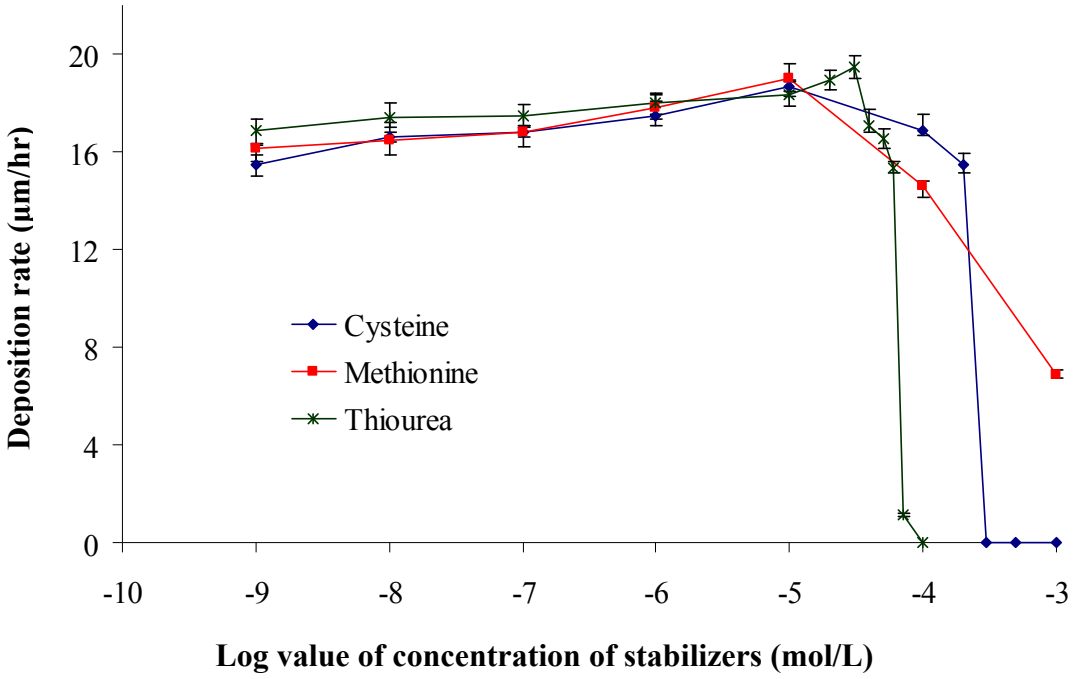

Figure 3.1 Influence of concentration of sulfur-containing amino acids on nickel deposition rate

As mentioned previously, the role of a stabilizer in the ENP system has been regarded as to inhibit the anodic process. On the basis of this perspective, we carried out anodic potentiodynamic scanning (PDS) from -0.8V to 0.1V, which checks the anodic current density of the working electrode (i.e., a Ni-P layer on brass). The current is generated from the oxidation of hypophosphite anions on the electrode when it is given a voltage relative to the reference electrode (Ag/AgCl). All of the measured anodic polarization curves (Figure 3.2) consist of two peaks, where the first peak (ca. -0.41V vs Ag/AgCl) reflects oxidation of hypophosphite ion and the

second (ca. -1.4V) indicates the dissolving of Ni-P layer (Lyaukonis, 1983; Ohno, 1985; Gyanutene, 1996; Han, 1997; Sotskaya, 1997; Khaldeev, 2000). As the plating (i.e., the cathodic reaction) is governed by the anodic current density, the peak value reflecting the maximum oxidation rate of hypophosphite ion could therefore be taken as a measure of the ENP rate with respect to the concentration of a particular stabilizer. Hence, for each stabilizer, the peak values of the anodic current density were plotted as a function of the stabilizer concentration (Figure 3.3). Indeed, both curves of current density vs logC show a pattern similar to those displayed in Figure 3.1, namely, regardless of the metal deposition rate or the anodic current density experiences a slow increase with increasing stabilizer concentration but a rapid drop when the stabilizer concentration is higher than 10^{-5} M (Figure 3.3). At the same time, it can also be seen that cysteine works more effectively to repress the anodic reaction of hypophosphite than methionine in the concentration range (10^{-9} to 10^{-5} M) that could not be clearly discerned in the deposition rate vs concentration curves (Figure 3.1). In comparison with these two stabilizers, thiourea gives an intermediate anodic current density in the low concentration range as indicated above.

The Pearson Hard Soft (Lewis) Acid Base (HSAB) principle offers a qualitative theoretical model to interpret the capabilities of the three S-containing compounds to inhibit the anodic current density. If the electron polarizability of the sulfur atoms in the three organic groups is used to gauge the hardness of the Lewis base, the order RSR' > RSH > R_2C=S could be established. On the other hand, a Ni(0) atom was regarded as a soft Lewis acid relative to a secondary amine ligand (Haack, 1997), so it could fit better with a soft sulfur atom. Of the two amino acid compounds of interest, cysteine (RSH type) is thought of to have a stronger affinity with Ni(0)

atoms on the ENP surface because of their analogous Lewis acid-base hardness characteristics. Indeed, cysteine results in the lowest anodic current density in the concentration range below 10^{-6} M.

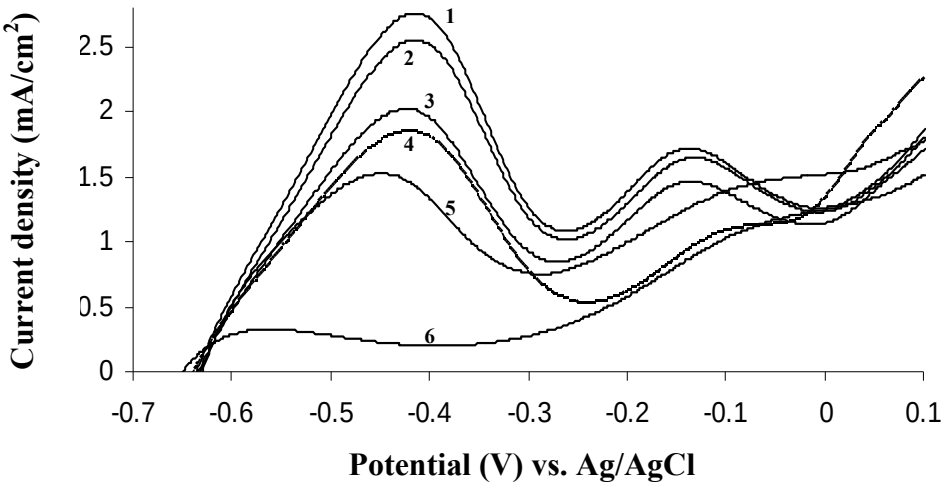

Figure 3.2 Current-potential curves of anodic oxidation of hypophosphite on nickel at different cysteine concentrations (mol/L). 1) 10^{-5}, 2) 10^{-6}, 3) 10^{-8}, 4) 0, 5) 2×10^{-4}, 6) 10^{-3}

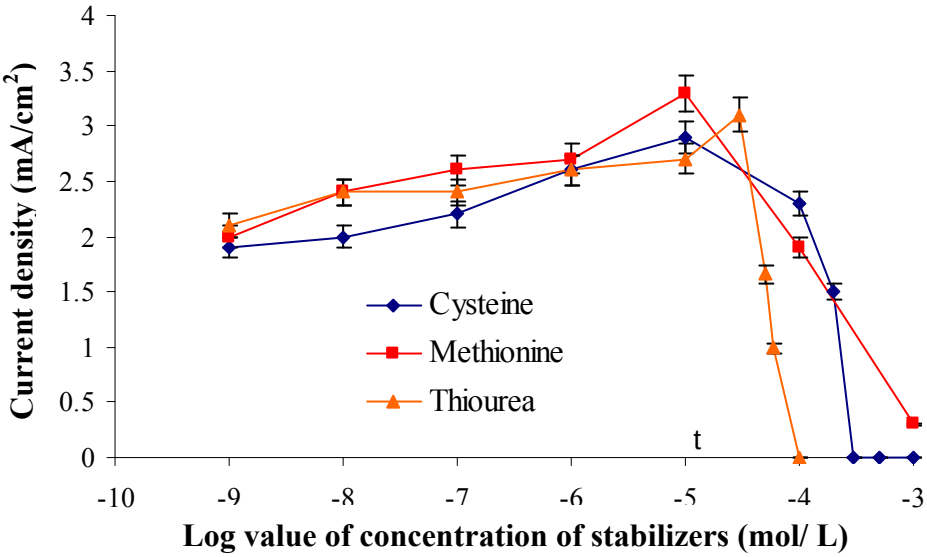

Figure 3.3 Peak values of anodic current density vs. the corresponding concentrations of sulfur-containing amino acids

Regarding the chemistry that governs the dual roles of the three S-containing compounds, previous studies (Feldstein, 1971; Mallory, 1990; Han, 1996) considered that the accelerating role of cysteine lies in its interaction with hypophosphite ion, through which the oxidation of hypophosphite is promoted. The oxidation of hypophosphite ion involves the transformation of a P-H bond to a P-OH bond. Nevertheless, neither of the two amino acids nor thiourea was found to associate with hypophosphite ion by UV-vis spectroscopy at room temperature. It is likely that either a thiol or sulfide group might participate only transiently in stabilizing the positively charged phosphorous center when a $H_2PO_2^-$ ion releases two electrons to the plating surface via its oxygen "tentacles" (Figure 3.4) (Yin, 2004). Such a mediating action is presumed to cause the gradual increase of the anodic current with increasing stabilizer concentration before the threshold. In addition to the anodic effect, this work also pursued the question of whether these two amino acids affect the cathodic reaction, specifically through complexation with Ni^{2+} ions in aqueous media. It was found, based on UV-vis spectroscopy (Figure 3.5), that cysteine does not form a coordination complex with Ni^{2+} ion, but methionine-$Ni(SO_4)_2$ solution displays an additional shoulder peak comopared to the single-component absorption spectrum in the near-UV range (251 nm). This shoulder peak can be attributed to the adsorption of methionine-Ni^{2+} complex ion that presumably has the structure shown in Figure 3.6. Compared with the UV-vis absorption of the hydrated nickel ion complex $[Ni(H_2O)_6]^{2+}$ (at 390, 650 and 720 nm)(Jolly, 1991), the shoulder peak appears at the high-energy side. This implies that methionine is a stronger filed ligand than water as defined by the crystal field theory. The different Lewis acid-base properties bring about the different

complexing tendencies of these two amino acids with Ni^{2+} ions. In the following section, the role of the methionine-Ni^{2+} complex is further elaborated.

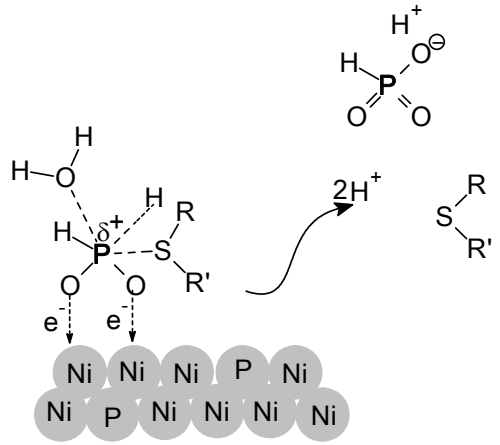

Figure 3.4 Schematic graph for interaction between sulfur-containing amino acids and positively charged phosphorous center at plating surface

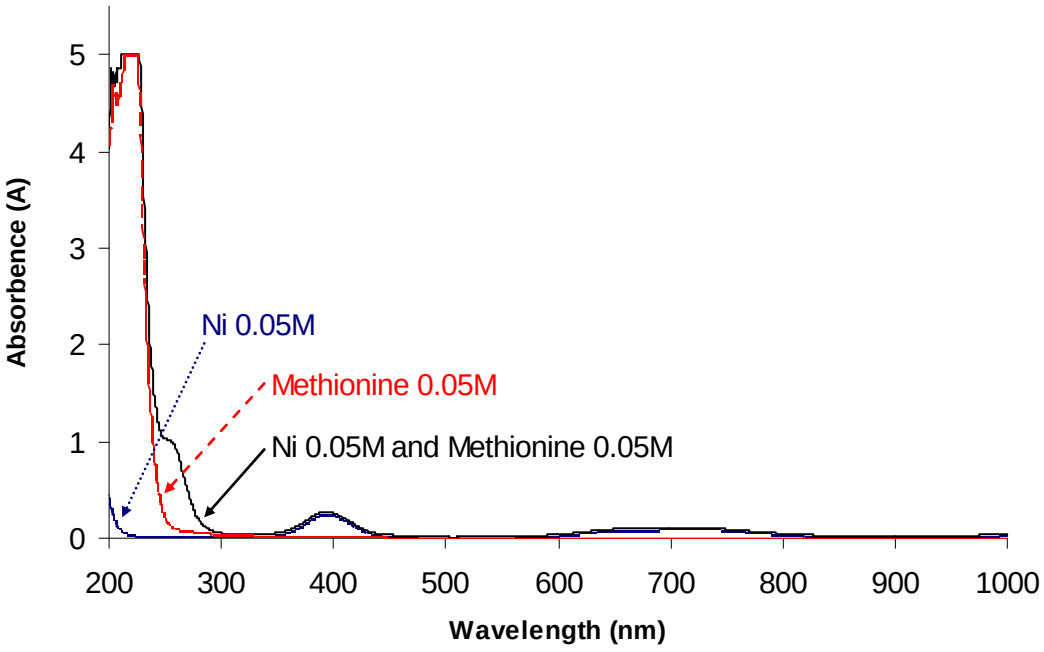

Figure 3.5 The UV-Vis spectra of nickel solution with methionine as stabilizer 1) Methionine 0.05M, 2) Nickel sulfate 0.05M, 3) Methionine 0.05M + Nickel sulfate 0.05M

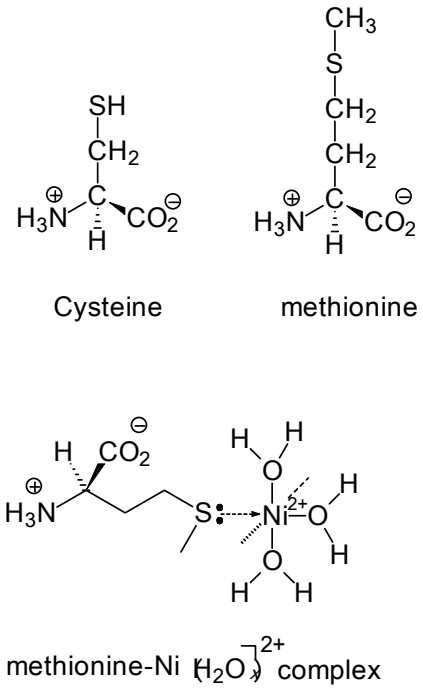

Figure 3.6 The structures of cysteine, methionine and methionine-Ni^{2+}

The inhibiting role of the two amino acids arises from competition with hypophosphite to occupy reactive Ni(0) sites on the plating surface. The oxidation rate of hypophosphite will be impeded if the reactive Ni(0) surface sites are not readily accessible, and this is why the nickel deposition rate or the anodic current density decreases quickly above the critical concentration of stabilizer. These active Ni surface sites refer to those nickel atoms having highly unsaturated coordination environments. Since they are handful on a normal plating surface, it is experimentally difficult to detect the adsorbed amino acid molecules on an ENP surface.

A model system was designed to investigate the adsorption of the two amino acids on the nickel surface. In this model system, the adsorbent was nickel fine particles and an amino acid was present while the Ni particles were generated by chemical reduction (section 3.2.6). In principle, fine particles have a large specific surface area and a plentiful number of reactive surface sites. Therefore, in situ adsorption of the amino acid molecules to the Ni particles would take place if they had adequate chemical affinity. Thiourea was employed as a refence adsorbate and a pristine Ni powder as reference adsorbent. The four powders made by the solution reduction were examined by XPS.

They all show Ni-$2P_{3/2}$ peak at about 855.5 eV, which can be deconvoluted into two components with binding energies (BEs) at about 855.4 and 856.8 eV (Figure 3.7). These peaks are attributed to the surface Ni(II) and Ni(III) species with oxygen as the counter ions (Moulder, 1992; Davidson, 1996). The broad satellite (centred at about 861.5 eV for NiO and NiOOH) was due to a predominant surface plasmon loss (Grosvenor, 2006). Obviously, a significant amount of the surface nickel atoms were oxidized as soon as they were generated in the preparation system. However, it is important to note that the XPS spectrum of the pristine Ni powder exhibits Ni(0) species with a binding energy at 852.8 eV, whereas this peak is not observed in the other three spectra. It is rational to consider that the remaining Ni(0) species are covered by the adsorbed S-containing species. This inference was then supported by the XPS of sulfur and the IR spectra of these three powders.

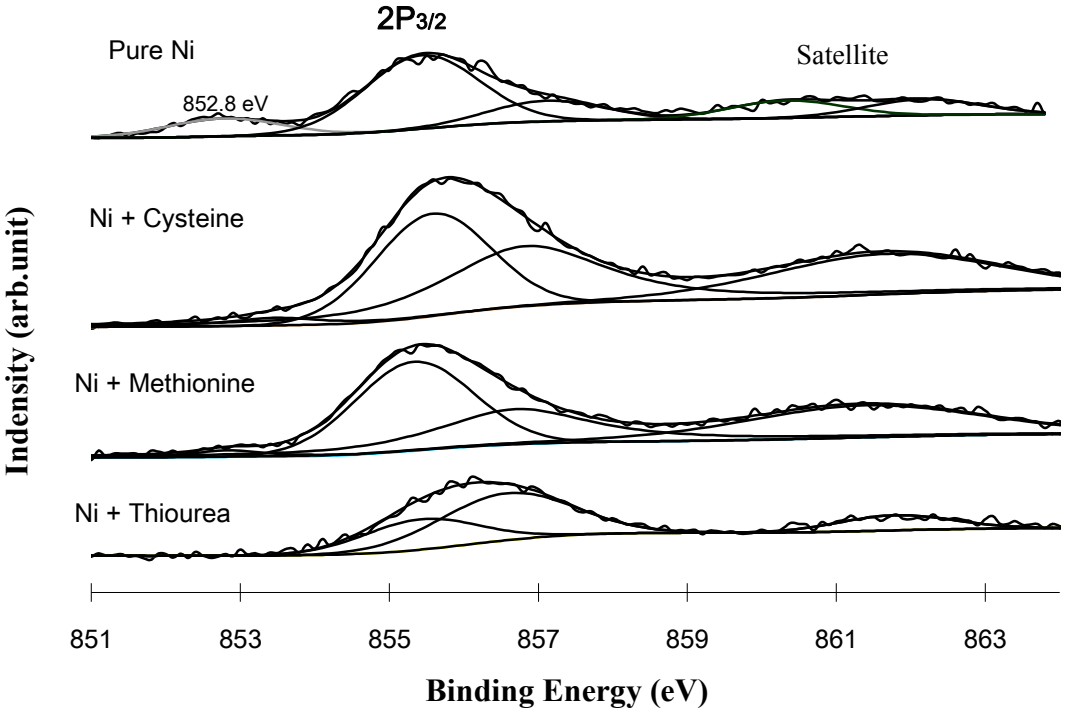

Figure 3.7 XPS spectra of Ni 2P3/2 in four samples together with curve fitting

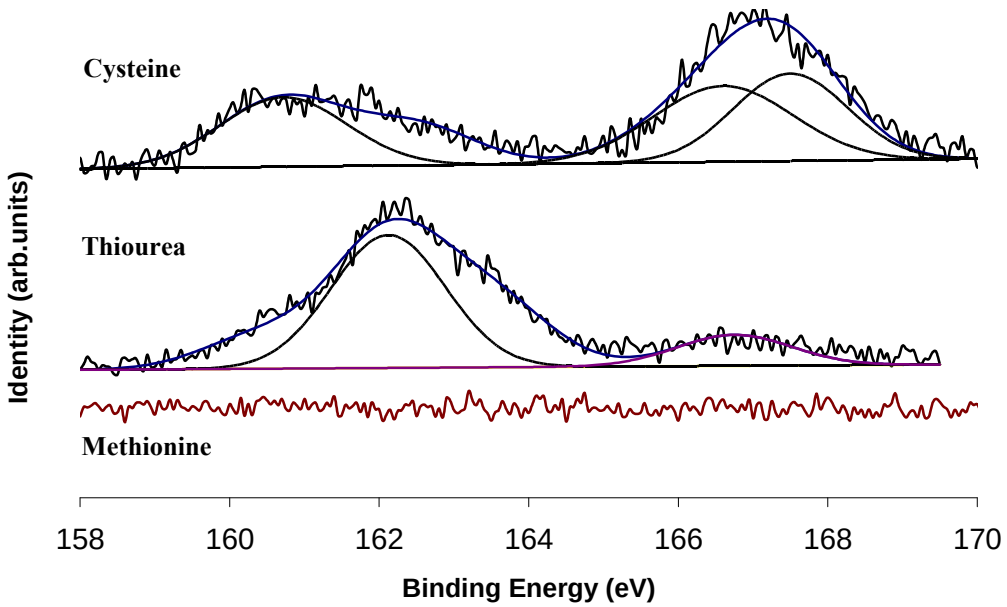

Figure 3.8 XPS spectra of S 2P3/2 in three samples together with curve fitting

Although it was still rather weak, the S-$2p_{3/2}$ XPS peak displayed by both the Ni-cysteine and Ni-thiourea powders represents the presence of surface S-containing species (Figure 3.8). The adsorbed mercapto (-SH) group shows the peak at 160.8 eV, and the adsorbed thiourea (>C=S) exhibits a peak at 162.3 eV as was also reported by Yagi (1995 & 2003). In addition, the major S-$2p_{3/2}$ XPS peak of Ni-cysteine appears at the higher-BE side (167.2 eV), which can be assigned to oxidation products of mercapto group (S=O at 166.5 eV and $S_2O_3^{2-}$ at 167.7 eV)(Moulder, 1992). The FT-IR spectrum of Ni-cysteine also displays a rather strong S=O vibration absorption band (Figure 3.9). Similarly, the Ni-thiourea also presents two S-$2p_{3/2}$ XPS peaks, but the adsorbed thiourea is less oxidized because the peak with the higher BE (at 167.2 eV) is much weaker than the corresponding peak in S-$2p_{3/2}$ XPS spectrum given by the former sample. Moreover, the IR spectrum of the Ni-thiourea powder shows a strong absorption band of the adsorbed thiourea but a weaker S=O absorption band. In contrast to thiorurea and cysteine, methionine does not form adsorption species on the in-situ generated nickel particles. This was also verified by the IR spectrum, in which no organic absorption peaks are present. It is clear now that methionine does not have the HSAB affinity required for the combination with Ni(0) atoms. This contrasts with what revealed in Figure 3.5, where only methionine forms a complex with Ni^{2+} ion because of their matching HSAB properties. Furthermore, as mentioned previously, the Ni-$2P_{3/2}$ XPS spectrum of this powder sample showed essentially no Ni(0) species, similarly to what was found for the pristine nickel powder. It could be inferred that it is methionine-Ni^{2+} complex but rather methionine that retards the oxidation of hypophosphite on the Ni plating surface by occupying the reactive sites. Moreover, the gradual decrease in plating rate at methionine concentrations above 10^{-5} M (Figure 3.1) can be explained

by the occurrence of this particular adsorbate. In the end, the adsorbed complex ions will be washed away during the purification, and the reactive Ni(0) sites that are opened will be readily covered by oxygen to form an entire NiO surface.

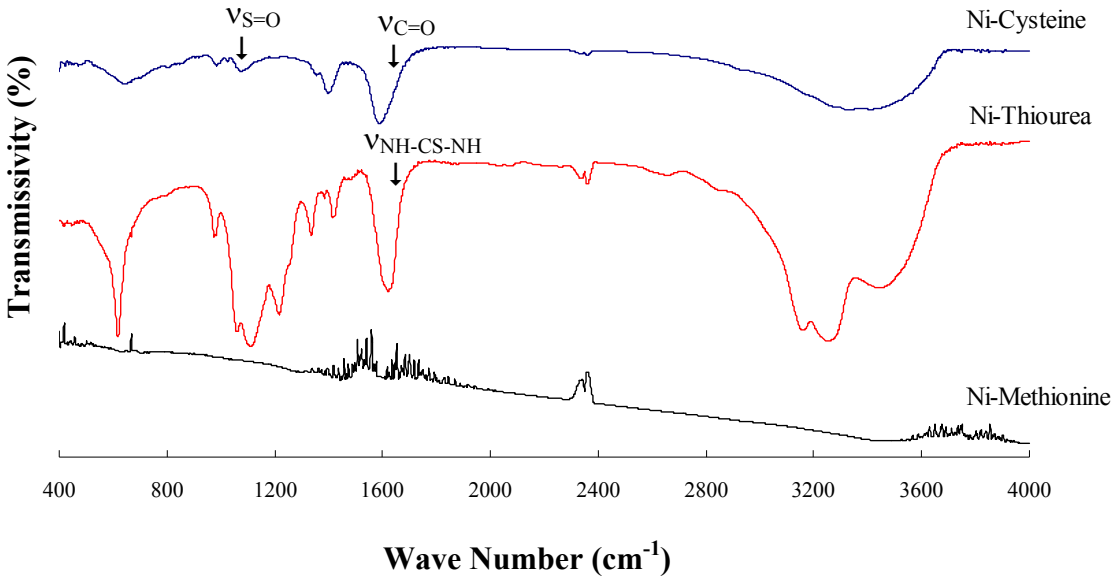

Figure 3.9 FT-IR spectra of Ni-thiourea, Ni-cysteine and Ni-methionine

3.3.2 Nature of S-containing group and the composition of Ni/P deposition layer

It is important to understand whether the composition of the nickel plating layer is affected by the sulfur groups of amino acid used, in addition to the concentration of the stabilizer. Table 3.2 summaries EDX measurement data on the nickel and phosphorus contents (weight percentage) of the plating layers obtained under different conditions. Here the Ni and P contents are absolute values. Judging from the tabulated data, the two amino acids essentially did not lead to any noticeable difference in nickel and phosphorus contents. However the concentration of both

cysteine and methionine had a certain effect on the phosphorus-content (P-content), which showed a pattern that the maximum P level was obtained in the middle (10^{-7} mol/L) of the concentration range investigated. At the same time, it can also be noted that the EDX surface analysis did not indicate the presence of residual sulfur species in the plating layer in the systems in which cysteine and methionine were used. This is because the very low concentrations of these two amino acids ($\leq 10^{-5}$ mol/L) led to low concentrations of sulfur adsorption species that were below the EDX detection limit.

Table 3.2 Composition of Ni-P deposition layer based on EDX analysis

Concentration of stabilizers (mol/L)	Cystein		Methionine	
	Ni wt.%	P wt.%	Ni wt.%	P wt.%
0	87.2	12.8	87.2	12.8
10^{-9}	87.9	12.1	87.3	12.7
10^{-8}	86.9	13.1	86.9	13.1
10^{-7}	85.9	14.1	86.5	13.5
10^{-6}	87.0	13.0	86.7	13.3
10^{-5}	88.4	11.6	88.3	11.7
10^{-4}	88.3	11.7	88.2	11.8

To examine the long-term stability of the EN bath containing either of these two amino acid stabilizers, a four-MTO continuous plating process (as stated in Section 3.2.4) was evaluated. Neither plating-out nor decomposition occurred in the plating bath after 4 MTOs had been completed, despite a very slight decrease in the plating rate (Figure 3.10). The P-content in the plating layer could be roughly maintained at a stable level throughout the four MTOs (Table 3.3). In addition, the ENP layers developed in the cysteine-containing bath yielded slightly higher P-content than those developed in the methionine-containing bath. This phenomenon is consistent

with the different electrode stabilizing roles as concluded above: cysteine has a stronger anodic passivation capability than methionine. As a result, a lower Ni deposition rate leads to a relatively high P-content.

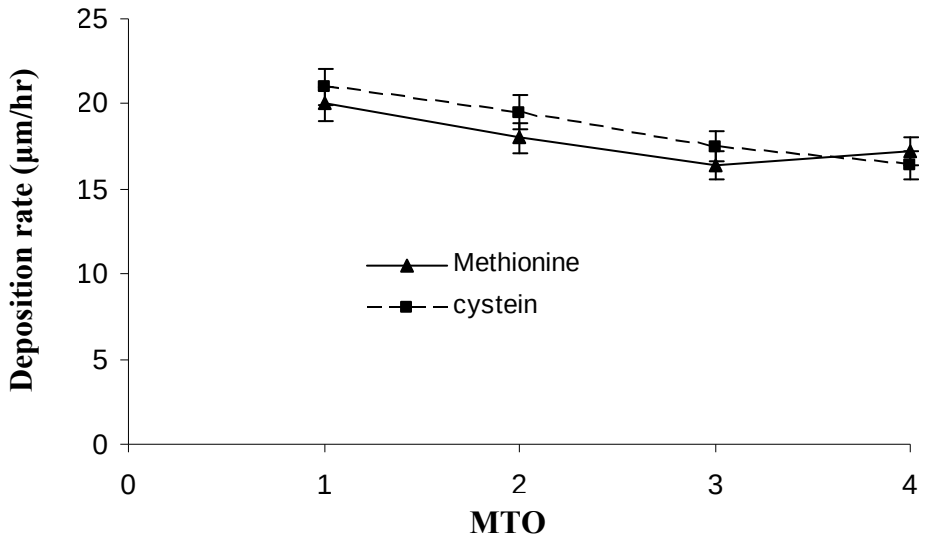

Figure 10 Effect of MTO on nickel deposition rate with cysteine or methionine as the stabilizer

Table 3.3 Change of the Ni and P contents in the plating layer with MTO

Round of MTO	Cysteine		Methionine	
	Ni wt.%	P wt%	Ni wt.%	P wt.%
1st	89.0	11.0	89.5	10.5
2nd	88.6	11.4	89.4	10.6
3rd	88.8	11.2	89.9	10.1
4th	89.4	10.6	89.3	10.7

Concentration of cysteine and methionine: 10^{-5} mol/L

The potentiodynamic scanning (PDS) technique (Section 3.2.5) was employed to study the chemical corrosion resistance of the plating layers obtained from different MTOs, and representative PDS curves for samples with methionine as the stabilizer

are shown in Figure 3.11. The respective cathodic (corrosion) current densities of the two MTO investigation systems obtained from the PDS diagrams are summarized in Figure 3.12. It is noteworthy that the plating layer formed in the second MTO displays the highest corrosion resistance amongst the four layers, regardless of the amino acid used. This outcome suggests that the surface morphology of the plating layer, which is apparently affected by the rate of evolution of H_2 from the plating surface, is another factor affecting the corrosion resistance.

We found that the two sets of plating layers (corresponding to the two stabilizers) formed in the last two MTOs (third and fourth) display somewhat different surface morphologies from the preceding ones (Figure 3.13). Both layers from the first two MTOs share similar surface morphologies, are shown in Figure 3.14 for the methionine-based set. It is clear that the second MTO produced the smoothest surface, which hence gives rise to the smallest corrosion current density. Furthermore, the plating layers generated from the third and fourth MTOs show increasingly vulnerable corrosion resistance due, in general, to the codeposition of insoluble tiny particles. In addition, the cysteine-based plating layer (from the fourth MTO) has a higher corrosion current density than its methionine-based equivalent. This phenomenon can be attributed to the adsorption of cysteine onto the plating surface according to previous characterizations. The adsorption becomes severe with the accumulation of stabilizer in the plating solution and the formation of rough domains on the plating surface. It is likely that the absorbed organic sulfur species favors electron transfer between the amino acid and the deposit and leads to a decease in the corrosion resistance.

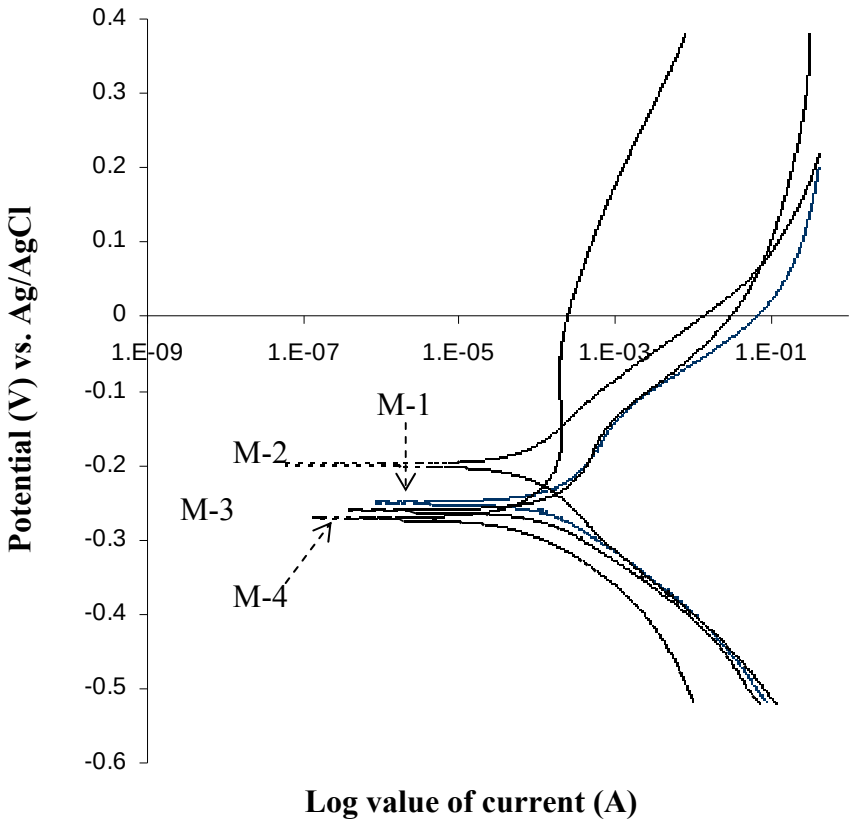

Figure 3.11 PDS curves of Ni-P coatings with methionine as stabilizer in different rounds of MTO. M-1: 1st MTO, M-2: 2nd MTO, M-3: 3rd MTO, M-4: 4th MTO

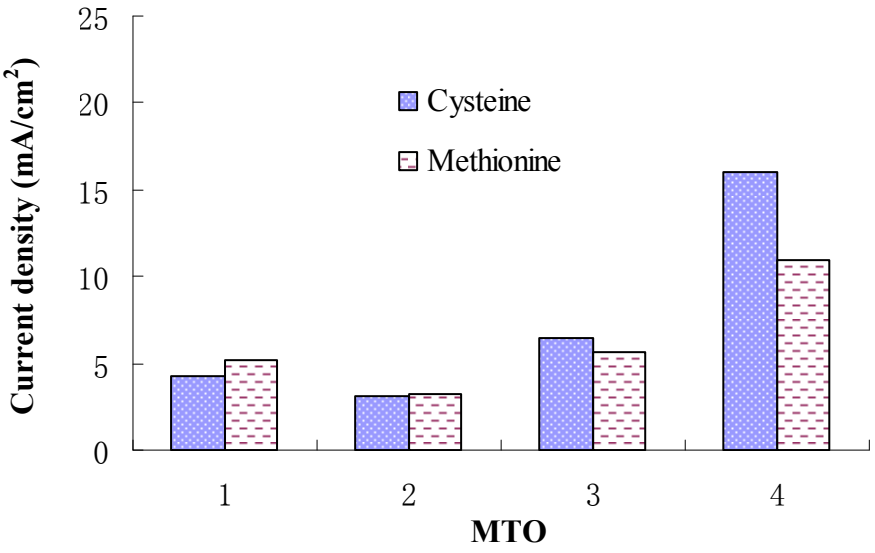

Figure 3.12 Corrosion current density vs MTO for cysteine and methionine

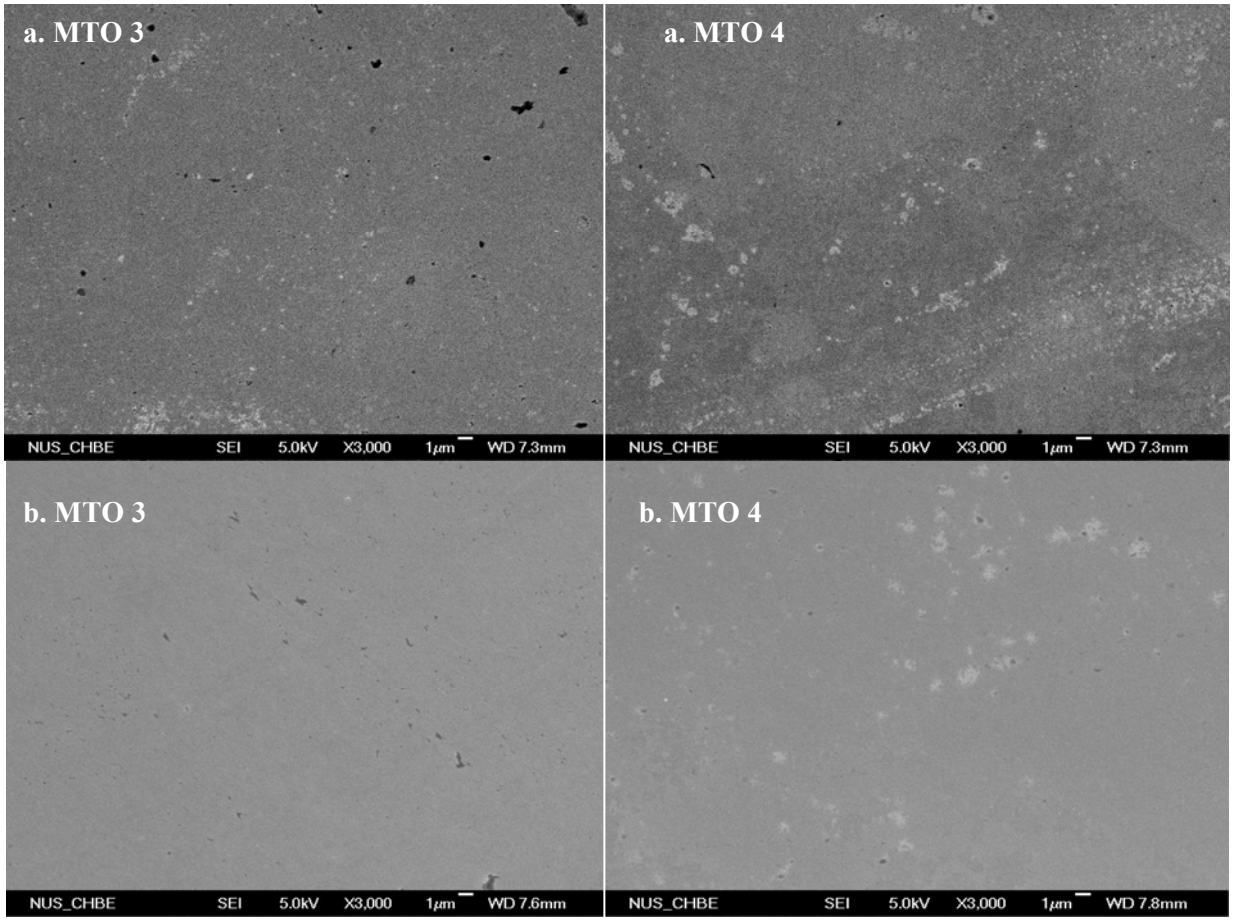

Figure 3.13 Surface morphology of the 3rd and 4th MTO samples for a) cysteine or b) methionine as the stabilizer

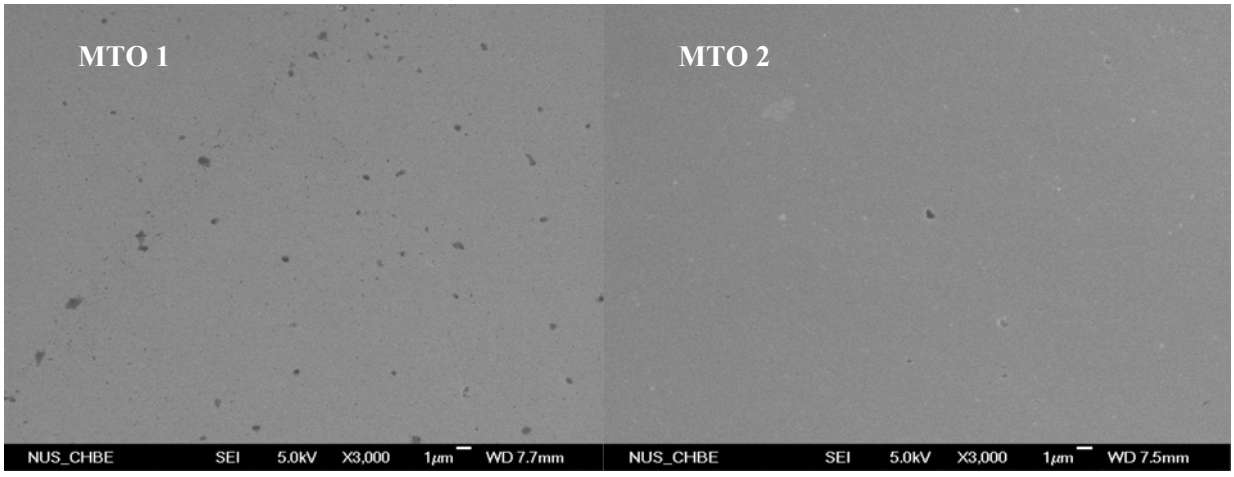

Figure 3.14 Surface morphology of the 1st and 2nd MTO samples for methionine as the stabilizer

3.4 Conclusions

In this chapter, two sulfur-containing amino acids, cysteine and methionine, were investigated as the bath stabilizer in a lead-free electroless nickel plating (ENP) system. To benchmark the performance of these two amino acids, thiourea, a commonly used organic stabilizer, was employed in parallel studies. The relations of the ENP deposition rate versus concentration for the different stabilizers were established. Both cysteine and thiourea displayed a clear cutoff for dramatically decreasing the deposition rate at a concentration near 10^{-5} M, but methionine revealed a gradual decreasing trend because a methionine-Ni^{2+} complex rather than methionine itself provided a stabilizing role. Furthermore, the anodic reaction of hypophosphite on a Ni-P electrode in the presence of one of the stabilizers was tested by measuring the anodic current density. The current density – concentration profiles resulting from this test match well with the deposition rate – concentration profiles, which means the role of sulfur-containing amino acids in ENP process is to control the oxidation rate of hypophosphite ion at the plating surface. In this test, the order of anionic current density could be clearly discerned as methionine > cysteine > thiourea; i.e., methionine provided the highest deposition rate of the three.

The most important test carried out in this work was the adsorption of these three sulfur-containing compounds on the in-situ generated Ni particles. This is because the normal ENP surface has a small number of coordination-unsaturated Ni sites but the Ni particles contain a large number of such surface sites; hence chemical adsorption of these compounds on an ENP layer could be magnified. From this test,

only cysteine and thiourea exhibited stagnant adsorption on the Ni particles, whereas methionine did not, according to XPS and IR evidence. On the other hand, a UV-vis study showed that methionine formed a soluble complex with Ni^{2+} ions. We are inclined to believe that methionine forms a complex with Ni^{2+} ions and that the complex acts to stabilize the anodic reaction. In contrast, cysteine and thiourea act on their own to stabilize the EN bath.

The last part of this chapter presents the investigation of the durability of the two amino acids in stabilizing a four-MTO continuous ENP process. As a key parameter, the electrochemical resistance of the resulting plating layers was measured. The results showed that methionine gives rise to a more corrosion-resistant plating layer from the fourth MTO than cysteine and this is ascribed to its sulfur-free surface.

Chapter 4 The Role of Bi^{3+}-Complex Ions as the Stabilizer in the Electroless Nickel Plating Process

This chapter explores Bi^{3+}-complex ions to replace harmful Pb^{2+} ion as the stabilizer in electroless nickel plating (ENP) solution. The asymmetric derivatives of EDTA coordination ligands were identified to be effective in assisting with dissolution of Bi^{3+} ions in the acidic ENP solution. The critical stabilizing concentration of the Bi^{3+}-complex ions, from which the ENP rate drops sharply, was determined at ca. 10^{-5} mol/L. Besides experimental measurement, the deposition rates of both Ni and P were also simulated by a kinetic model that was developed on the basis of the double electric layer theory. The intrinsic instable trait of ENP system can be attributed to the occurrence of metal colloidal particles in the plating bath, and the Bi^{3+}-complex ion, behaving like the traditionally used Pb^{2+} ion, stabilizes ENP bath through the chemical displacement reaction at the surface of Ni deposition layer, which causes a passive plating surface. This investigation also verified that the properties of EN deposit were not significantly affected by the extension of plating time with employing Bi^{3+}-complex ion stabilizer.

4.1 Introduction

As discussed in Chapter 2 and Chapter 3, ENP is in nature an autocatalytic process in which reduction of Ni^{2+} ions from the plating solution is catalyzed by the nickel just being deposited. This autocatalytic nature leads to inherent instability of the ENP system. As the plating proceeds, colloidal particles of insoluble nickel and nickel phosphite provide highly efficient catalytic sites due to their tremendously large specific surface area, and an overwhelming deposition of nickel black will be triggered, known as a "self-accelerating chain reaction" or the plating-out process, and result in failure of plating bath (Section 2.8 in Chapter 2 & Section 3.1 in Chapter 3).

As aforementioned, Pb^{2+} ion had been traditionally employed as the stabilizer in commercial ENP solution for a long time. However, as the public has become aware of the harmful effects of lead to human being especially children in recent years, the lead containing products have been strictly barred. Therefore, the development of lead-free ENP baths has therefore become obligatory (Section 2.8 in Chapter 2 & Section 3.1 in Chapter 3). In Chapter 3, two sulfur-containing amino acids – cysteine and methionine – were successfully evolved to replace Pb^{2+} ion as the stabilizer in ENP solution. But the use of such sulfur-conatining stabilizers also cost the corrosion resistance of EN deposits. This deteriorating effect was clearly observed in the 4-MTO continuous test because of the co-deposition or adsorption of sulfur species in/on the deposits. Such a negative effect of sulfur-containing stabilizers on EN deposits was also reported by other researchers in recent years (Das, 1996; Han, 1997; Lin, 2002; Cheong, 2004 & 2007[a,b]).

In this Chapter, a particular type of Bi^{3+}-complex ions is prepared and employed as ENP stabilizer. Among heavy metals, bismuth is unusual because its toxicity is much lower than that of its neighbors in the periodic table such as lead, thallium, and antimony. Actually bismuth has widely used as a lead substitute in industries (Ketkar, 2006; Zylberberg, 2007), because the toxicity of bismuth and its salts is dose-dependent and only large doses can be fatal (Serfontein, 1979; Sano[a,b], 2005). Furthermore the existence of insignificant amounts of bismuth in a Ni-P plating layer does not reduce its corrosion resistance. Alfons (2004) and Bobrovskays (1993) reported their studies on replacing lead by bismuth (III). Nevertheless, their studies did not explore the aquatic chemistry of Bi^{3+} ion because Bi^{3+} ion undergoes quick hydrolysis in ENP solution if there is not a pertinent ligand present to hold the ion. Moreover, the ligand effect on reactivity of Bi^{3+} ions makes the stabilization role of complex ion more complicated than that of Pb^{2+} ion. Hence it is imperative to have an insight into the coordination chemistry of Bi^{3+} in ENP system in order to understand the performance of the ENP process this stabilizer maintains.

In this chapter the derivatives of EDTA (ethylene diamine tetraacetic acid) but rather EDTA itself constitute a unique type of ligands that preserve Bi^{3+} ions in the weak acidic ENP solution medium. White bismuch precipitate would, otherwise, occur in the solution without the presence of a coordination ligand of this type. Moreover, finite structural differences among these ligands were identified to bring about trivial leverages on performance of ENP, such as plating rate, deposit composition, surface morphology and bath service life etc. Hence the focus of this study is placed on clarifying how the coordinated Bi^{3+} participates in ENP process. In addition, a simple model was developed using the concept developed in our prior work (Yin,

2004) to explore the stabilization mechanism of Bi^{3+} ion in ENP system and predict the deposition rates of nickel (R_{Ni}) and phosphorus (R_P) respectively. It was found that Bismuth(III) not only acts as a stabilizer in the ENP process, but also competes with nickel ions in the metal reduction. The extension of bath service life to at least four metal-turnovers (MTOs) did not noticeably affect the properties of EN deposit. Moreover, according to the revised mathematic model, it was also verified that once Bi^{3+}-complex ion exceeded its critical concentration an exponential reduction in both nickel and phosphorus deposition rates occurred concurrently.

4.2 Experimental

4.2.1 Materials

Ethylenediaminetetraacetic acid disodium salt (***EDTADSS***), N-(2-hydroxyethyl)-ethyleneddiamine-triacetic acid (***EDTA-OH***) were purchased from Aldrich and ethylene glycol-bis(2-aminoethyl)-N,N,N',N",-tetraacetic acid disodium salt (***EGTADSS***) from Fluka. Other chemicals, brass substrate and DI water were the same as those described in Section 3.2.1 of Chapter 3.

4.2.2 Determination of characteristics of ENP process and deposit

The main components of ENP solution were remained the same as those listed in Table 3.1 of Chapter 3. In addition, the details of methods, used to determine the relations of plating rate and stabilizer concentration, to measure the oxidation rates

of hypophosphite at plating surface in the presence of different Bi^{3+}-comoplexes, to evaluate the electrochemical corrosion resistance of Ni-P in HCl, and to assess the ENP bath stabilities, have been described in Sections 3.2.2-3.2.5 of Chapter 3.

4.2.3 Other instrumental analyses

The surface morphology and chemical composition of Ni-P plating layer were analyzed the same as what descried in Section 3.2.7.; while transmission electron microscope (TEM, JEOL, JEM-2010, Japan) was used to analyze the colloidal particles collated from plating solutions.

4.2.4 Palladium titration

The stabilizing capability of Bi^{3+}-complex ion was evaluated using the palladium titration method as developed before (Yin, 2003). The aqueous $PdCl_2$ solution was prepared by dissolving 25mg of $PdCl_2$ in 5 mL concentrated hydrochloric acid (37%). The resulting solution was then diluted by DI water to 500mL in a volumetric flask. Before the titration, the pH of the plating bath was adjusted to 4.80±0.03 by adding ammonia solution. The $PdCl_2$ solution was dripped at a rate of ca. 0.05mL/s into 20 mL ENP solution, and the temperature was held at 60±2 ^oC. Sufficient magnetic stirring was upheld to disperse $PdCl_2$ added instantaneously. The titration was stopped at the moment the ENP bath turned black, a sign of large precipitation of metal colloids; and the $PdCl_2$ solution consumed was recorded as the decomposition volume V_d. For each concentration, the titration was repeated for at least 20 times to reduce the accidental error. In addition, a parallel study of

effectiveness of Pb^{2+} ion in the same plating system was also evaluated as benchmark.

4.3 Results & Discussion

4.3.1 Influence of Bi^{3+}-complex ion on anodic reaction of hypophosphite

Bi^{3+} ion can only exist in fairly strong acid solutions, because it undergoes rapidly hydrolysis in water to generate bismuth oxide (BiO^{+}), which finally precipitates as BiO·OH. Hence it is important to identify a suitable ligand that forms complex with Bi^{3+} ion in the weak acidic ENP medium and to ensure complete dissolution of the required bismuth salt.

It was found that three EDTA derivatives, namely, EDTADSS, DETA-OH and EGTADSS, in which the four chelating arms of diamine are non-equivalent as shown in Figure 4.1, could satisfactorily form water-soluble complexes with Bi^{3+} ion. In contrast, their counterparts with equivalent chelating arms all cause precipitates in ENP solution. This phenomenon implies that free arms other than those that grab Bi^{3+} ion must be available in the complex in order to maintain the solubility of complex. We further examined the three complexes using UV-Vis spectroscopy, and found that they all showed an extremely strong absorption band at 270 nm in contrast with the pristine ligands, which revealed only a very weak absorption band at ca. 256 nm. The same investigation also showed that none of the three ligands

formed complex with Ni^{2+} ion. Hence, Ni^{2+} ions would not substituted for Bi^{3+} ion in the complexes in the ENP bath.

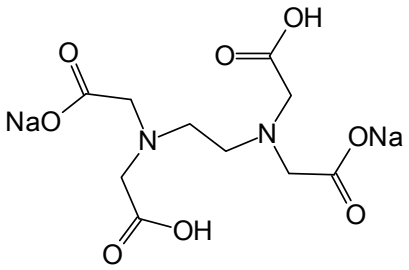

EDTADSS

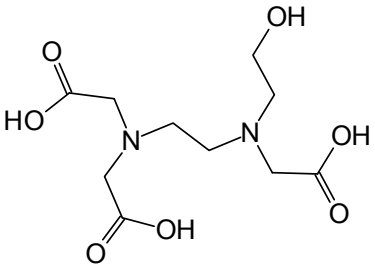

EDTA-OH

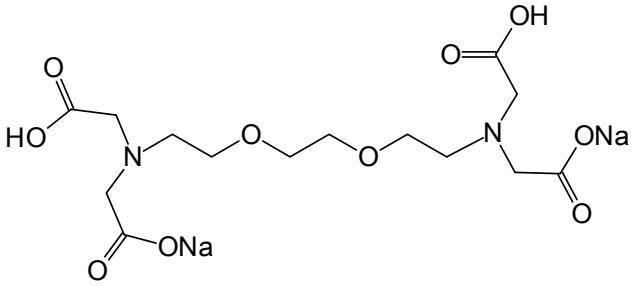

EGTADSS

Figure 4.1 Structures of three EDTA-derivatives

The curves of ENP rate vs. the concentration of Bi^{3+}-complex ion are shown in Figure 4.2. All of them show a critical concentration at ca. 10^{-5} mol/L ($C_{Bi\text{-}C}$), above which the nickel deposition rate is decelerated rapidly. In the concentration range from 10^{-9} mol/L to 10^{-5} mol/L, Bi^{3+}-complex ion does not noticeably disturb the nickel deposition rate. In addition, structural differences of the three EDTA-derived ligands did not affect deposition rate in the concentration range below $C_{Bi\text{-}C}$.

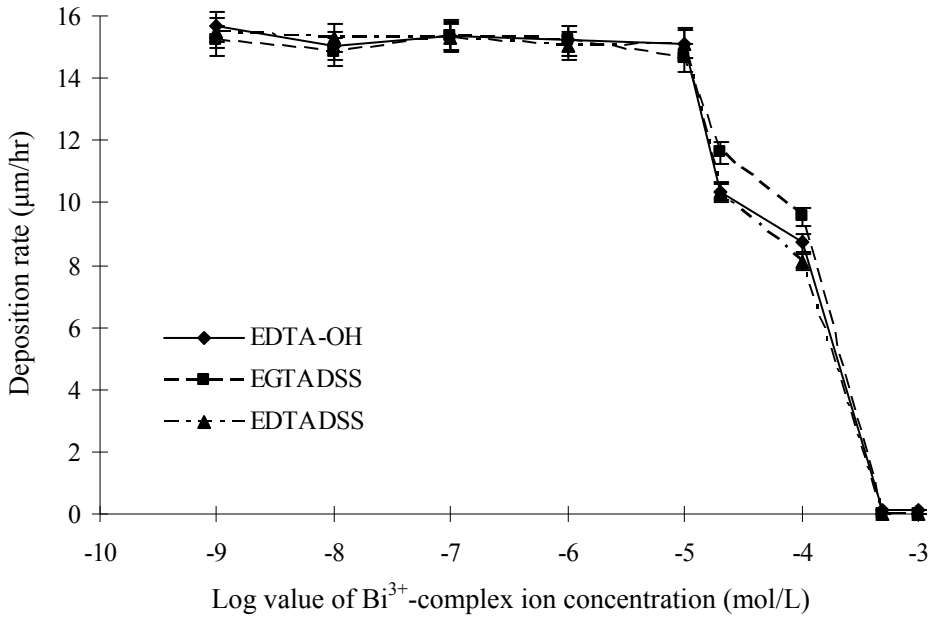

Figure 4.2 Influence of existence of Bi^{3+}-complex ions on nickel deposition rate

In principle ENP can be split into the cathodic reaction (Ni-P deposition) and the anodic reaction ($H_2PO_2^- + H_2O \rightarrow H_2PO_3^- + 2H^+ + 2e^-$). The anodic half reaction is deemed to be the rate determining step of the whole ENP (Section 3.3.1 in Chapter 3). Hence, the Bi^{3+}-complex ion is expected to act on retarding the anodic reaction when its concentration is above $C_{Bi\text{-}C}$. To verify this concept, the anodic potentiodynamic scanning test, which checked the anodic current density of the working electrode (i.e. a Ni-P layer on brass) generated from the oxidation of hypophosphite anion on the electrode when it was given a series of lower biases relative to the reference electrode (Ag/AgCl), was carried out.

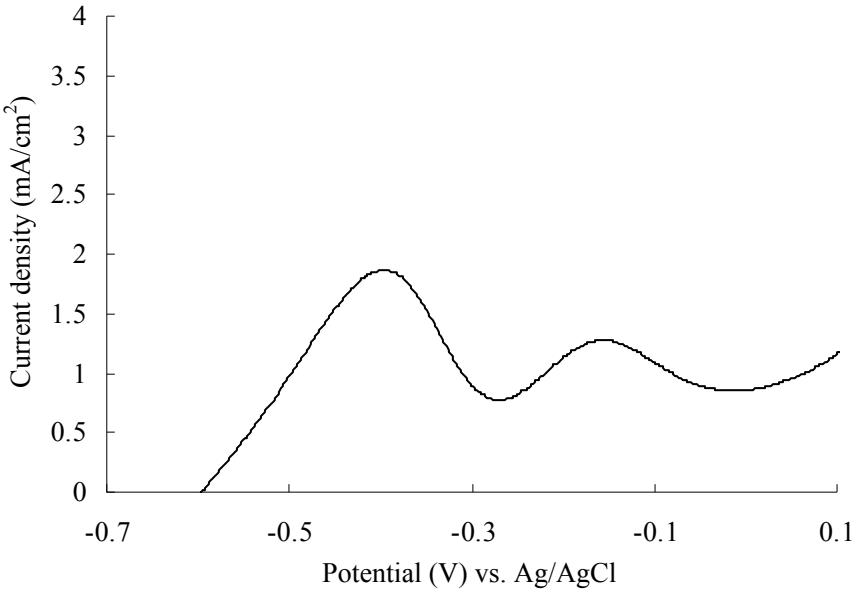

Figure 4.3 Current-potential curve of anodic oxidation of hypophosphite on Ni-P electrode in solution containing 0.24 mol/L hypophosphite and 10^{-6} mol/L Bi^{3+}-EDTADSS

It was observed that, the same as what showed in Figure 3.2 in Chapter 3, the anodic polarization curve (Figure 4.3) consists of two peaks, of which the first peak (ca. -0.41V vs. Ag/AgCl) reflects oxidation of hypophosphite ion, the second one (ca. -0.14V) the dissolving of Ni-P layer (Section 3.3.1 of Chapter 3). As the plating rate, namely the cathodic reaction, is governed by the anodic current density or supply of electrons from anodic reaction, the peak intensity that reflects the oxidation rate of hypophosphite ion could, therefore, be taken as the measure of ENP rate about a particular concentration of stabilizer. Hence, with respect to a stabilizer, a curve consisting of the anodic current density (amplitude of peak) versus concentrations of stabilizer was plotted (Figure 4.4). Indeed, the current density ~ logC relationship is similar to the deposition rate ~ logC relationship presented in Figure 4.2. This

resemblance verifies the attribute that the oxidation of hypophosphite determines the ENP rate.

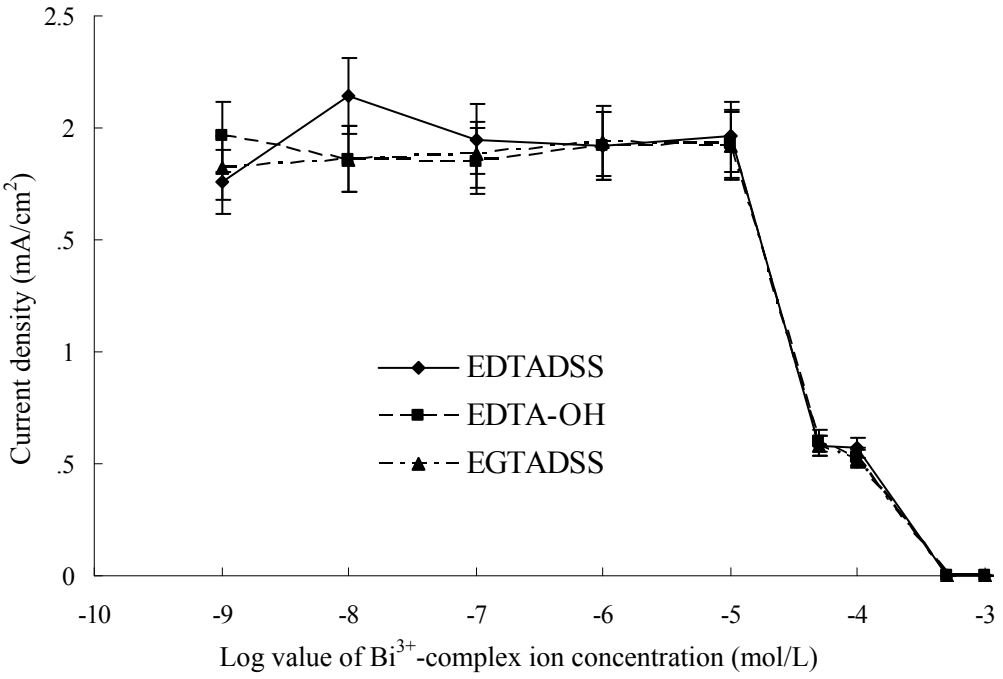

Figure 4.4 Peak values of anodic current density vs. the corresponding concentrations of Bi^{3+}-complex ions

Similar to the effect of Pb^{2+} ion in the inhibiting of anodic process of ENP, when the concentration of Bi^{3+}-complex is below its critical level ($C_{Bi\text{-}C}$), a handful amount of Bi^{3+} ions will replace the surface Ni atoms through the chemical displacement reaction $Bi^{3+} + \frac{3}{2} Ni \rightarrow Bi + \frac{3}{2} Ni^{2+}$ that is driven by spontaneous thermodynamic tendency ($\Delta G^o \cong 82.5\, kJ \cdot mol^{-1}$). The Bi atoms generated occupy the surface lattice sites of Ni atoms due to their close atomic radii ($r_{Ni} = 124\ pm$ vs. $r_{Bi} = 150\ pm$). The sparse Bi atoms distributed over the surface Ni lattice make the substrate passive to ENP according to the theoretical model developed previously (Yin, 2004). It is,

however, difficult to detect by XPS the presence of Bi at the deposit surface (Figure 4.5 (a)) due to substantially low contents, such as, in the two spectra corresponding to the initial stabilizer concentrations of 10^{-5} and 10^{-6} M, respectively.

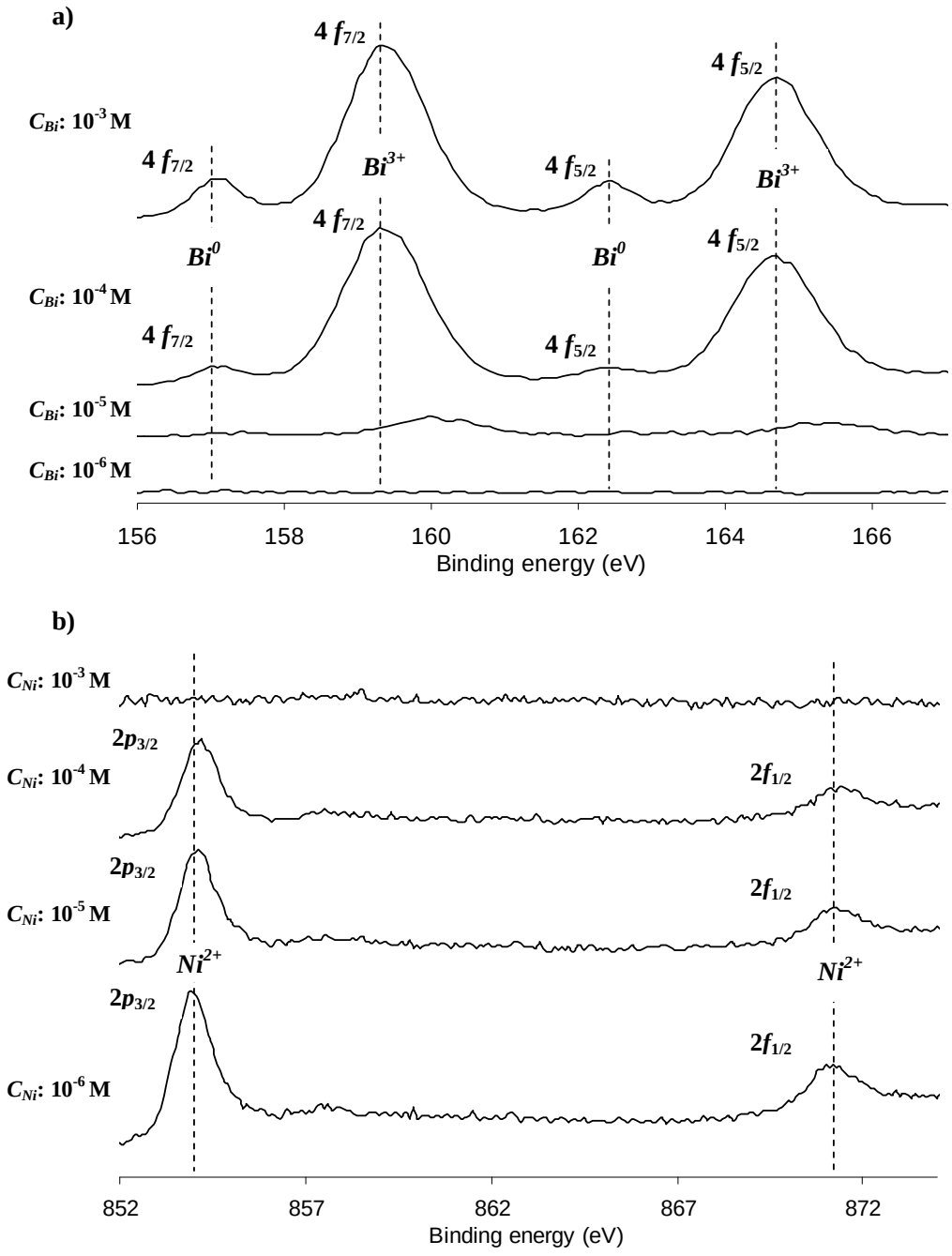

Figure 4.5 The XPS spectra of (a) Bi 4f and (b) Ni 2p in four samples after plated in ENP bath at different Bi^{3+}-complex ion concentrations for 30 mins

In order to verify experimentally the happening of chemical displacement process, two higher concentrations of Bi-complex ion (10^{-4} M and 10^{-3} M) relative to C_{Bi-C} were tested in the same plating system as that designed for generating plots of Figure 4.2. Although no perceptible Ni deposition (e.g. H_2 bobbling) took place on brass since the stabilizer concentration was above C_{Bi-C}, Bi species were still detected on the two samples prepared on account of XPS Bi 4*f* doublet peaks (Figure 4.5 (a)). Correspondingly, the XPS Ni 2*P* doublet disappeared from the spectrum of the sample with using the stabilizer concentration of 10^{-3} M (Figure 4.5 (b)). It is rational to believe that a thin layer of Ni was deposited on a brass plate at the very moment when ENP was initiated by touching the plate with a Ni wire, but the Ni layer was subsequently replaced by Bi through the chemical displacement reaction. Meanwhile, it may be also worthy noting that under the same conditions Bi^{3+}-complex ion cannot be reduced by hypophosphite, hence the deposition of Bi species on the brass substrates was solely due to the chemical displacement reaction with Ni atoms.

A further confirmation was undertaken with using EDX analysis. The samples were prepared in the solution containing the stabilizer of 10^{-3} M but with different plating times. The result supports the above supposition (Figure 4.6): a shoulder peak of Ni was observed on the main Cu peak but no Bi peak appeared on the spectrum after 1min plating. Such a weak Ni peak stands for a thin Ni layer formed since the moment when the brass substrate was connected to a nickel wire. However, this initially deposited Ni was quickly replaced by Bi^{3+} from the solution, which could be proven by the EDX spectrum of the sample with plating time of 2 min. Such a trend continued as reflected by the EDX spectra of the other two samples for longer

plating time. Furthermore, when inspecting the XPS binding energy of Bi4*f* peaks, we see two sets of Bi 4*f* doublets consisting of the Bi $4f_{7/2}$ peak and the Bi $4f_{5/2}$ peak, where both peaks have a span of 5.3-5.6 eV. Bi $4f_{7/2}$ peak at 159.3 eV and Bi $4f_{5/2}$ peak at 164.6 eV indicate the presence of Bi^{3+} cations (Moulder, 1992); while for Bi(0) the two peaks appear at 156.9 eV and 162.5 eV, respectively (Suezer, 1999). In comparison with the surface concentration of Bi(0) species, a much higher surface concentration of Bi^{3+} species is exhibited according to XPS analysis, and this result could be attributed to fast oxidation of Bi(0) when the sample was exposed to air because the sample was carefully cleaned by DI water to remove solution attached to surface before the analysis.

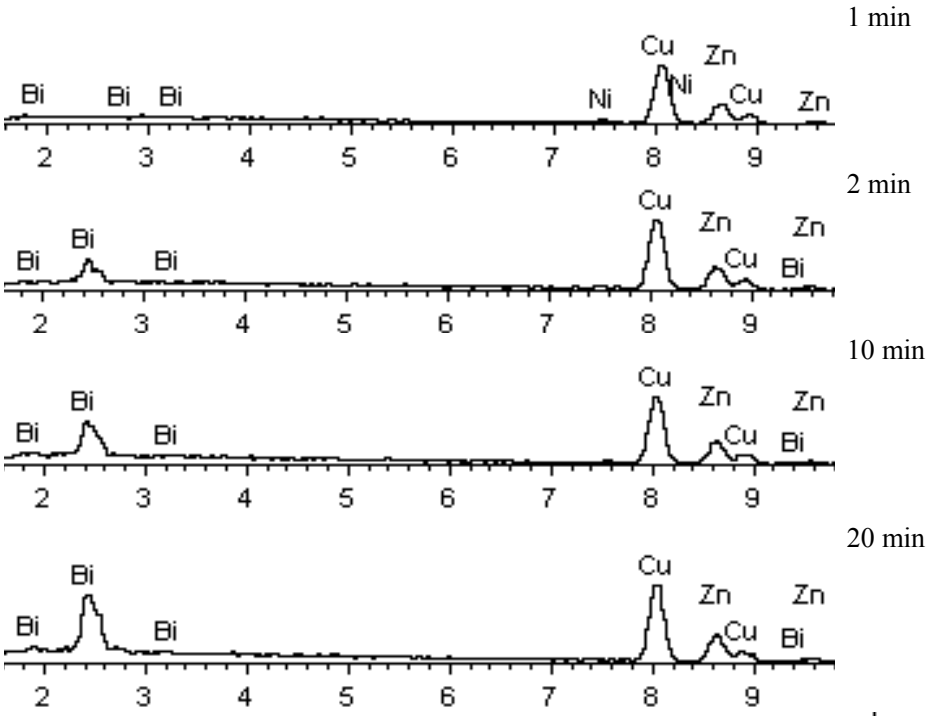

Figure 4.6 EDX spectra of samples plated in ENP solution of $[Bi^{3+}]=10^{-3}$ mol/L for different times: a) 1 min, b) 5 min, c) 10 min, d) 20 min (i.e., starting to count from the moment when the brass substrate is touched by Ni wire)

Using the theoretical model developed before (Yin, 2004) to simulate the effects of the stabilizer concentration (C_s) on the deposition rates of nickel (R_{Ni}) and the phosphorus (R_P) were attempted. This model assumes that the electrical double layer developed on the surface of substrate in the plating solution governs the transport of different species involved. According to this model the participation of stabilizer atoms like Bi onto the surface lattice of Ni will cause lifting of its Fermi level and then impair the oxidation of hypophosphite in anodic reaction. This model is represented by the following two equations:

$$R_{Ni} = R_{Ni}^0 \sqrt{\frac{E_f^0 + 4\pi\, pa\left(C_S - C_S^c\right)}{E_f^0}} \exp\left[\left(64\pi\, pa - \frac{4\pi\, pak_G}{kT}\right)\left(C_S - C_S^c\right)\right] \qquad (4.1)$$

$$R_P = R_P^0 \exp\left[-\frac{4\pi\, pak_G}{kT}\left(C_S - C_S^c\right)\right] \qquad (4.2)$$

where p is the dipole moment, a is a constant, E_f^0 is the Fermi energy level without the stabilizer, k_G is the $H_2PO_2^-$ adsorption constant, k is the Boltzmann constant, R_{Ni}^0 is the nickel deposition rate without stabilizer, R_P^0 is the phosphorus deposition rate without stabilizer, C_S is the stabilizer concentration and C_S^c the critical stabilizer concentration.

If the term $4\pi\, pa\left(C_S - C_S^c\right) << E_f^0$, Equation (1) is then simplified to:

$$R_{Ni} = R_{Ni}^0 \exp\left[\left(64\pi\, pa - \frac{4\pi\, pak_G}{kT}\right)\left(C_S - C_S^c\right)\right] \qquad (4.3)$$

Then we can simplify Eqs (2) and (3) as:

$$R_{Ni} = K_1 \exp\left(K_2 (C_S - C_S^c)\right) \tag{4.4a}$$

$$R_P = L_1 \exp\left(L_2 (C_S - C_S^c)\right) \tag{4.5a}$$

In Equation 4.4a and 4.5a, there are four physical terms, K_1, K_2, L_1 and L_2, whose values are to be determined. This is realized through simulation of these two theoretical models by using the experimental data as shown in Figure 4.7. Substitution of the parameters obtained from simulation into Equation 4.4a and 4.5a, the nickel deposition rate, R_{Ni}, and the phosphorus deposition rate, R_P, in mg/cm^2hr, are established as follows:

$$R_{Ni} = 11.679 \exp\left(-10837 (C_S - C_S^c)\right) \tag{4.5b}$$

$$R_P = 1.6449 \exp\left(-7060.9 (C_S - C_S^c)\right) \tag{4.5b}$$

From the above theoretical models, how the Bi^{3+}-complex ion exerts its effect on the deposition rates of Ni and P is now quantified.

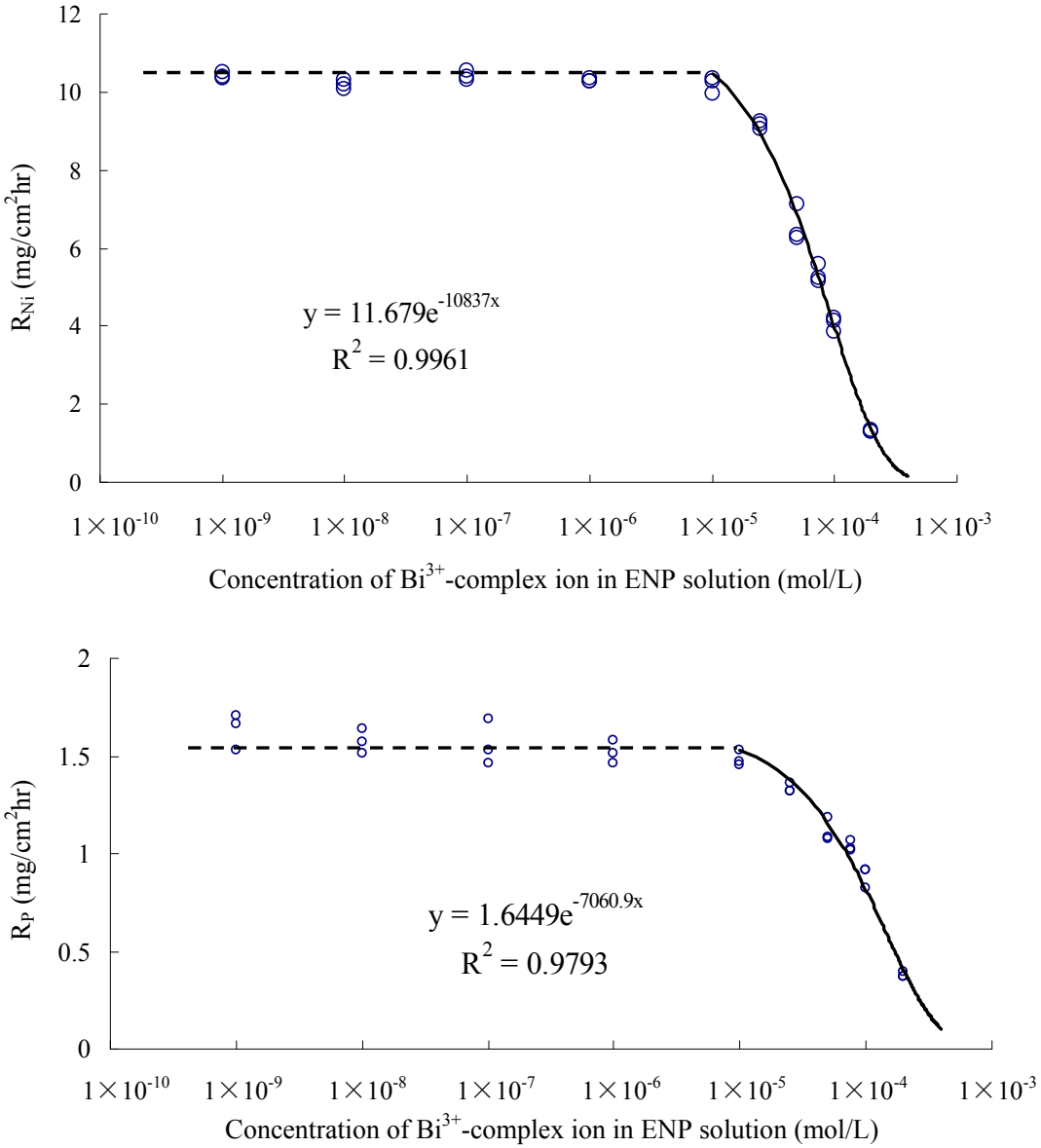

Figure 4.7 Influence of the Bi^{3+}-complex ion concentration on the deposition rate of a) nickel and b) phosphorus

4.3.2 The critical role of metal colloidal particles generated in ENP solution

There is always a trace amount of Ni atom clusters detaching from the plating frontier and entering into the bulk solution during the ENP process. These colloidal

particles are deactivated due to the chemical displacement of Bi^{3+} on their surface. To verify the presence of metal colloidal particles, a number of drops of solution were collected from a plating bath containing Bi^{3+}-complex ions of 10^{-5} M after plating of 1h, and the liquid sample was dried gradually on a copper grid, colloidal particles were observed on the copper grid by TEM (Figure 4.8). The EDX analysis showed that these colloidal particles are enriched with nickel and bismuth in contract to the background. In the mean time, no such tiny particles were spotted if the fresh solution was sampled.

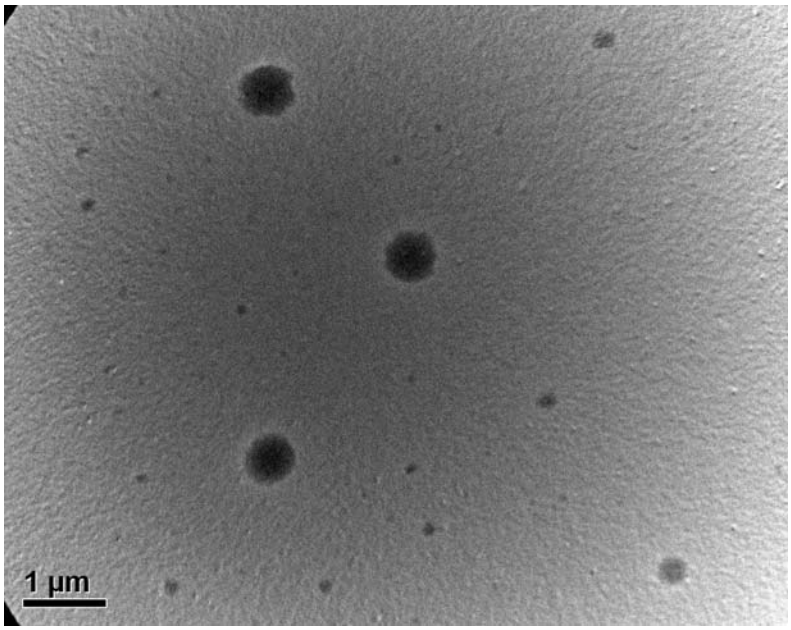

Figure 4.8 TEM photograph of colloidal particles collected from plating bath with addition of 10^{-5} mol/L Bi^{3+}-EDTADSS after a 1 hr plating process

Palladium titration is another method to test the stabilizing capacity of an ENP bath (section 4.2.4). Metal nuclei were generated instantaneously when the $PdCl_2$ solution was dropped into the bath, but the bath still remained clear until an adequate volume of $PdCl_2$ solution (V_d) was introduced, at that moment a black cloud was observed

suddenly. Unlike Ni^{2+} ion, Pd^{2+} ion could be reduced by hypophosphite ion at around 40 ^{o}C. On the Pd particles generated a quick Ni deposition would take place and initiate overwhelming metal powder deposition. Before the moment when the bath decomposition was triggered out, the metal colloidal particles (Ni/Pd) were turned passive due to the occupation of Bi species on surface sites of these miniature particles.

It is interesting to note that V_d undergoes almost negligible increase with the increasing concentration of stabilizers in the concentration range below $C_{Bi\text{-}C}$ and a steep increase when their concentration exceeds this critical point (Figure 4.9).

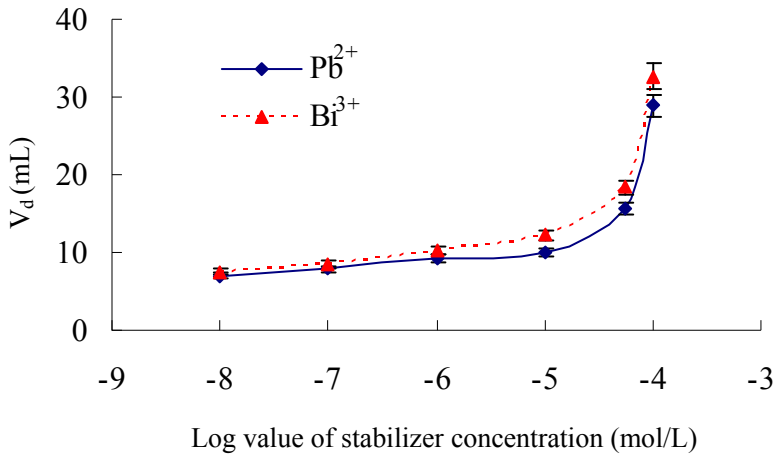

Figure 4.9 Dependence of decomposition volume (V_d) on concentration of added stabilizers

The appearance of such a plateau followed by a hill profile implies that deactivation of metal colloidal particles only requires a substantially low concentration of stabilizer (e.g., 10^{-8} M), in other words, a metal particle become passive when a small number of its surface sites is occupied due to the lift of its Fermi level (Yin,

2004). The additional stabilizer increases only the surface coverage of existing particles (corresponding to magnitude of V_d), and the turning point in between (10^{-5} and 10^{-4} M) marks reach of saturation coverage. After this margin extra amount of stabilizer will be needed to tackle the newly generated metal particles. This test also reveals that Bi^{3+}-complex ion has slightly better stabilizing effect than Pb^{2+} ion.

4.3.3 The effect of stabilizer concentration on the performance of ENP bath

It is imperative to understand how the composition of nickel plating layer is affected by the variation of Bi^{3+}-complex ion concentration. Table 4.1 concludes EDX measurement data of Ni-content and P-content in weight percentage of the plating layers obtained from different plating bath conditions. The Ni/P atomic ratio in the plating layer maintained approximately 3.5 regardless of which kind of EDTA-derived ligand was used to form Bi^{3+}-complex ion.

Table 4.1 Composition of Ni-P alloy deposit layer based on EDX analysis

Concentration of Bi^{3+} ion (mol/L)	EDTADSS		EDTA-OH		EGTADSS	
	Ni wt.%	P wt.%	Ni wt.%	P wt.%	Ni wt.%	P wt.%
0	86.81	13.69	86.81	13.69	86.81	13.69
10^{-9}	86.02	13.98	87.13	12.87	86.23	13.77
10^{-8}	86.65	13.35	86.97	13.03	86.24	13.76
10^{-7}	85.94	14.06	87.79	12.21	87.19	12.81
10^{-6}	86.70	13.30	87.24	12.76	87.53	12.47
10^{-5}	87.04	12.96	87.11	12.89	87.69	12.31

To examine the long-term stabilizing effect of Bi^{3+}-complex ions in ENP bath, a 4-MTO continuous plating process (as stated in Section 3.2.4) was carried out. None of plating-out in the plating bath after 4-MTO was observed despite a very slight

dropping of plating rate for every Bi^{3+}-complex ion (Figure 4.10). Although insignificant discrepancy in the plating rates caused by ligand type was found, there were still perceptible differences in the rates of 4th-MTO.

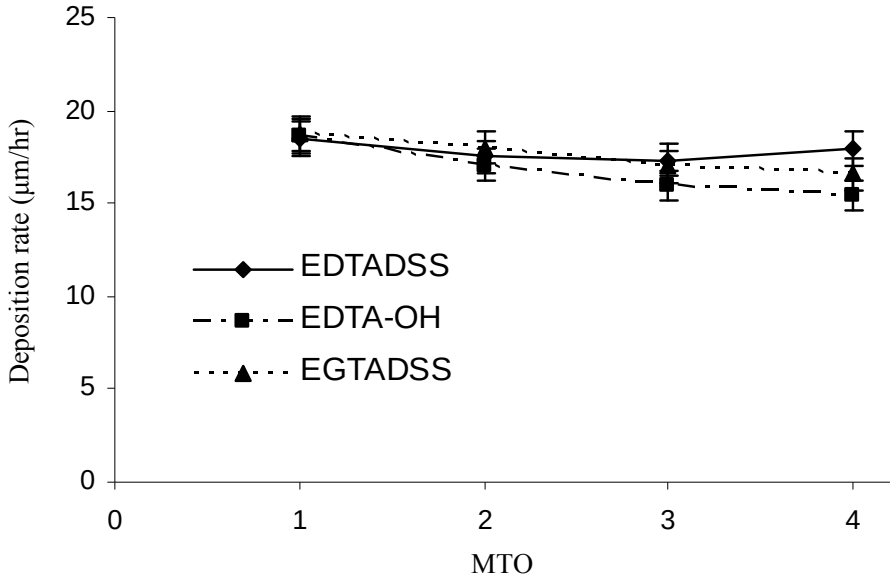

Figure 4.10 Effect of MTO on nickel deposition rate with using Bi^{3+}-complex ions as the stabilizer

Judging from the tabulated data in Table 4.2, the three Bi^{3+}-complexes essentially did not lead to any noticeable difference in Ni and P contents throughout the four MTOs, where the P-content in the Ni/P plating layer in all samples was above 10 wt.%. This is regarded as the high phosphorus EN deposit that is generally considered to possess good corrosion resistance (Luke, 1986; Carbajal, 1988).

Table 4.2 Change of the Ni and P contents in the plating layer with MTO

Round of MTO	EDTADSS		EDTA-OH		EGTADSS	
	Ni wt.%	P wt.%	Ni wt.%	P wt.%	Ni wt.%	P wt.%
1	88.94	11.06	89.46	10.54	88.56	11.44
2	88.88	11.12	89.07	10.93	88.37	11.63
3	88.14	11.86	89.24	10.76	88.16	11.84
4	87.96	12.04	89.24	10.76	88.45	11.55

Concentration of Bi^{3+}-complex ions: 2×10^{-6} mol/L

To verify this feature, the potentiodynamic scanning (PDS) technique (Section 3.2.5 of Chapter 3) was used to study the chemical corrosion resistance of the plating layers obtained from different MTOs (Figure 4.11). It turns out that the corrosion potential (E_{corr}) was shifted to negative direction with the increase in cycle of MTO. Generally the anodic polarization curves observed can be divided into two regions (use M-1 curve as an example): The first region is at potentials between E_{corr} and approximately -0.1 V (wrt. Ag/AgCl), where the dissolution of Ni-P deposit is kinetically limited. The anodic current density increases slowly with potential moving positive. The second region is at potentials above -0.1 V, where the transpassive dissolution of Ni/P alloys begins and the anodic current density increases quickly with potential moving toward positive direction (Lo, 1994; Ashassi-Sorkhabi, 2004).

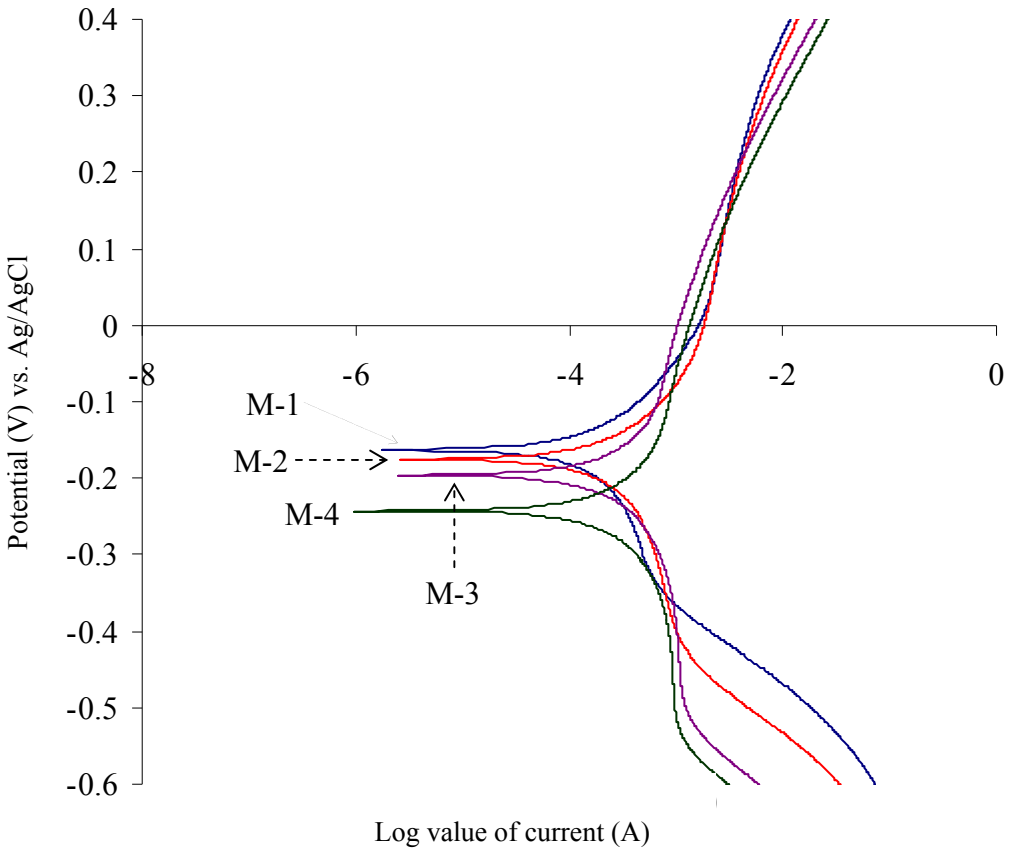

Figure 4.11 PDS curves of Ni-P coatings with Bi^{3+}-EGTADSS complex as stabilizer in different rounds of MTO

The overall results of the three ENP baths showed that the anodic (corrosion) current densities increased with the extension of operation time regardless of which kind of ligand was employed to form complex ion stabilizer (Figure 4.12). As noted previously that the MTO does not bring about significant changes in the Ni/P ratio of plating layer, surface morphology would likely be another factor reducing the corrosion resistance, as it has been elaborated in Section 3.3.2 of Chapter 3.

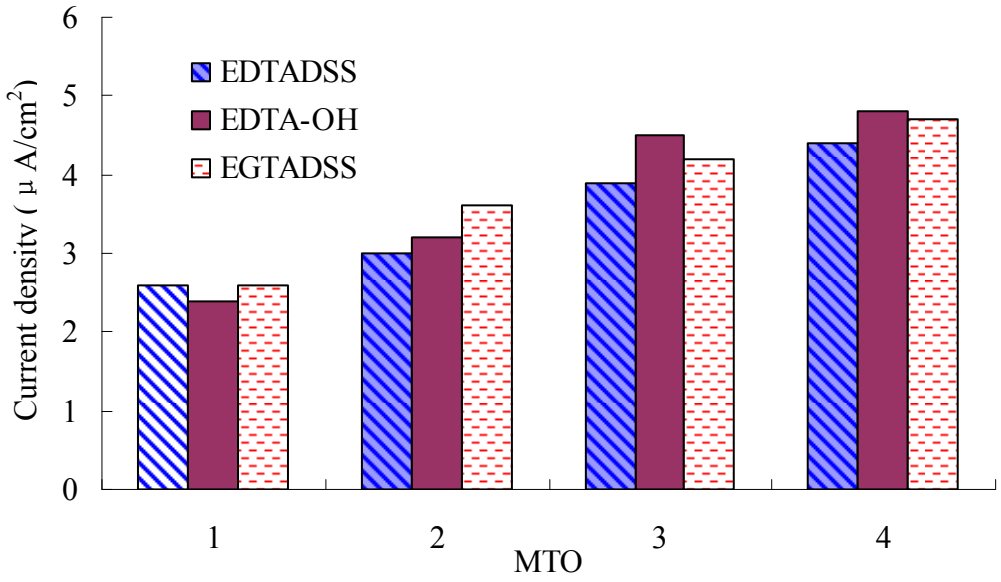

Figure 4.12 Corrosion current density vs MTO for three bismuth complexes

The plating layers generated from the bath using Bi^{3+}-(EDTA-OH) complex ion as stabilizer are chosen as demo samples (Figure 4.13). The first MTO cycle produced the smoothest and cleanest surface among the four samples. It thus gave rise to the smallest corrosion current density. Nevertheless, the plating layers generated from later MTO cycles showed more heavier co-deposition of insoluble tiny particles on their surfaces, which is deemed to increase susceptibility to galvanic corrosion.

Compare Figure 4.12 with Figure 3.12, it is clear that Ni-P deposits, obtained from the ENP bath carrying Bi^{3+}-complex ion stabilizers, display better corrosion resistance than those where sulfur-containing amino acids were employed as stabilizer, such superiority being especially true for the 4^{th} MTO. It is, therefore, suggested that the adsorbed sulfur species is more reactive than bismuth in promoting electron transfer between the acidic liquid medium and the Ni-P deposit,

resulting in a poorer corrosion resistance. In other words, protons in corrosive medium find it easier to gain electrons from sulfur-Ni sites than from Ni sites.

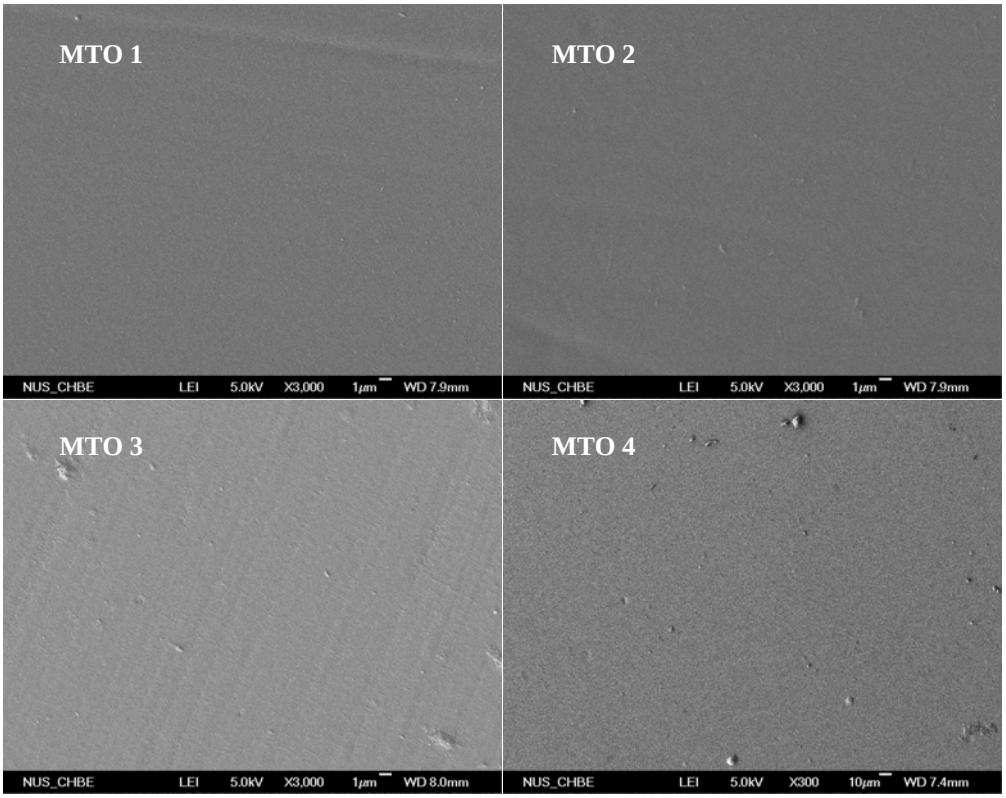

Figure 4.13 Surface morphology of the 4 MTO samples by using Bi^{3+}-(EDTA-OH) complex as the stabilizer

4.4 Conclusions

This work investigated a lead-free ENP bath in which three Bi^{3+}-complexes were tested respectively as the bath stabilizer. Three EDTA derivatives – EDTADSS, EDTA-OH and EGTADSS – were found to be able to form soluble complexes with Bi^{3+} ion in the acidic EN solutions. The relation of nickel deposition rate with the stabilizer concentration was investigated; all the three types of Bi^{3+}-complex ions

displayed a dramatically decrease of deposition rate at the critical concentration near 10^{-5} M. Below this critical concentration, bismuth does not show significant effect on the nickel deposition rate and the composition of plating layer.

Furthermore, the anodic reaction of hypophosphite on a Ni-P electrode in the presence of one of the stabilizers was tested via measuring the anodic current density. The current density – concentration plots resulted from this test are similar to the deposition rate – concentration plots. According to the potentiometry test and EDX and XPS analysis, Bi^{3+}-complex ions undertake chemical displacement reaction with Ni(0) atoms, in which Bi(0) atoms are produced and passivate the anodic reaction of hypophosphite ion. Consequently, both nickel and phosphorus deposition rates are reduced due to short of electrons. A modified kinetic model was established through successful simulation of the experimental curves of deposition rate-stabilizer concentration relation.

The last part of this work investigated the durability of the Bi^{3+}-complex ion in stabilizing a 4-MTO continuous ENP process. As a key parameter, the electrochemical corrosion resistance of the resulting plating layers was measured. The result showed that the corrosion resistance only decreases moderately with extension of plating time due to primarily co-deposition of tiny particles. Furthermore, compared with samples obtained from ENP solution using sulfur-containing amino acids as the stabilizer the samples based on using Bi^{3+}-complex ion stabilizer exhibit better corrosion resistance.

Chapter 5 Exploring the Phosphine Ligands as Stabilizer for the ENP System

Phosphine (R_3P) is well known to be a type of coordination ligand having tunable affinity with nickel atom. Hence, in this chapter the question of whether phosphine could also act as a plating stabilizer in the electroless nickel plating (ENP) system was investigated. Three types of phosphine compounds, triphenyl phosphine (TPP), bis(diphenylphosphino)methane (BDPPM), and triphenylphosphine-3,3',3"-trisulfonic acid trisodium salt (TPPTS), were employed to carry out the study. Of them the hydrophobic TPP and BDPPM were converted to become partially hydrophilic through forming complexes with lactic acid molecules in advance. Hence the partners formed were marginally soluble in ENP solution and the resulting concentrations suited the requirement of a stabilizer; while TPPTS is highly water soluble. This study has identified that the phosphine compounds work to prevent ENP process from decomposing in the bulk of solution through suppressing the rapid reduction of Ni^{2+} ions on those highly reactive surface sites, and noticeably none of them exhibits a concentration threshold for a sharp ceasing of plating. Being the stabilizer of cathodic type, the phosphine compounds, especially TPPTS, give rise to a gradually increase in phosphorus-content (P-content) in the Ni-P plating layer with the increase of their concentrations. In addition, this work has also investigated the corrosion resistance of the as-plated and the annealed Ni-P plating layers by electrochemical impedance spectroscopy (EIS) and depth profile analysis. Finally the bath stabilizing capabilities of the three phosphine compounds were evaluated respectively using the metal-turn-over (MTO) test.

5.1 Introduction

In Chapter 3 and Chapter 4, the roles of sulfur-containing amino acids and Bi^{3+}-complex ions as the stabilizers in ENP solutions have been discussed in detail respectively. These two kinds of stabilizers are anodic type that is generally deemed to impede the oxidation of hypophosphite during plating. In this chapter, the three phosphine ligands were examined at great length and demonstrated to be a unique type of stabilizer that controls the ENP process in a different way from the above two types.

As mentioned previously, to date, a number of non-lead chemicals, such as thiourea (Han, 1997; Lin, 2002) and cupric sulfate (Chen, 2006), have been proposed to be in place of Pb^{2+} as the stabilizer in ENP bath. But the presence of sulfur (from thiourea) or copper (from cupric sulfate) in the Ni-P plating layer will be likely to undermine the corrosion resistance of ENP deposits (Das, 1996; Armyanov, 1999; Petukhov, 1999; Cheong, 2004; Tarozaite, 2006; Touir, 2006).

According to ASTM 733B-04 standard, a Ni-P deposition layer can be classified as low P (1-4 wt.%), medium P (5-9 wt.%) or high P (10 wt.% and above) type according to its P-content (Cui, 2006). When the P-content exceeds approximately 7-8%, the resulting Ni-P deposition layer has an amorphous matrix, which is desirable to most of industrial applications since it possesses sound corrosion resistance, low friction coefficients and suitable refined surface (Mai, 1988; Lambert, 1989; Martyak, 1994; Kumar, 1996; Baskaran, 2006; Krolikowski, 2006). In order to achieve a high-P deposition layer, there is always a trade-off between deposition

rate and phosphorus content. The basic strategy is to suppress the cathodic reaction rate ($Ni^{2+} \rightarrow Ni^{0}$) via employing stronger coordination ligands of Ni^{2+} ion to formulate ENP solutions (Mallory, 1998; Cheng, 2008). Since the ENP bath stabilizers used in industry are primarily anodic type, the P-content in EN deposits is not significantly affected by the change of stabilizers in terms of type and dose. The present work explored the possibility of using phosphine compounds, represented by the generic formula (R_3P), to stabilize ENP system. Phosphine has been prevalently used in many homogeneous catalytic reactions as ligand to form coordination complex catalysts with transition metal atoms or ions, and among them Ni^{0}-phosphine complex is an important type of organometallic catalyst (Baird, 1995; Miedaner, 1997; Norris, 1999; Tamao, 2002). The fact that phosphine does not form complex with Ni^{2+} ion is an important property allowing it to function as a bath stabilizer, e.g., only a substantially low dose of phosphine in ENP bath is adequate for maintaining normal operation of ENP system. The phosphine stabilizers also reveal the unique characteristic of inhabiting the cathodic reaction but rather the anodic reaction, which has been identified in this work through the anodic current measurement and adsorption of phosphine species on active Ni(0) sites. It is because of this cathodic stabilizing role, increasing the concentration of phosphine stabilizers in an ENP bath could help raise P-content in the plating layer.

It was also confirmed that the properties of EN deposit, such as deposition rate and surface morphology, were insignificantly affected by the extension of bath service life to 4 MTOs. Similarly as other kinds of stabiliers, a slight reduction in the corrosion resistance of the Ni-P deposition layer was also found with the extension of operation time. However, the difference in corrosion resistance of samples from

different MTO was not significant. In light of this, a further interest was to learn whether the use of phosphine stabilizers can result in a particular metallurgical structure so that the as-deposited Ni-P plating layer can be further annealed to promote its corrosion resistance. This attempt has indeed been proven; the heat-treatment at 500 ^{o}C for 1 hour largely improved the corrosion resistance of Ni-P deposition layer. A detail investigation has been conducted to understand the root-cause.

5.2 Experimental

5.2.1 Materials

Triphenyl phosphine (TPP) and bis(diphenylphosphino)methane (BDPPM) were purchased from Fluka and triphenylphosphine-3,3',3"-trisulfonic acid trisodium salt (TPPTS) from Aldrich. Other chemicals, brass substrate and DI water were the same as those described in Section 3.2.1 of Chapter 3.

5.2.2 Determination of characteristics of ENP process and deposit

The main components of ENP solution were remained the same as those listed in Table 3.1 of Chapter 3. In addition, the details of methods, used to determine the relations of plating rate and stabilizer concentration, to measure the oxidation rates of hypophosphite at plating surface in the presence of different phosphine ligands

and to assess the ENP bath stabilities, have been described in Sections 3.2.2-3.2.4 of Chapter 3, except the type of stabilizers.

5.2.3 Heat treatment of as-deposited Ni-P layer

The heat treatment of the as-deposited electroless Ni-P plated brass specimens was carried out in a furnace (Carbolite, CWF1300, England) at a constant heating rate of 10 ^{o}C/min from ambient temperature to 500 ^{o}C. After calcining at 500 ^{o}C for 1 hr, the specimens were gradually cooled down to the room temperature within 5 hr. The whole annealing process was conducted in the nitrogen atmosphere to prevent deep oxidation in the plating layer.

5.2.4 Evaluation of corrosion resistance

The corrosion resistance of Ni-P layer was assessed by electrochemical impedance spectroscopy (EIS). The measurement was conducted in the three-electrode electrochemical system, the same setup as that was used to measure the anodic oxidation rate (Section 3.2.3). To minimize the influence of the ENP film thickness on the electrochemical measurement, all the samples were controlled to have a thickness close to 8 μm. For EIS measurement, an AC voltage in a sine wave form with amplitude of 10 mV was used as imposing signal, and the measurement frequency was varied in the range from 100,000 to 0.01 Hz. Before the EIS test, each specimen was immersed in the testing solution for 30 min to reach a stable open-circuit potential (OCP). The testing solution was a aqueous NaCl solution (3.5 wt.%).

5.2.5 In situ adsorption of the three phosphines on fresh nickel powders

Four aqueous solutions (20 mL of each): 0.05M $NiSO_4$, 0.05M $NiSO_4$ + 0.025M TPPTS, 0.05M $NiSO_4$ + 10^{-5} M TPP and 0.05M $NiSO_4$ + 10^{-5} M BDPPM were prepared, and an excess of sodium boron hydride ($NaBH_4$, 0.1g) was added to each of the solutions under vigorous stirring. The same treatment was taken as described in Section 3.2.6 of Chapter 3, before the resultant powders obtained were investigated by XPS (XPS, Kratos Axis HiS System) to examine whether there were chemically adsorbed phosphine species on the nickel metal particles. The binding energies of XPS peaks were calibrated using the carbon 1s peak that was corrected to 284.6 eV. The curve fitting was carried out by XPS PEAK (version 4.1).

5.2.6 Other instrumental analyses

The EDX analysis and SEM (or FESEM) (Section 3.2.7 of Chapter 3) were employed to examine the compositions and the surface morphologies of EN deposits, respectively. To minimize the influence of nonhomogeneous P distribution in the Ni-P layers, three zones in each specimen were chosen at random for EDX analysis. The structure of the as-deposited Ni-P alloys was analyzed with an X-ray diffractometer (XRD; Shimadzu, XRD-6000, Kyoto, Japan) using a Cu Kα X-ray as the radiation source. The scanning was performed through 30-80^o (2θ), with a step size of 0.04^o and counting time of 1 s/step.

5.2.7 Palladium titration

The effectiveness of phosphine on holding back nickel deposition on metal colloidal particles was evaluated using palladium titration method as we used in Section 4.2.4 of Chapter 4.

5.3 Results & Discussion

5.3.1 The state of phophine compounds in ENP aqueous solution

Three phosphine compounds selected as ENP stabilizer in this work could be distinguished by their water-solubility. Triphenylphosphine-3,3′,3″-trisulfonic acid trisodium salt (TPPTS) is highly water-soluble, whereas triphenylphosphine (TPP) and Bis(diphenylphosphino) methane (BDPPM) are strongly hydrophobic and completely insoluble in water. Their molecular structures are shown in Figure 5.1. Clearly, direct dissolving of TPP or BDPPM in the ENP solution is not possible. An appealing method was developed to promote water-solubility of these two phosphines: they are firstly dissolved in highly concentrated lactic acid (LA) up to 10^{-2} mol/L at around 200 ^{o}C with vigorously stirring. The resulting solution remains homogeneous while cooled down to and stable for a substantially long "shelf life" at room temperature. Secondly, no precipitation occurs when either of the these two types of phosphine-lactic acid solutions is introduced into the ENP solution at operation temperature as long as the concentration of phosphine in the plating solution is below 5×10^{-4} mol/L.

Triphenylphosphine-3,3′,3″-trisulfonic acid trisodium salt (TPPTS)

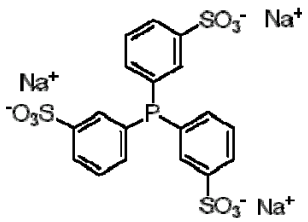

Triphenylphosphine (TPP)

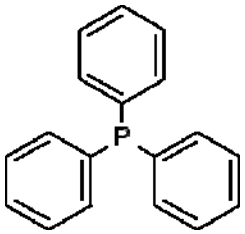

Bis(diphenylphosphino) methane (BDPPM)

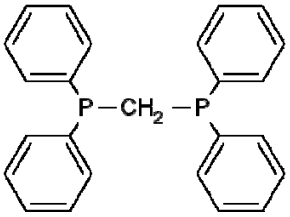

Figure 5.1 Molecular structures of the three phosphines.

To prove the existence of strong association between lactic acid molecules with TPP molecules, a sample made by mixing the TPP-LA solution (~0.1ml) with KBr powder was subject to evaporation in an oven for enough time to remove the majority of free LA and then analyzed by infra-red spectroscopy. A parallel sample using pure LA was designed to check the evaporation extent of free LA. The IR spectrum of the former sample showed similar intensity of characteristic absorption peaks of LA and TPP, whereas the spectrum intensity of LA became rather weak in the latter sample.

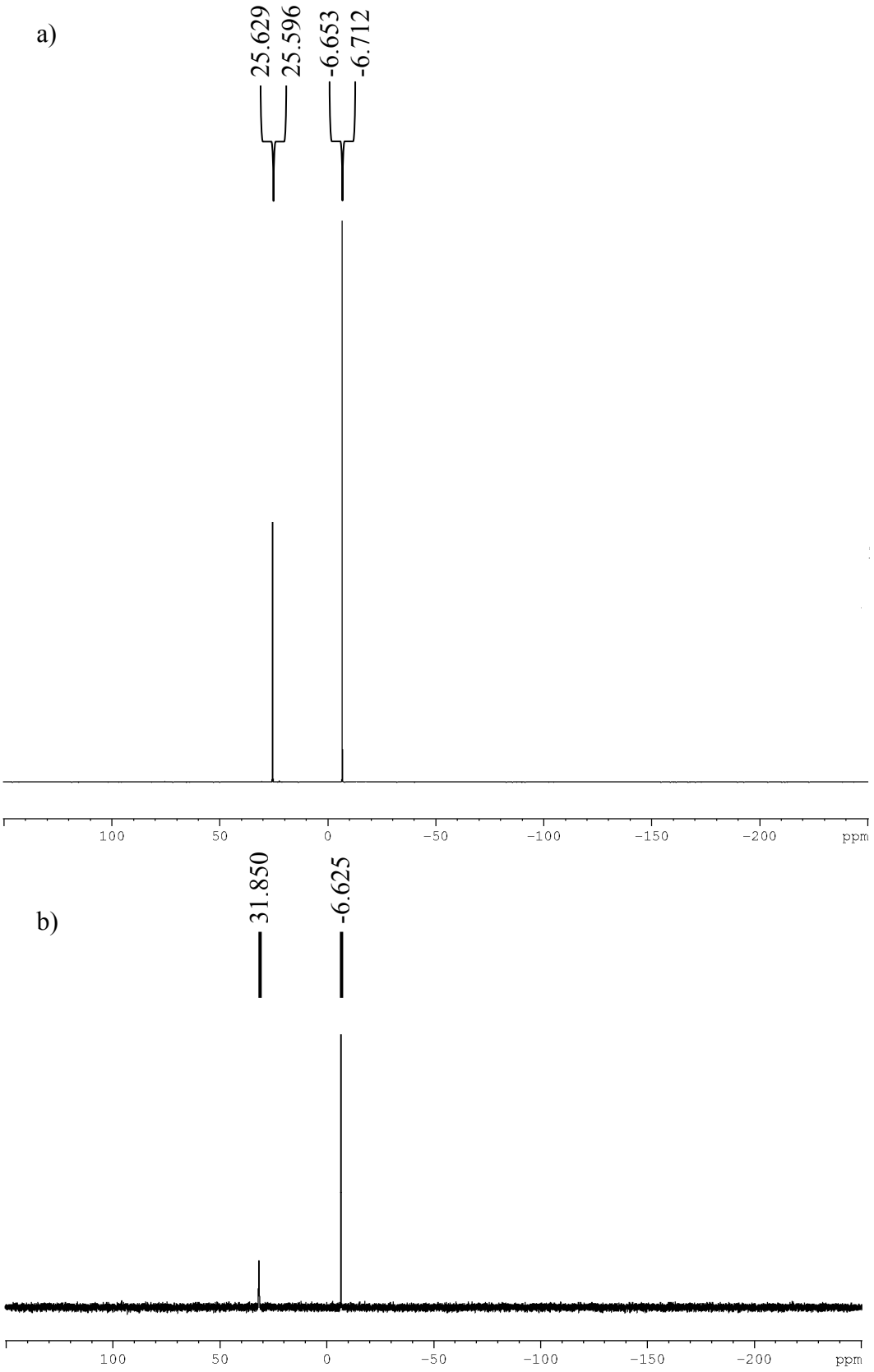

Figure 5.2 P31 NMR spectra of (a) 10 mg TPP in 5 ml DMSO-d_6 and (b) 5×10^{-5} mol/L TPP-LA complex in 5 ml DMSO-d_6

Besides IR characterization, ^{31}P-NMR spectra of the pristine TPP and LA-TPP were also examined on the basis of the following assumption. There is a strong interaction between at least a lactic acid molecule and a TPP molecule, in which phosphorus atom of TPP is the nucleophilic moiety that interacts with lactic acid molecules. Hence this interaction must cause a variation of chemical shift of ^{31}P isotope.

Figure 5.2 shows the ^{31}P-NMR spectra of the two samples. The relative change of the chemical shift of TPP from 25.6 to 31.8 ppm (moving to down field) indicates that the electron density on phosphorus atom of TPP becomes lower due to the complexation of TPP with lactic acid.

Although detail structure of the TPP-LA associate is still unclear, it is presumed to have a surfactant-like structure with the hydrophilic LA moieties and the hydrophobic TPP moiety, namely, there is a strong association between each TPP molecule and a few LA molecules and this association permits TPP to be dissolved in aqueous medium. Similar association should also occur between BDPPM and LA molecules. An important note is that either TPP or BDPPM cannot be dissolved directly in an ENP solution even though the solution contains a high concentration of LA. As aforementioned, these two phosphine compounds could be dissolved only in highly concentrated or pure LA solution, and the phosphine-LA associate becomes stable once it is formed when dissolved in water. As to TPPTS, it has an intrinsically amphiphilic molecular structure and is thus highly soluble in water. In conclusion, the three phosphine compounds possess different extents of surface activity in the ENP solution.

5.3.2 A study on how the phosphines influence the ENP deposition rate

Unlike the known ENP stabilizer systems (Han, 1997; Yin, 2004; Chen, 2006), the curves of ENP deposition rate *vs.* the concentration of phosphines (Figure 5.3) don't show a dramatically decreasing of plating rate at the so-called critical concentration that is usually observed when the other types of stabilizers, such as Pb^{2+} ion, sulfur-containing amino acids and Bi^{3+}-complex ions are used (Section 3.3.1 in Chapter 3 and Section 4.3.1 in Chapter 4). The deposition rate displayed a stagnant response to the concentration variation of phosphines in the range from 10^{-9} to 10^{-4} mol/L. A continuous increase in the concentration of TPP or BDPPM to 10^{-3} mol/L caused appearing of a thin emulsion due to agglomeration of their associates with LA, and tiny particles were generated. Figure 5.4 displays a particle-embedded plating surface. Alternatively, regarding the highly water-soluble TPPTS, it gave rise to only a slight decrease in deposition rate at the concentration of 10^{-3} mol/L.

It is noteworthy that the deposition rates displayed by the three curves (in Figure 5.3) are slower than the instance (about 15μm/hr) when no stabilizer was employed in the same plating solution. This is abnormal as compared with the sulfur-containing stabilizers (Section 3.3.1 in Chapter 3) that promote nickel deposition rate before the critical concentration, although both R_2S and R_3P compounds are considered to be Lewis base. Such a rate-suppression phenomenon implies that the phosphines work in a different way to decelerate the ENP rate. Also from Figure 5.3, it can be seen that among the two hydrophobic phosphine compounds, TPP exhibits a slightly stronger rate-suppression effect than BDPPM. This may be attributed to the bulky

structure of BDPPM, which results in a bigger size of BDPPM-LA associate. It is thus cannot behave as efficiently as TPP-LA associate to shield the cathodic reaction.

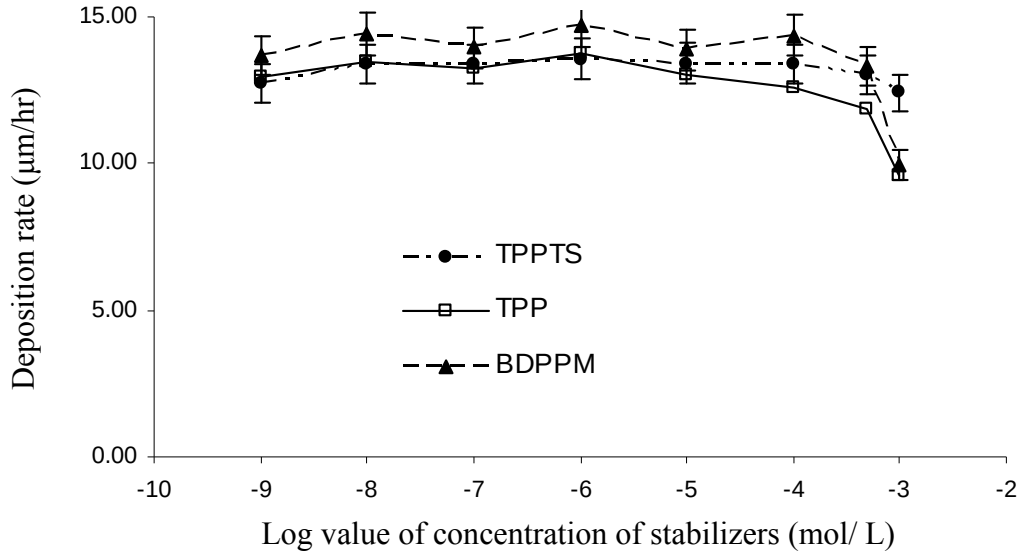

Figure 5.3 Influence of concentration of phosphines on Ni-P deposition rate

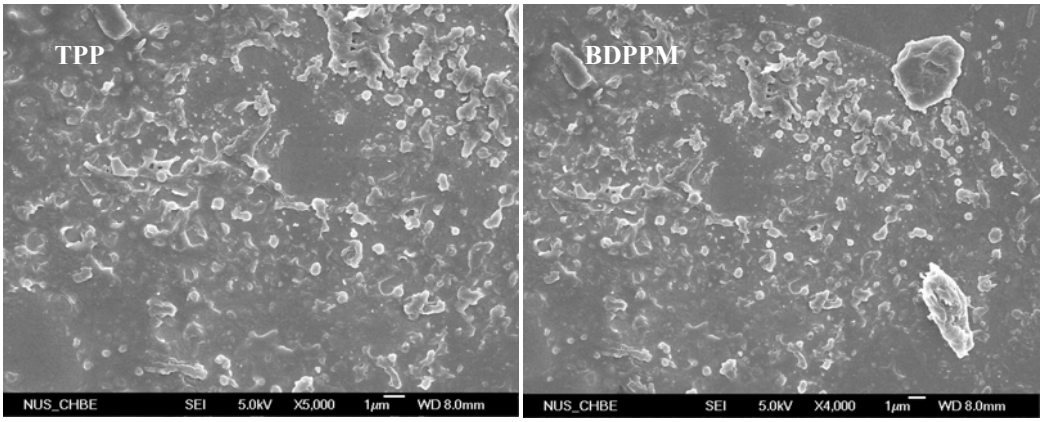

Figure 5.4 The co-deposition of TPP or BDPPM insoluble particles on the plating surface at high concentraton (10^{-3} mol/L)

Normally the role of a stabilizer in the ENP system has been regarded as inhibition of the anodic process, since this can tighten up the electron stream when the cathodic reactions run away (Han, 1996 & 1997; Sotskaya[a,b], 2003).

$$H_2PO_2^- + H_2O \rightarrow H_2PO_3^- + 2H^+ + 2e^-$$

$$Ni^{2+} + 2e^- \rightarrow Ni^0 \quad \text{and} \quad H_2PO_2^- + e^- + 2H^+ \rightarrow P + 2H_2O \qquad (6.1)$$

On the basis of this perspective, an anodic potentiodynamic scanning measurement was carried out as described in Section 3.2.3 of Chapter 3, from which the anodic current density of the working electrode (i.e. a Ni-P layer on the brass substrate) was obtained (Figure 5.5). In this test the peak height of current density reflected the oxidation rate of hypophosphite ion on the working electrode. With respect to a particular phosphine compound used, the anodic current density values were plotted versus the corresponding concentrations of this phosphine. It is worthy of the observation that the current density values (~2.7-2.8 mA/cm^2) especially in the low concentration range (<10^{-7} mol/L) is greater than what could be obtained (~2.4-2.5 mA/cm^2) when the other stabilizers, such as Pb^{2+} or thiourea, are used. This is opposite to their rate-suppression behavior as seen in Figure 5.3. Hence with employing the phosphine as stabilizer, a direct correlation between the anodic oxidation rate of hypophosphite and the ENP deposition rate becomes no longer valid because this type of stabilizer does not impair the anodic reaction. The role of phosphine molecules in the ENP solution is, consequently, postulated to affect the cathodic process.

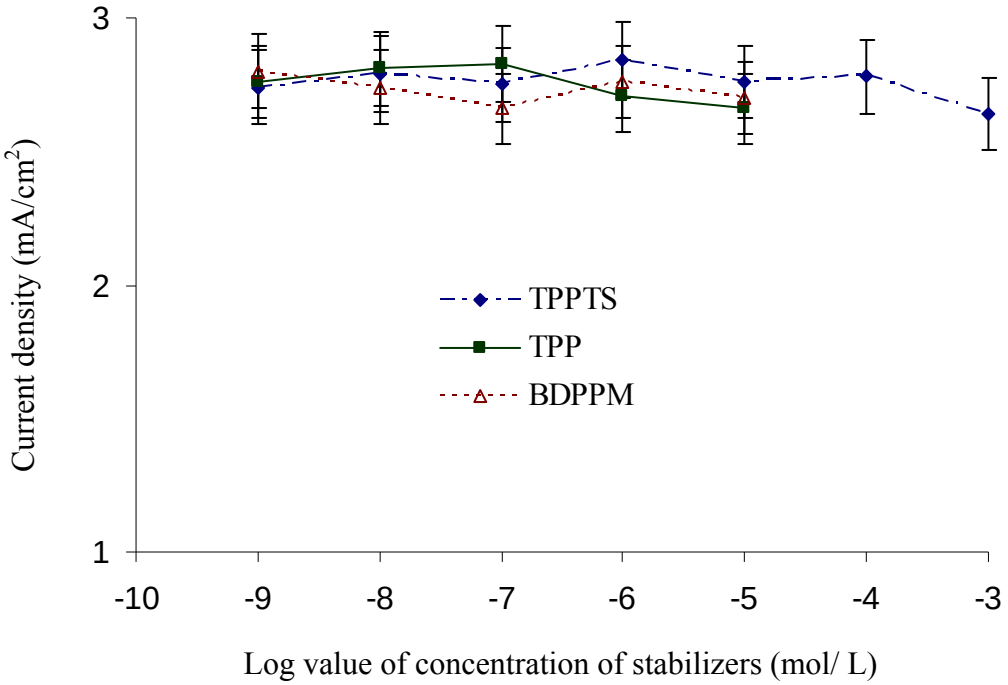

Figure 5.5 Peak values of anodic current density vs. the corresponding concentrations of phosphines. (For TPP and BDPPM the tested concentration is up to 10^{-5} mol/L, because neither of them can be completely dissolved under the experiment conditions above this concentration).

Yet, since the phosphine type of ligands is known to form complexes preferentially with Ni^0 but rather with Ni^{2+} ion, it is unlikely that the phosphine molecules intervene with the cathodic reaction through the formation of coordination complexes with nickel ions in the plating solution so as to lower the availability of Ni^{2+} ions. Our UV-vis spectroscopy experiment indeed showed no evidences for the complexation of phosphine ligand with Ni^{2+} ion. It has been identified in the above section that the three phosphine molecules are surface active in the ENP solution. They are thought of forming an adsorption layer at the surface of plating substrate, as illustrated in Figure 5.6, due to the hydrophobic driving force. Namely, the adsorbed TPP (or BDPPM)-LA species should adopt an opposite orientation to those

of the adsorbed TPPTS at the plating surface. In addition, from the results of plating rate and anodic current density it could be inferred that such an adsorption layer would block the access of hydrated Ni^{2+} ions to the plating surface, or in other words they function primarily as a cathodic stabilizer.

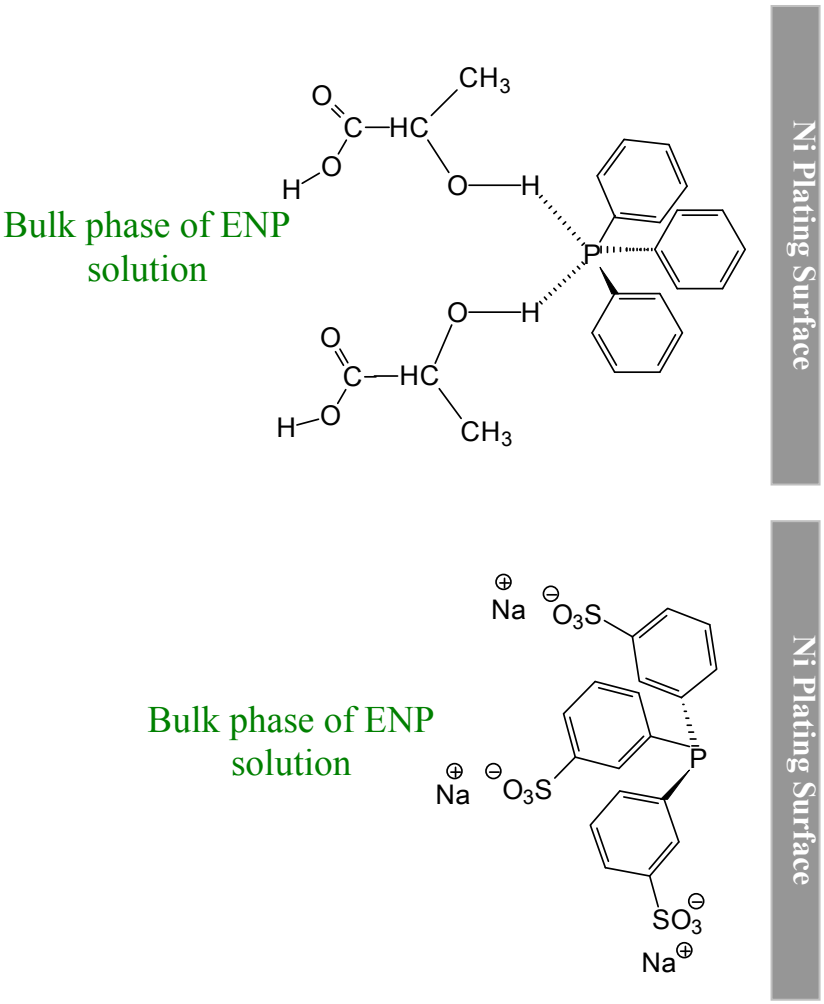

Figure 5.6 Schematic presentation of adsorption of TPP and TPPTS on the Ni plating surface

In regard to the coordination environments of nickel atoms on a plating surface, there would always be a small number of active surface Ni sites, which have highly unsaturated coordination environments, as compared with the majority of surface Ni atoms. However, the active surface Ni sites are plenty on colloidal particles that are generated in any an ENP bath and are considered as the initiating sites of a large extent of deposition of nickel blacks (Yin, 2004). It is therefore necessary to assess the adsorption capability of the three phosphine compounds on these active Ni sites. A model system, similar to the one used in Section 3.3.1 of Chapter 3, was then adopted to undertake the investigation, in which the adsorbent was very fine nickel particles and one of the three phosphines was present while the Ni particles were generated by chemical reduction (Section 5.2.7). In principle, fine particles possess a large specific surface area and a plenty number of active Ni sites. In-situ adsorption of the phosphine molecules to the Ni particles would, therefore, take place if they could access the active sites properly. Meanwhile, a clean Ni powder was employed as reference adsorbent in this examination. The powders generated in this model system were examined respectively by XPS after proper cleaning. Although the P(2p) peaks in the three samples added with phosphine stabilizers are quite weak, they still prove the existence of phosphorus species on the in-site generated Ni particles by compared with the pure nickel sample. Furthermore, the Ni-TPPTS sample displays stronger P(2p) peak than other two phosphine-involved samples (Figure 5.7). The right adsorptive state of TPPTS as indicated in Figure 5.6 could account for this outcome since this adsorptive state favors coordination of the phosphine to the active nickel sites.

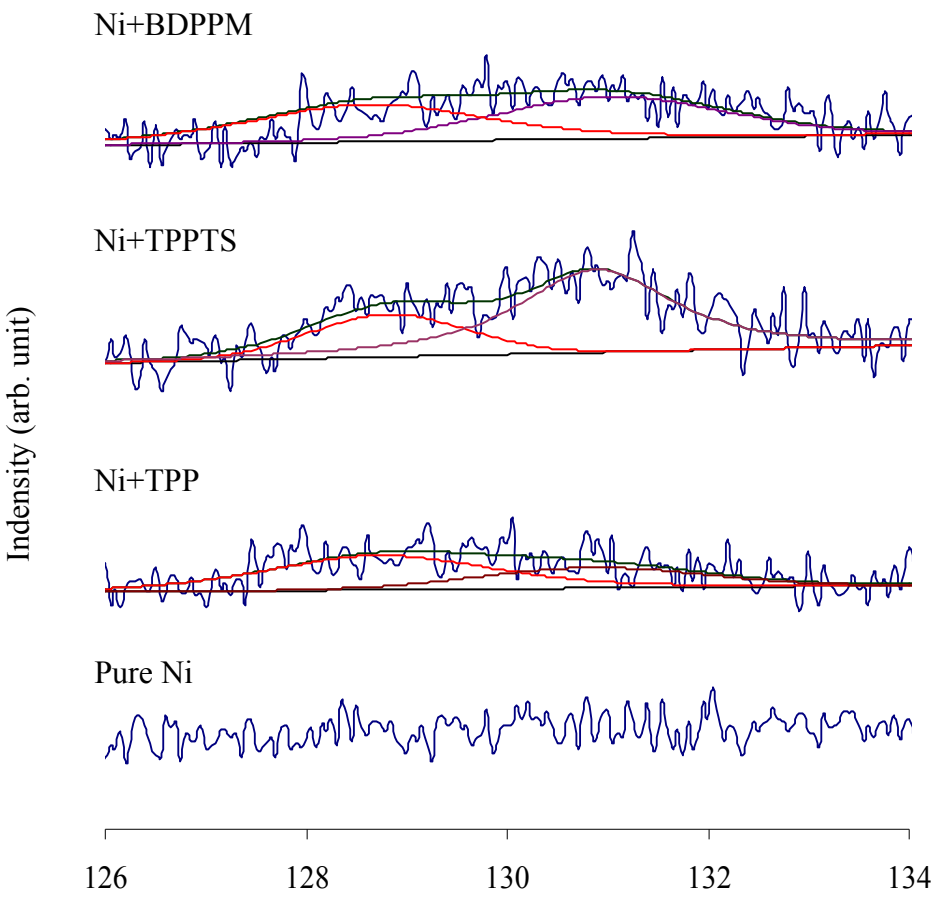

Figure 5.7 XPS spectra of ether with curve fitting

It is then important to understand whether there is a relation between the adsorption capability of phosphines on Ni colloidal particles and their action on restraining the propagation of metal colloidal particles in the ENP solution. With this aim, the palladium titration method, as described in Section 4.3.2 of Chapter 4, was employed in this work as well. This method probes the buffering capacity of an ENP bath through a continuous increase of the concentration of metal nuclei by deliberately introducing $PdCl_2$ into the bath until decomposition takes place. Unlike Ni^{2+} ion, Pd^{2+} ion could be reduced by hypophosphie ion at around 40^{o}C. The Pd particles generated in-situ act as an excellent catalyst to trigger a quick Ni deposition, which will eventually become rampant with the increase in number of particles.

Nevertheless, Ni deposition will not go further anymore if the Pd particles are deactivated upon generation owing to the adsorption of phosphine molecules on them. As such, the $PdCl_2$ solution consumed until the moment when the black cloud generated in the EN solution is taken as a measure of the tolerance of ENP solution to the increasing of Pd particles in it. The volume of $PdCl_2$ solution added is defined as the decomposition volume V_d. The decomposition volume V_d vs. the concentration of respective stabilizers was plotted (Figure 5.8). Same as what we did in Chapter 3, lead nitrate was used as the benchmark to the three phosphines examined in this test.

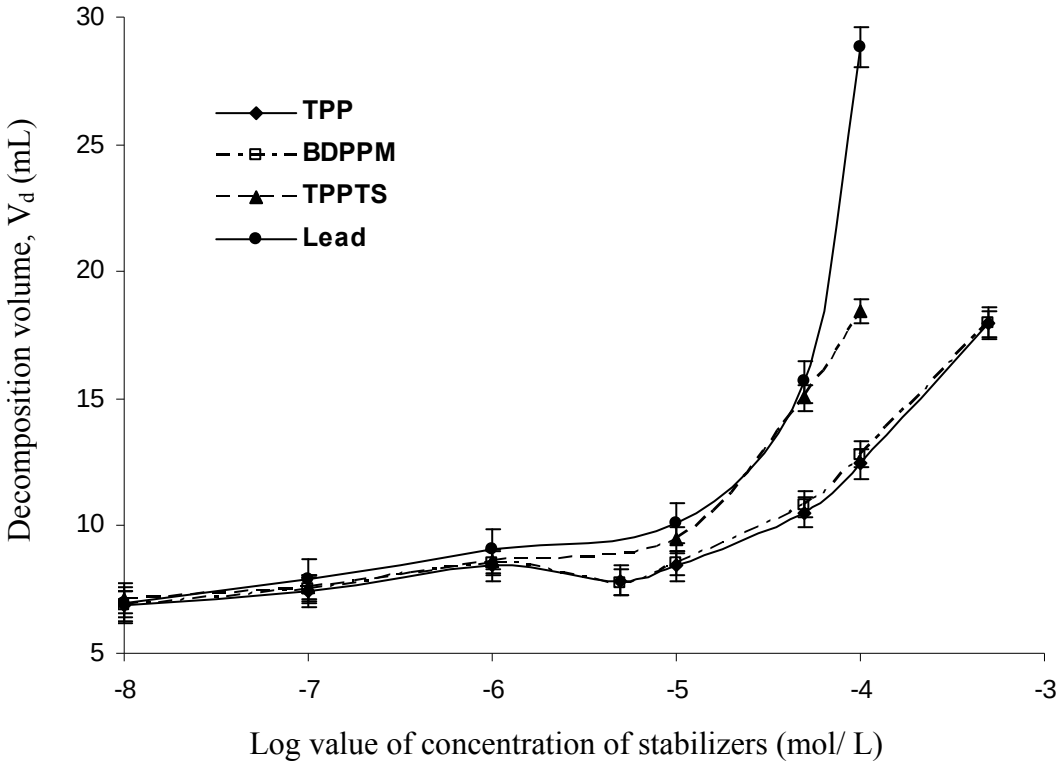

Figure 5.8 Dependence of decomposition volume on added concentration of stabilizers

For the ENP solution without a stabilizer, its V_d is 6.36±0.50 ml, while for the other solutions containing a stabilizer, V_d values are all above this baseline at the lowest stabilizer concentration level (i.e. log[stabilizer]=-8) and climb up with the increase in stabilizer concentration. The V_d~log[Pb^{2+}] curve displays a clear upward turning when log[Pb^{2+}]>-5, which is in fact the critical concentration of Pb^{2+} stabilizer, meaning that a concentration above this value will bring about a significant increase in solution stability but a dramatic decrease in nickel deposition rate. Therefore a fast increase in V_d is incurred as observed. The V_d~log[TPPTS] curve displays a profile slightly below the V_d~log[Pb^{2+}] curve in the range log[TPPTS]<-4.7. But beyond this margin, Pb^{2+} manifests a much stronger idling power than TPPTS due to its unique stabilizing mechanism (Yin, 2004). Also according to the V_d~log relation, of the three phosphine compounds studied, TPPTS shows obviously stronger ENP bath stabilizing power than the other two. This fact is supported by the above XPS results, in which both TPP and BDPPM present only rather weak adsorption capability. Besides this, the other two inferences could be drawn from Figure 5.8 are: firstly, the three phosphine compounds present no substantial difference in stabilizing capability than Pb^{2+} ion in the concentration range below 10^{-6} M, which is stabilizer concentration level normally selected in an industrial ENP system; and secondly, TPP and BDPPM show nearly the same stabilizing capability throughout the entire concentration range investigated because their adsorptive states share the same orientation.

5.3.3 How will phosphines improve corrosion resistance of Ni-P deposit?

Whether the phosphine stabilizers could more effectively boost the P-content in ENP deposition layer than the other types of stabilizers is a meaningful question to investigate, because the P-content of Ni-P alloy strongly affects the corrosion-proof performance of the ENP deposition layer. The usual way to achieve a high P-content deposition layer is to suppress the cathodic reaction, namely to enhance coordination stability of Ni^{2+} complex ions by means of increasing concentration of ligands or using ligands that have greater K_s values with Ni^{2+} ion (Cui, 2005; Wu, 2005).

In light of the present system, there are two mechanisms contributing to the increase in the P-content in the ENP deposition layer when TPP or BDPPM is employed, which are the repression of cathodic reaction that occurs in the stabilizer concentration range below 10^{-5}M; and the attachment of tiny LA–phosphine aggregations on the plating surface in the higher concentration range, i.e., 10^{-5}–10^{-4} M in Table 5.1. Unlike these two phosphines, the highly water-soluble TPPTS pushes up the P-content in the concentration range of 10^{-5}–10^{-4} M, purely through suppression of the cathodic reaction of ENP. Now with respect to the effect of stabilizer on P-content, the P-content in the deposit based on using Pb^{2+} ion as stabilizer, on the whole, was lower than those using a phosphine ligand stabilizer according to the parallel experimental results.

Furthermore, our experiments showed that the plating rate was dramatically decreased if $[Pb^{2+}] \geq 10^{-5}$ M and the P-content in EN deposits decreased with increasing concentration of Pb^{2+} ion. The same phenomenon was also reported by

Yin (2004). This is because Pb^{2+} ion is a typical anodic stabilizer, when lead atoms enter in the Ni-P lattice they reduce the work function of the plating frontier, and thus clogging up the oxidation of hypophosphite. Consequent, both Ni plating rate and P-content in the deposit are reduced (Yin, 2004). Nevertheless, the phosphine compounds belong to the cathodic stabilizer that promotes P-content with an increase in the concentration of itself by suppressing the cathodic nickel reduction.

Table 5.1 Ni & P Contents in the Ni-P Deposits

Concentration of phosphine (mol/L)	TPPTS		TPP		BDPPM	
	Ni wt.%	P wt.%	Ni wt.%	P wt.%	Ni wt.%	P wt.%
10^{-9}	87.62	12.38	87.79	12.21	87.66	12.34
10^{-8}	86.25	13.75	86.72	13.28	86.39	13.61
10^{-7}	86.01	13.99	85.66	14.34	85.89	14.11
10^{-6}	85.79	14.21	85.32	14.68	85.60	14.40
10^{-5}	85.54	14.46	85.01	14.91	85.05	14.95
10^{-4}	84.84	15.16	84.68	15.32	84.60	15.40
10^{-3}	84.66	15.34				

The electrochemical impedance spectroscopy (EIS) was employed to examine the corrosion resistance of ENP deposition layer. Plating samples produced from the TPPTS-containing ENP solutions were selected as demo type to carry out this test. Here arc-shape Nyquist plots (Figure 5.9) other than tafel plots were used for investigation; because, through simulation, Nyquist plots could provide the information (equivalent circuit) about the anti-corrosion structure for deposits. These arcs differ in their amplitude as well as the span over the frequency range scanned.

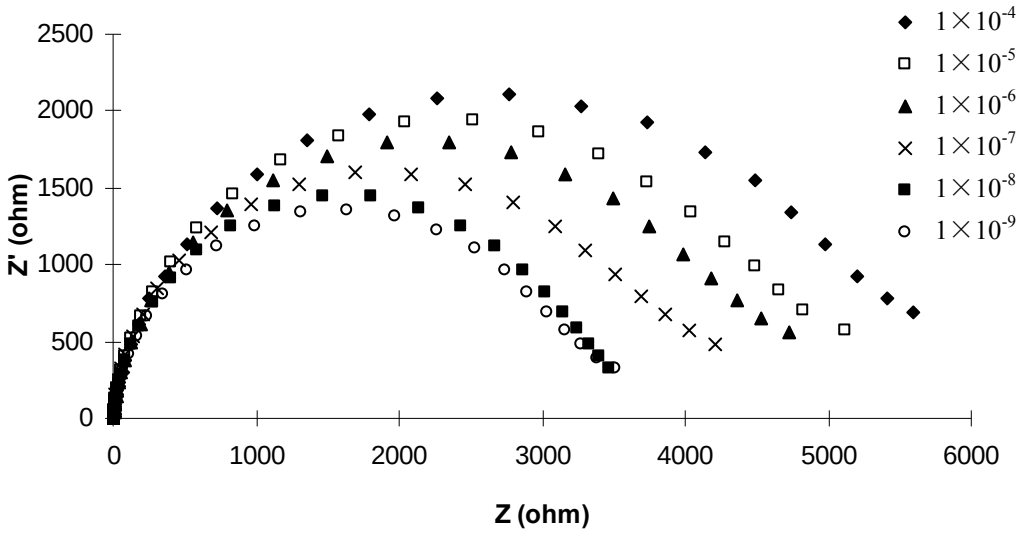

Figure 5.9 Nyquist plots obtained for as-plated EN deposits plated from ENP bath using TPPTS as the stabilizer in 3.5% NaCl solution

These Nyquist plots were fitted by the equivalent circuit as illustrated in Figure 5.10 to simulate the metal/solution interface where the constant phase element (CPE) resembles a capacitor but the phase angle is not 90^{o}. CPE describes inhomogeneous distribution of solid/liquid interface. The fitting results are shown in Table 5.2, in which parameter *n* evaluates CPE. With the approaching of *n* value to unity, the capacitor component in CPE increases. It is noteworthy that accompanying the increase of P-content in the deposition layer (Table 5.2) the Rc values increase but the values of CPE decrease. This trend reflects the improvement on corrosion resistance of the deposition layer. The result is in agreement with the study of other groups (Rajam, 1990; Lo, 1994; Cui, 2006).

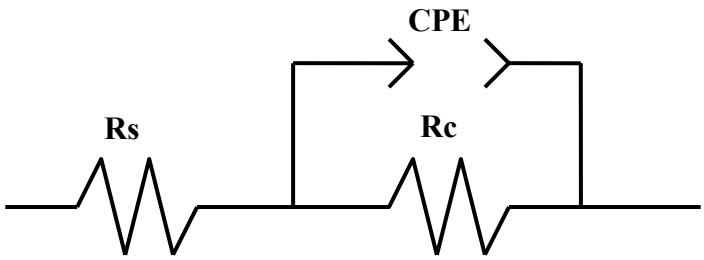

Rs: Resistance of the Solution
Rc: Corrosion Resistance of the Coating
CPE: Constant Phase Element

Figure 5.10 Equivalent circuit for EIS measurements on corrosion resistance of as-deposited Ni-P deposits plated from ENP bath using TPPTS as the stabilizer

Table 5.2 Fitted results of Nyquist plots for EN deposits on equivalent circuit described in Figure 5.10

Phosphine Conc./M	10^{-9}	10^{-8}	10^{-7}	10^{-6}	10^{-5}	10^{-4}
Rs/Ω	1.377	1.568	1.574	2.617	1.413	1.408
Rc/Ω	3772	3894	4341	4669	4983	5575
CPE/F	1.420e-4	1.313e-4	1.210e-4	1.187e-4	0.8658e-4	0.6638e-4
n	0.9197	0.9107	0.9179	0.9208	0.8871	0.8980

5.3.4 How will the use of phosphine stabilizer affect the heat treatment effect?

It is well known that annealing of an ENP deposition layer causes significant changes in properties and structure. In general, the hardness and wear resistance of the thermally treated layer can be boosted drastically (Wing, 1997; Keong, 2003).

But reports about leverage of annealing on the corrosion resistance of ENP deposition layer are controversy. Schenzel (1990), Singh (1995) and Ashassi-Sorkhabi (2004) reported that the corrosion resistance of the annealed EN deposits was increased. Yet, it is the usual viewpoint that heat treatment undermines corrosion resistance of the plating layer (Duncan, 1983; Singh, 2006). For this, we are inclined to believe that whether or not the corrosion resistance is improved is related to the plating history, in particular, the influence of the use of different concentrations or type of stabilizer.

To explore how the use of TPPTS affects this feature, the samples as demonstrated in Section 5.2.3 were subjected to annealing at 500^{o}C for 1 hr. As a result, the amorphous as-plated ENP layer became crystalline due to formation of Ni_xP_y phases (Figure 5.11), and correspondingly the grain-boundary surface morphology was generated (Figure 5.12).

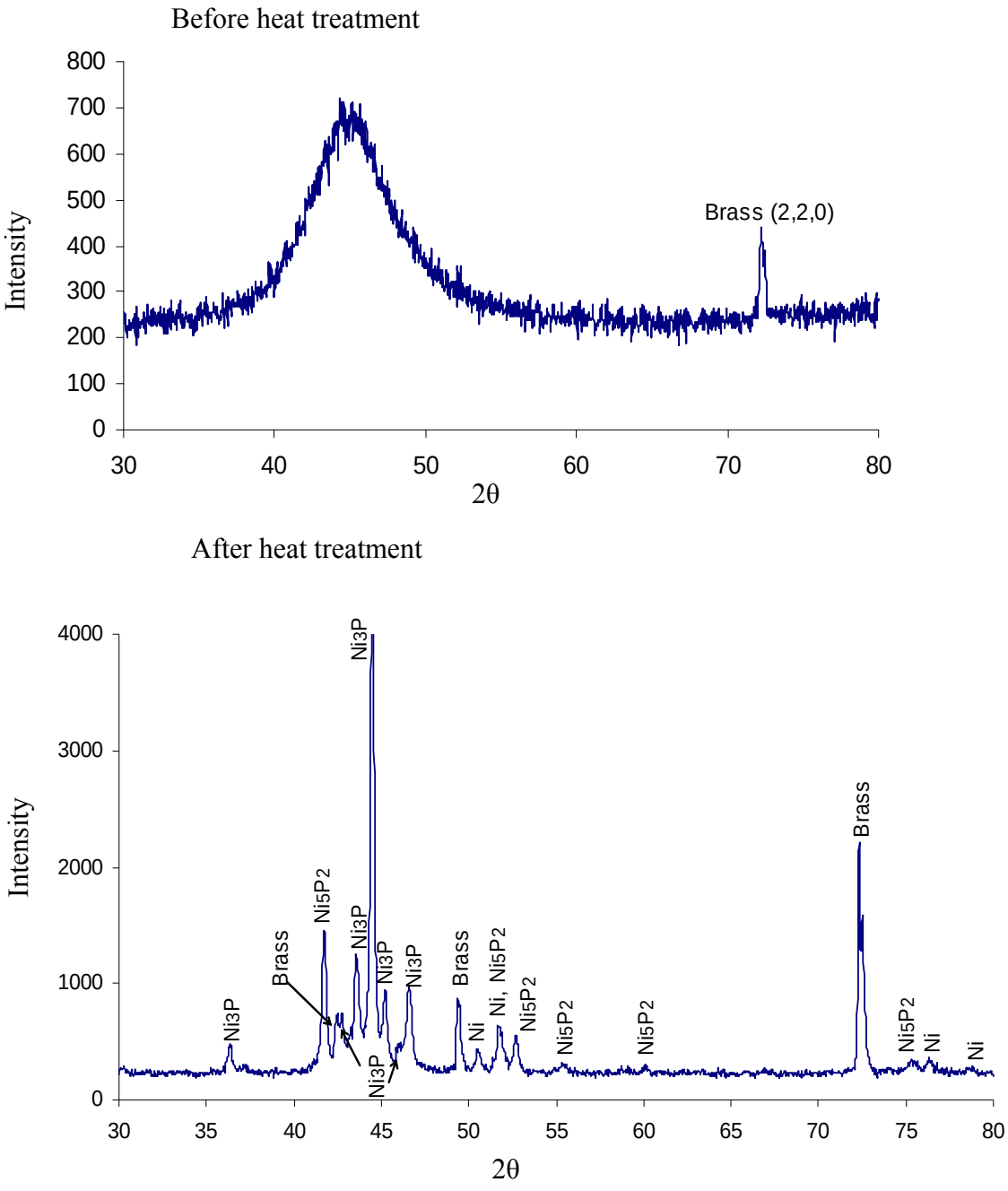

Figure 5.11 X-ray diffraction pattern of ENP deposition player before and after heat treatment

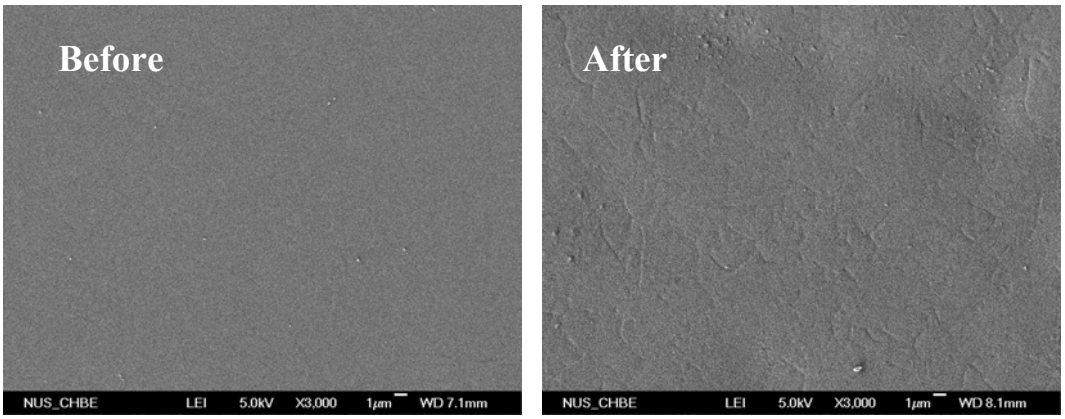

Figure 5.12 Surface morphology of ENP deposit layer generated from the bath containing TPPTS of 10^{-5}M before and after annealing treatment

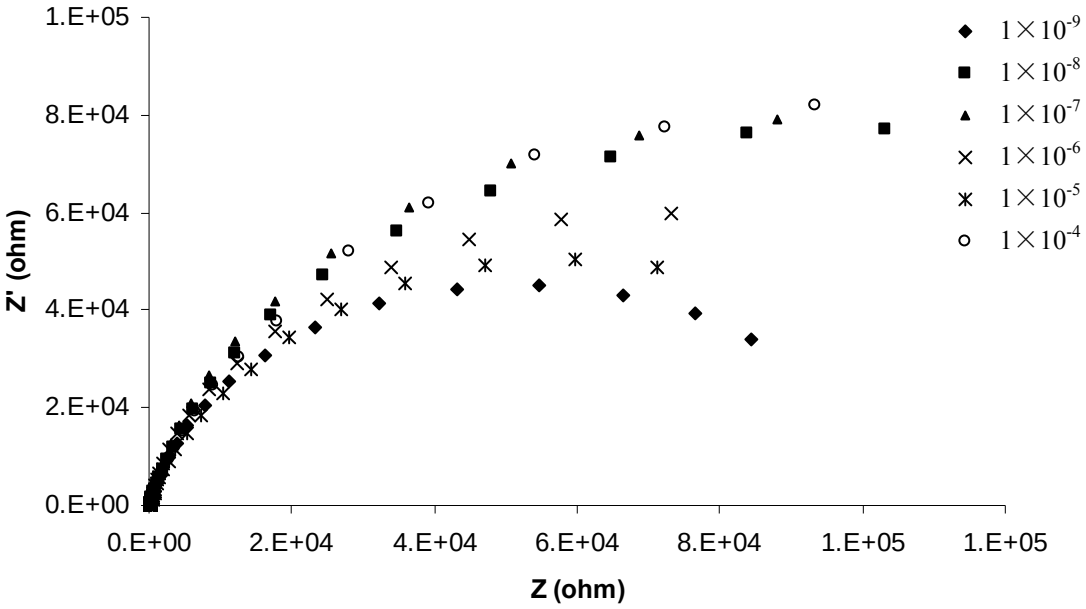

Figure 5.13 Nyquist plots obtained for heat-treated EN deposits in 3.5% NaCl solution

A set of Nyquist plots (Figure 5.13) of the annealed deposition layers was obtained from the same evaluation system as that of Figure 5.9. A rather different equivalent circuit (Figure 5.14) from that describing the as-plated samples was figured out via simulating the Nyquist plots. It contains the two electric components, CPE_1/Rc_1 and CPE_2/Rc_2, which can be viewed as the two interfacial layers. The parameters of fitting are listed in Table 5.3. The corrosion resistance of the outer layer (Rc_1) is negligible compare with that of the inner layer (Rc_2). The corrosion resistance of the EN coatings almost comes from the inner layer. From the Nyquist plots obtained we could see a unique pattern between the P wt% (the second column in Table 5.1) with corrosion resistance (Rc_2) excluding the two samples with both the highest and lowest P wt%, namely a lower P wt% gives rise to a greater Rc_2 after the annealing treatment. Taking the sample prepared from the bath containing 10^{-5} TPPTS for example, one can find that the corrosion resistance is enhanced by more than 20 times.

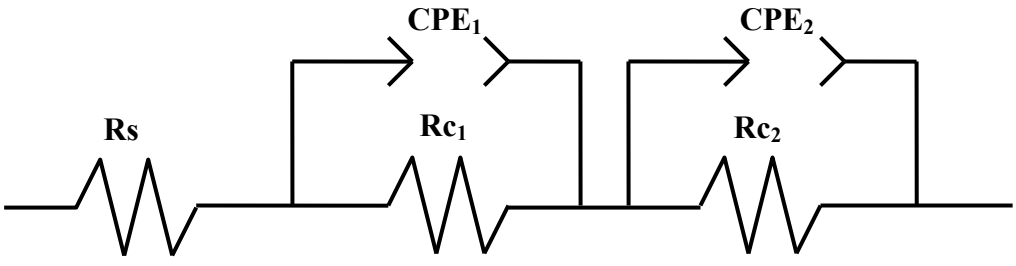

Rs: Resistance of the Solution
Rc: Corrosion Resistance of the Coating
CPE: Constant Phase Element

Figure 5.14 Equivalent circuit for EIS measurements on corrosion resistance of heat-treated Ni-P deposits

Table 5.3 Fitted results of Nyquist plots for EN deposits on equivalent circuit described in Figure 5.14

Phosphine Conc./M	10^{-9}	10^{-8}	10^{-7}	10^{-6}	10^{-5}	10^{-4}
Rs/Ω	1.336	1.644	2.527	0.542	0.598	1.575
Rc_1/Ω	93.8	68.0	58.1	235.9	205.1	72.6
CPE_1/F	0.1723e-5	0.3224e-5	0.4895e-5	0.9704e-6	0.8589e-6	0.2852e-5
n_1	0.7146	0.7503	0.8195	0.7141	0.7405	0.7408
Rc_2/kΩ	110.7	186.1	193.3	139.4	120.5	200.1
CPE_2/F	0.2425e-4	0.2716e-4	0.4012e-4	0.5095e-4	0.3881e-4	0.3636e-4
n_2	0.8753	0.8767	0.8893	0.8958	0.8790	0.8781

To understand this phenomenon, the depth elemental distribution profiles of this sample before and after annealing were analyzed (Figure 5.15). It can be seen that annealing causes diffusion of nickel and phosphorus as well towards the bulk phase of substrate. Such diffusions make the crystallization of Ni and P difficult to undertake because atoms of these two elements are plugged in the lattice of brass, hence the two diffusion Ni-P layers constitute two anti-corrosion protective screens. Two factors are deemed to be critical, the presence of P atoms in the diffusion layer and the thickness of diffusion layer. For the lower P-content deposition layer, the diffusion of Ni-P atoms might be more easily to take place, and hence thicker diffusion layers are generated. In light of the two end P-content cases, e.g., 12.4% and 15.2%, their corrosion resistance is predominated by the P-content in the diffusion layers.

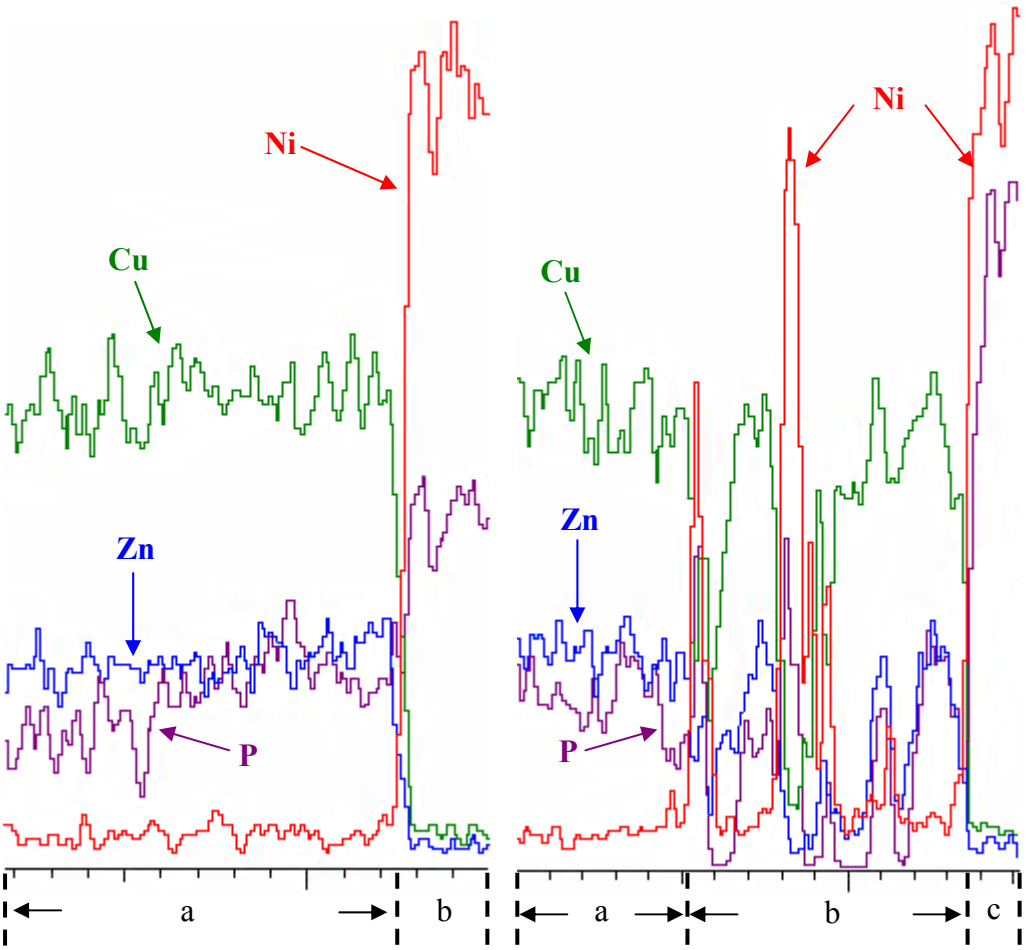

As-deposited EN deposit: a) brass substrate; b) EN deposit

Heat-treated EN deposit: a) brass substrate; b) diffusion layer; c) crystalline layer

Figure 5.15 Element Analysis on the cross section for EN deposits before and after heat treatment

5.3.5 The performance of phosphines in a continuous ENP process

The ENP bath stabilization capabilities of the three phosphine compounds were further examined in a 4-MTO continuous plating process (as stated in Section 2.4). The plating solution that contained regardless of any of the phosphine compounds could remain homogeneous after completing of 4-MTOs despite a very slight falling of plating rate (Figure 5.16). Here Pb^{2+} ion was used as the reference. The moving down of ENP rate with the prolongation of reaction time is due to the accumulation of stabilizer, by-products, buffers etc. in the solution. The P-content in the plating layer could be roughly maintained stable throughout the four MTOs (Table 5.4). On the other hand, the surface morphology generated from the bath using TPP as stabilizer was chosen as the demo samples (Figure 5.17). All of the four samples show a quite smooth surface; expect there some co-deposited particles in the surface of sample from the 4^{th} MTO. Due to the extension of operation time, undesired impurities, such as Ni colloidal particles, insoluble $NiHPO_3$ and the dusts from the air bubbles, inevitably accumulated in the ENP bath. Some of these impurity particles precipitate at the plating surface and then are embedded in the EN deposit, and then deteriorate the deposit quality.

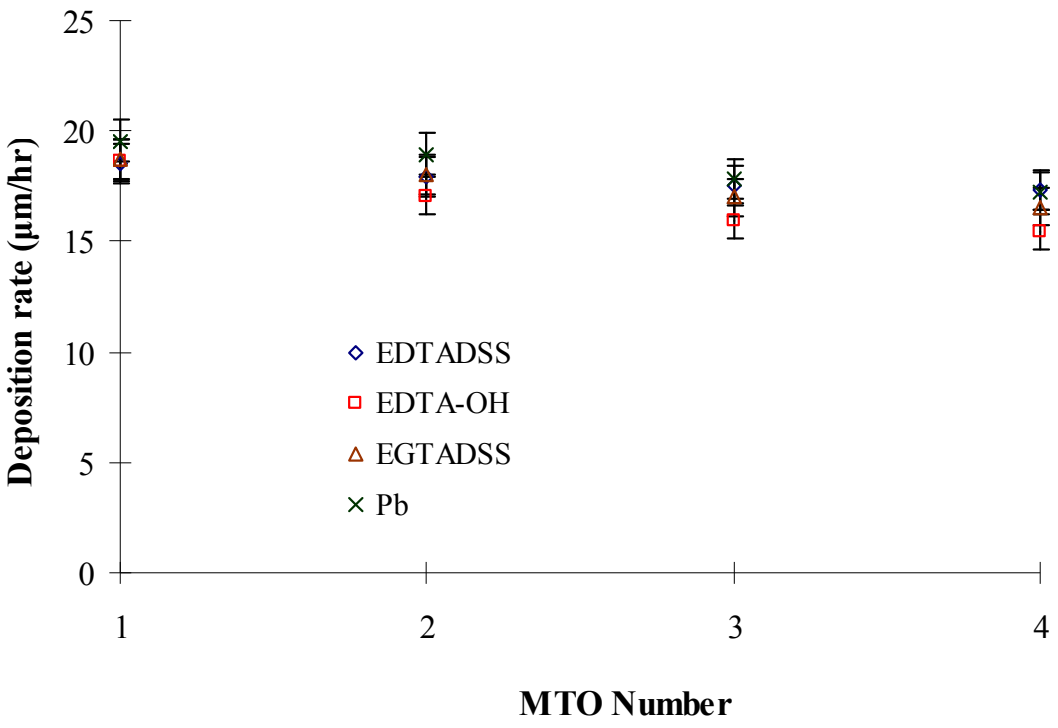

Figure 5.16 Effect of MTO on the deposition rate with using phosphines as the stabilizer

Table 5.4 Ni & P contents in the Ni-P deposits from 4 MTO

MTO	TPPTS		TPP		BDPPM	
	Ni wt.%	P wt.%	Ni wt.%	P wt.%	Ni wt.%	P wt.%
1	87.48	12.52	87.70	12.30	87.78	12.22
2	87.10	12.90	87.96	12.04	87.60	12.40
3	87.31	12.69	88.11	11.89	88.22	11.78
4	87.54	12.46	88.06	11.94	88.49	11.51

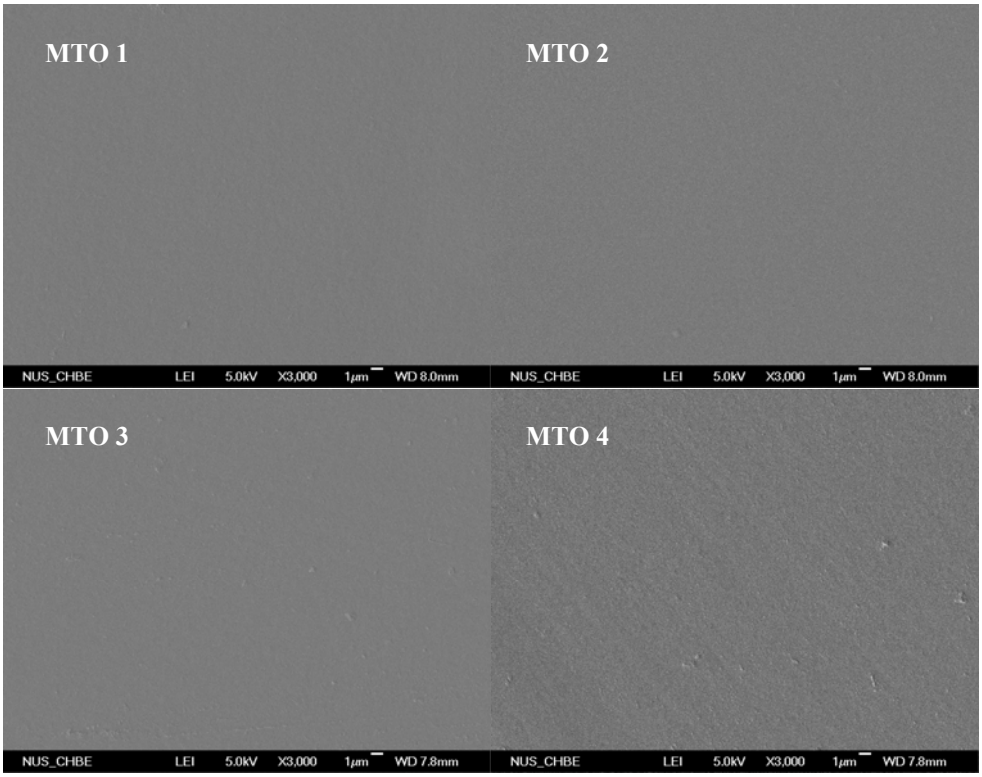

Figure 5.17 Surface morphologies of the EN deposits from each MTO round with TPP as the stailizer

5.4 Conclusions

In this chapter, three phosphine compounds – TPPTS, TPP and BDPPM – were proposed to replace Pb^{2+} ion in the ENP solution as the stabilizer. Among them, the hydrophobic TPP or BDPPM was successfully dissolved in the ENP solution up to 5×10^{-4} mol/L through arranging them to form complex with LA molecules in the high-concentrated lactic acid prior to the use. The relation of ENP deposition rate with the stabilizer concentration was investigated; none of them displayed a critical concentration like Pb^{2+}, Cu^{2+} and thiourea. This is because phosphine ligands are a

cathodic type stabilizer that prevents the ENP process from decomposition through suppressing the rapid reduction of Ni^{2+} ions at those highly reactive surface sites. Furthermore, the phosphine compounds, especially TPPTS, gave rise to a gradual increase of P-content in the Ni-P plating layer by increasing their concentrations in the solution, which led to improving the anti-corrosion property of as-deposited Ni-P plating layer. After annealing at 500 ^{o}C for one hour, the corrosion resistance of Ni-P deposition layer enhanced almost 20 times due to the formation of diffusion layer between the brass substrate and crystalline layer. In the last part of this work, the stabilizing capabilities of three phosphine compounds were tested in a 4-MTO process. The results showed that the properties, for example, surface morphology, deposit composition and plating rate, do not exhibit a perceivable change with the extension of operation time. Phosphine ligands are, therefore, regarded as a type of stabilizer that has great potential to replace lead in the future industrial applications due to several advantages that this compound could offer.

Chapter 6 Developing a Well-Adhered Ni/P Alloy Film on the Surface of Silicone Elastomer for Shielding Electromagnetic Interference (EMI)

Surface metallized silicone elastomer, poly(dimethylsiloxane) (PDMS), using electroless nickel plating (ENP) will find a niche in biomedical applications because it combines the biocompatibility of PDMS with the electromagnetic shielding capability of nickel thin film. However, PDMS is extremely hydrophobic and this makes ENP difficult to be carried out on its surface. In this paper, we report a simple and inexpensive chemical modification method, called the reverse surface roughning approach, which increases the wettability of the PDMS surface and thus the adhesion between the metallic deposit and PDMS substrate. In this method, an appropriate amount of surfactant was added into the PDMS matrix to enhance its surface wettability. Furthermore, TiO_2 was attached as an interlayer on the PDMS surface to increase the adhesion between the deposited metallic Ni-P film and the PDMS substrate. On the modified PDMS surface ENP can successfully proceed. Triton X-100 is found to be the most appropriate surfactant as compared to the other surfactants used in terms of its effect on the mechanical properties of PDMS, uniformity of TiO_2 layer and deposition of Ni-P film. The characteristics of the Ni-P deposit, such as structure, morphology, surface resistivity, adhesion and electromagnetic shielding are also investigated to highlight its potential applications in the future.

6.1 Introduction

Poly(dimethylsiloxane) (PDMS) is an important structural material that has broad applications in automotive, electric and electronics industries, food packaging, composite membranes, and medical/biomedical devices (Jershow, 2002; Iwasaki, 2007; Qi, 2007) due to its unique physical and chemical properties. PDMS is an elastic material at room temperature with high gas permeability and low curing temperature. Besides its good mechanical properties, PDMS is optically transparent, non-toxic, non-flammable and chemically inert (Auroux, 2002; Makamba, 2003; Roman, 2006; Qi, 2007). These properties make PDMS a very useful material.

Metallization of polymer substrate has major applications in the microelectronics industry such as magnetic storage devices and printed circuit boards (Yan, 2004; Azzaroni, 2006). In addition, suitably metallized polymers have potential applications in medical/biomedical industry (Metz, 2001; Gray, 2005). Different methods have been developed to metallize many polymers, for example, physical vapor deposition (PVD), chemical vapor deposition (CVD), and electroless plating (Mittal, 1998 & 2001; Kim, 2001; Carlo, 2002; Sipaut, 2007). However, reports have seldom been published for metallizing PDMS, likely because of its highly hydrophobic nature.

Compared with PVD or CVD, electroless plating, especially electroless nickel plating (ENP), is the most popular industrial method because of its low operation cost and simple equipment requirement. ENP is an autocatalytic redox reaction carried out in an aqueous environment, in which Ni^{2+} ions are reduced on a substrate

forming a nickel alloyed layer. A suitable polymer surface must be able to hold catalytic metal (Pd) nuclei as seeds to initiate the self-catalytic deposition (Azzaroni, 2006). Hence implantation of catalytic sites on the polymer surface before ENP becomes very important for the ENP process and the quality of the deposited Ni/P layer.

An appropriate surface modification of PDMS is, therefore, necessary before performing metallization by ENP on PDMS. Conventional techniques for PDMS surface modification could be classified as physical methods and chemical methods or both. In physical methods, PDMS surface is oxidized to increase its wettability by exposure to various energy sources such as plasma, ultraviolet and corona discharge (Hillborg, 1998; Vickers, 2006; Ye, 2006). But such techniques have a drawback of having a short lifetime before the hydrophobic recovery (Hillborg, 1998 & 2000). Prolonged hydrophilicity on PDMS surface has been achieved by chemical or physical-chemical methods. However, the complex protocols and huge operation cost in applying them are the issues to be addressed (Charbonnier, 2004 & 2006; Bodas, 2006).

Here we have developed a simple and inexpensive method to modify PDMS surface, which is the reverse surface roughening approach, to make it suitable for ENP. In this method, an appropriate amount of a surfactant is added into the PDMS matrix to increase its wettability; and TiO_2 nanoparticles are partially-embedded on the modified PDMS surface to improve the adhesion of Ni-P film to the PDMS substrate. ENP successfully proceeds on PDMS surface after this surface modification. The effect of different surfactants on the wettability of the modified

PDMS surface was evaluated by water contact angle measurements. The properties of the Ni-P deposit, such as structure, morphology, surface resistivity and adhesion, were also investigated to come up with a set of optimum plating conditions.

6.2 Experimental

6.2.1 Materials and sample preparation

Conventional P-25 TiO_2 powder (Degussa Co. Ltd., 30 nm average particle size) was first dispersed in 10 mL chloroform using ultrasonication to prevent coagulation, and then the resultant colloidal dispersion was transferred to a Petri dish and vacuum dried. A PDMS thin sheet was prepared by mixing a base (Sylgard 184, Dow Corning, Midland, MI, USA) and a curing agent at a volume ratio of 10:1 in chloroform solvent. The same mole amount (0.001mol) of one of the following surfactants, AOT, CTAB, Span-80 or Triton X-100, was then added to the PDMS mixture solution. After stirring for 5 min, the PDMS mixture solution was poured into the Petri dish containing the dried TiO_2 powder, and then was vacuum dried. When the solvent, chloroform, was completely evaporated, the Petri dish was transferred to a vaccum oven for 24 hr at 100 ºC. Then the cured PDMS was peeled off from the Petri dish and kept in DI water overnight at room temperature. Then the modified PDMS was stored in ambient conditions.

6.2.2 Deposition of catalyst

The modified PDMS sample was activated via a one-step process at room temperature in an acidic Pd-Sn colloidal dispersion, containing 1.0 g/L $PdCl_2$, 12 g/L $SnCl_2$ and 20 mL/L HCl, for 5 min. The PDMS sample was then dipped in a 1 M HCl solution for about 30 sec to remove the outer layer enriched in stannous species. The Pd particles left were used as the catalyst for further nickel deposition. After the activation, the PDMS substrate was rinsed with DI water and dried in air.

6.2.3 Electroless nickel plating

The ENP solution was prepared using the recipe given in Table 6.1. The pH of the plating bath was controlled at 4.80 ± 0.05 by adding 25% ammonium hydroxide during plating. The plating temperature was maintained at 90 ± 1 °C using the HAAKE DC30/W13 water bath. The modified PDMS substrates were plated by immersing them in the ENP solution for 20 min. After plating, the samples were rinsed by hot DI water thoroughly, kept in an oven for half an hour at 100 °C and followed by gradual cooling down from 100 °C to room temperature (over 2 hr).

Table 6.1 Composition of Acidic Hypophosphite Plating Bath

Components	Concentration
Nickel (II) sulfate hexahydrate	22.4 g/L
Sodium hypophosphite monohydrate	25 g/L
DL-Malic Acid	4 g/L
Sodium Acetate	8.5 g/L
Stabilizers	variable

6.2.4 Contact angle measurement

Static contact angles on PDMS samples modified with different surfactants were measured by the sessile droplet method using a Contact Angle (CA) Goniometer - Model 100-00 (Rame-Hart Inc., USA) with a CCD camera, and analyzed with the Rame-Hart Imaging 2001 software. The measurements were carried out at room temperature in air with DI water as probe liquid. Each contact angle reported here is an average of at least 3 measurements on the same sample.

6.2.5 Field emission scanning electron microscopy (FESEM)

The surface and cross-sectional images of the Ni-P deposit on modified PDMS were taken by FESEM (JSM-6700F, JEOL, Japan) equipped with energy dispersive X-ray spectrometry (EDX). Here the EDX was employed to analyze the chemical composition of the modified PDMS and the Ni-P deposit.

6.2.6 Atomic force microscopy (AFM)

AFM images for bare, modified and EN plated PDMS were obtained using a Digital Instruments Multimode AFM with Nanoscope IIIa Controller (Santa Barbara, CA, USA). The experiments were performed in the tapping mode using etched silicon tips under ambient conditions (Veeco Metrology Group).

6.2.7 Adhesion measurement

The adhesion of the metallic Ni-P layer on the modified PDMS was measured by the tape peel method. A piece of Scotch tape was applied to the surface of plated PDMS and smoothed to ensure good contact. Then the tape was peeled back at 180 ° in one smooth movement.

6.2.8 Measurement of magnetic property

Magnetization measurements were made at room temperature in magnetic fields up to 10 kOe using a vibrating sample magnetometer (Lakeshore 73045, Westerville, Ohio, USA).

6.3 Results and Discussion

6.3.1 Effect of surfactant on the crosslinking of PDMS

Some information on the surfactants used in this study is given in Table 6.2. The HLB (hydrophilic-lipophilic balance) value is an index varying from 1 to 20 for defining polarity of surfactants, namely the higher the HLB value, the more hydrophilic will be the surfactant. The mechanical properties of PDMS depend on the extent of its network formation, which may be affected by the presence of surfactant in the mixture of base polymer and curing agent. For AOT, Span-80 and Triton X-100, the degree of crosslinking in the resulting PDMS sheet does not show significant change relative to the pristine matrix except for requiring a longer curing duration. But the elasticity of modified PDMS film greatly decreases with using CTAB; it is easily broken under tensile laod. Therefore only AOT, Span-80 and Triton X-100 were used further as the wetting agents to increase the hydrophilicity of PDMS.

Table 6.2 Surfactants Used for the Preparation of Modified PDMS Films

Commercial Name	Charge Type	Chemical Name	HLB Value
AOT	Anionic	Sodium dioctyl sulfosuccinate	>10
CTAB	Cationic	N-Hexadecyl trimethyl ammonium bromide	10
Span-80	Non-ionic	Sorbitan mono-laurate	4.3
Triton X-100	Non-ionic	t-Octylphenoxypolyethoxyethanol	13.5

6.3.2 Wettability of modified PDMS

Because pure PDMS is highly hydrophobic, it is impossible to carry out ENP on pristine PDMS. To surmount this obstacle, it is necessary to increase the wettability of PDMS surface. Surfactants with specific molecular structures have been widely used for performing hydrophilization of hydrophobic materials (Adamson, 1997; Seo, 2006). In this work the PDMS base, curing agent and surfactant were mixed together and polymerized. After polymerization the modified PDMS film was immersed into DI water, so that the surfactant in the bulk of the film would move toward the surface of PDMS to improve its wettability (Seo, 2006). The advantages of this method lie in its low cost and simple operating procedure. The hydrophility of a surface is commonly evaluated by water contact angle. The contact angles of DI water on glass, pure PDMS and modified PDMS are compared in Figure 6.1. All the measurements were taken after 10 seconds of DI water droplet deposition. Here the contact angle of DI water on glass is used as the benchmark, as glass is a typical hydrophilic material. Before modification the contact angle on PDMS is 108.6º, showing its hydrophobic nature. After incorporation of a designated surfactant, the contact angle decreases to 45.9º, 74.9º and 80.5º for Triton X-100, AOT and Span-80, respectively. This observation suggests that surfactants mingle into the PDMS matrix and decrease the solid-liquid interfacial tension. Especially, Triton X-100 renders PDMS a hydrophilic surface after modification. The differences in the contact angles for the three surfactants could be explained from their HLB values. Triton X-100 has the largest HLB value among the three hence it gives rise to the greatest improvement in the hydrophilicity of PDMS.

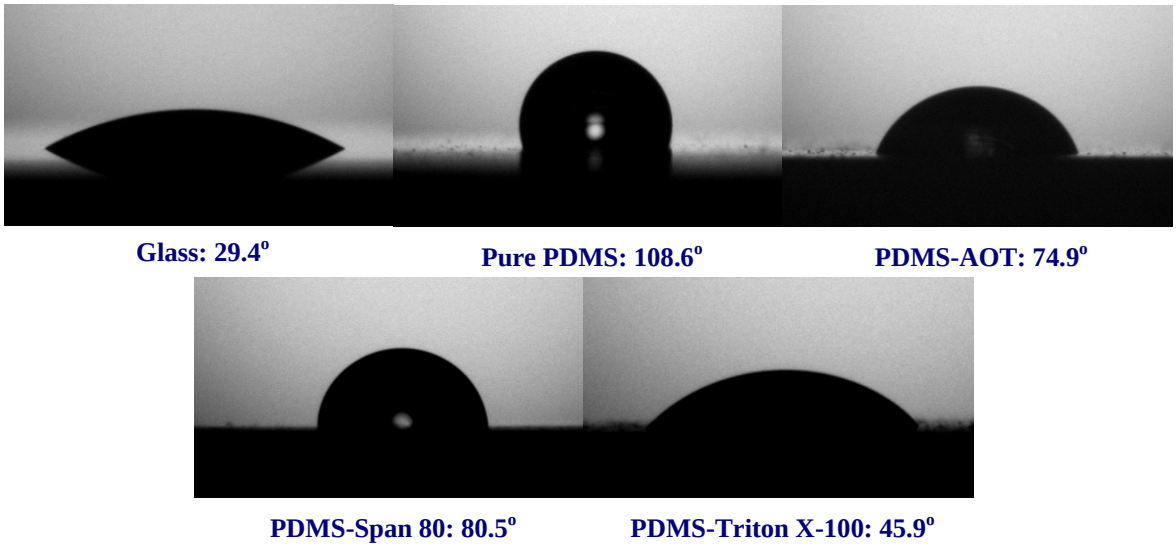

Figure 6.1 Contact angles of water on PDMS before and after incorporating a surfactant

6.3.3 Attaching a TiO_2 layer to the PDMS surface via gluing approach

Another problem that hampers ENP on a polymer is the low adhesion between the Ni-P deposit and the substrate because of the structural incompatibility in terms of physicochemical bonding and other unmatched materials properties. Therefore, the interfacial adhesion strength often limits the performance of a metallized polymer (Mittal, 1989; Charbonnier, 2003). TiO_2 nanoparticles are mechanically interlocked in the surface of PDMS and, therefore, offer both pertinent polarity and micro-roughness to assure adsorption of Pd/Sn colloidal particles on the PDMS surface. It is noted that TiO_2 nanoparticles could not be coated onto PDMS surface without modification with surfactants due to their greatly different hydrophilicity. It is experimentally confirmed that the presence of a TiO_2 transitional layer enhances the adhesion between the Ni-P deposit and the PDMS substrate. Figure 6.2 shows the

XPS spectra of Ti species on the modified PDMS surface, which signifies that TiO_2 particles are not fully covered by PDMS. The Ti peaks are observed only on samples modified by Span-80 and Triton X-100 but not by AOT. This phenomenon suggests that the kind of surfactant used affects the state of TiO_2 on PDMS surface. Only non-ionic surfactants could work in this technique. The peak intensity of Ti in the sample modified by Triton X-100 is significantly stronger than in the sample modified by Span-80. This difference might be related to their different affinities with PDMS matrix. Namely, the hydrophilic moiety of Span-80 molecules has stronger tendency to reject the PDMS matrix than that of Triton X-100 molecules, thus they push down the TiO_2 particles and take up the entire surface, while Triton X-100 molecules could better share surface with TiO_2 nanoparticles.

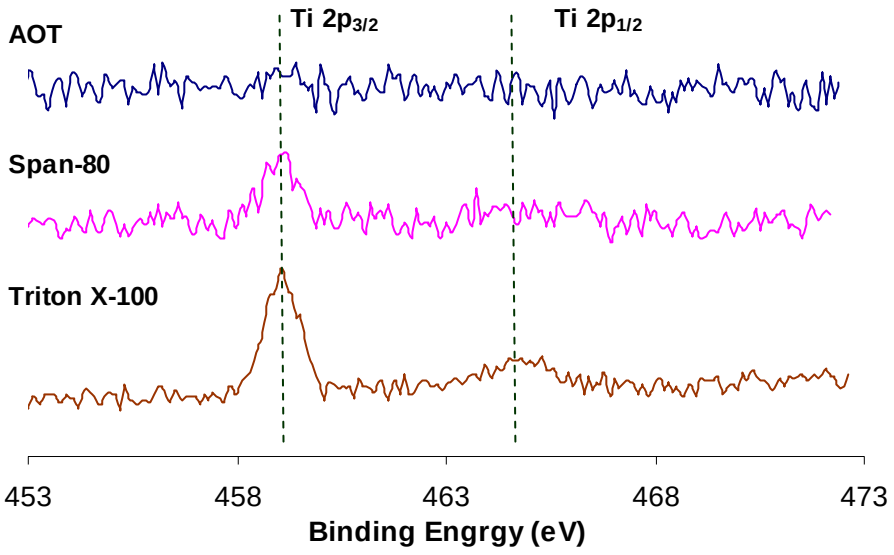

Figure 6.2 XPS analysis of the three PDMS surfaces where TiO_2 nanoparticles were embedded

6.3.4 Appearance of modified PDMS

The pictures of pure and modified PDMS films are shown in Figure 6.3. Pure PDMS is a smooth, colorless and shiny material with optical transparency. After incorporating a surfactant in its matrix and embedding TiO_2 particles into its surface, the PDMS film becomes milky and opaque. In addition, the surface of modified PDMS is rougher than that of the pure form and thus is beneficial for fixation of the catalyst seeds during the activation and the nickel deposition in ENP.

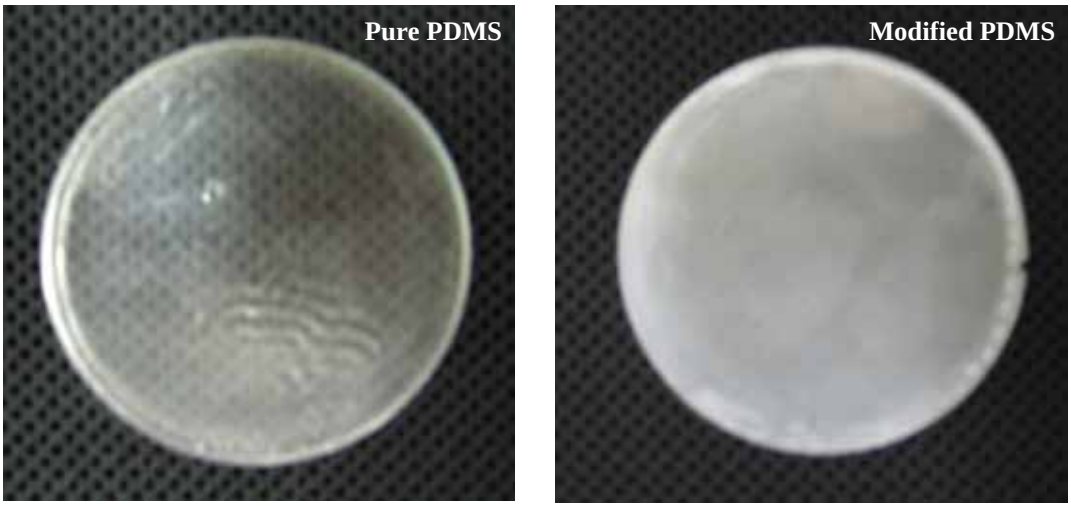

Figure 6.3 The appearances of pure and modified PDMS (Before modification PDMS was colorless and transparent and became milky after modification)

6.3.5 Deposition of Pd on modified PDMS

Currently, a one-step activation process has been widely adopted for undertaking ENP on polymer substrates. In this process the polymer substrate is first activated in the $PdCl_2/SnCl_2$ mixed colloidal dispersion and dipped in an acidic solution to remove the outer layer of Sn^{2+} species surrounding the metallic Pd/Sn core of the

adsorbed colloidal particles. This step makes the Pd/Sn initiation sites on PDMS surface ready (i.e. activated) for ENP (Nicolas-Debarnot, 2006). Creation of catalytic sites on PDMS surface is a crucial step for ENP. The performance of ENP on PDMS is largely affected by the adhesion of the colloidal particles to PDMS surface during the activation process.

The XPS analysis of the activated PDMS surface (Figure 6.4) showed a doublet Pd $3d_{5/2}$ and Pd $3d_{3/2}$ due to spin-orbit-split with a bonding energy difference between them of about 5.3 eV (Moulder, 1992). Under each peak above two sub-peaks could be discerned using the curve fitting procedure, and therefore the two sets of doublets obtained are the doublets of Pd^0 and Pd^{2+}, respectively. The doublet with $3d_{5/2}$ peak at around 335.2 eV is assigned to Pd^0 species, which resulted from the redox reaction described in Equation 6.1 (Nicolas-Debarnot, 2006).

$$Pd^{2+} + Sn^{2+} \rightarrow Pd^{0} + Sn^{4+} \qquad (6.1)$$

The Pd^0 species are known to be the sites where the subsequent nickel deposition will be initiated. The doublet with the $3d_{5/2}$ peak at about 337.8 eV is attributed to the Pd^{2+} species.

Similarly, a double-peak pattern, Sn $3d_{5/2}$ and Sn $3d_{3/2}$, was observed in Sn XPS spectra as well, and the difference in binding energy between them is about 8.6 eV (Moulder, 1992). From curve fitting, the lower binding energy at 486.0 eV for Sn $3d_{5/2}$ is attributed to SnO; while the higher one is assigned to $SnCl_2$ or SnO_2 (Moulder, 1992).

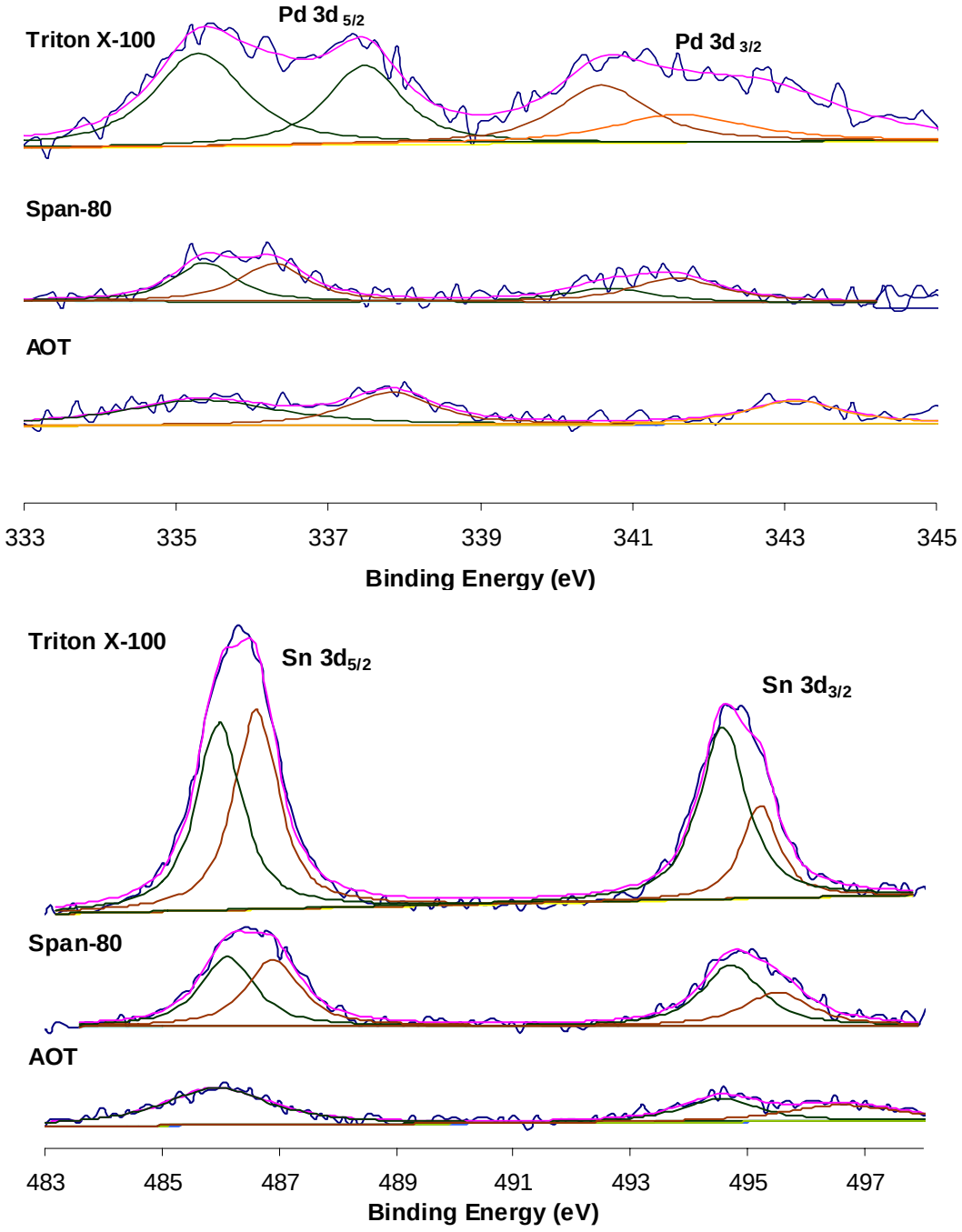

Figure 6.4 XPS spectra of Pd and Sn on the PDMS surfaces of the three samples (distinguished by different surfactants used) after they were activated in acidic Pd-Sn colloidal dispersion

It can concluded, based on the comparison of XPS peak intensities of Pd and Sn detected from different surfaces of modified PDMS sheets, that using Triton X-100 provides a suitable surface to hold colloidal Pd seeds at the maximum density; in contrast, using AOT leads to the least extent of catalyst attachment. On the other hand, induction time of ENP is the time elapsed before Ni plating is initiated. This parameter could also reflect the surfactant effect: Span-80 brings about slower initiation and poorer coverage than Triton X-100; while for AOT, the ENP could not be initiated at all. Thus, only the PDMS substrate modified with Triton X-100 was selected for carrying out ENP and property assessment in the following section.

6.3.6 Surface/cross-sectional morphology and composition of Ni deposit on modified PDMS

It has been established in previous sections that the type of surfactant affects the embedding state of TiO_2 nanoparticles on the PDMS surface, i.e., the roughness of the resulting surface. Promoting surface roughness in an appropriate range is imperative to enhance the adhesion between ENP layer and the PDMS film. Surface morphologies of the pure PDMS, the modified PDMS and the plated PDMS are shown in Figure 6.5. It is obvious that the smooth surface of pure PDMS becomes rough after modification and its rough topography is propagated to the subsequent ENP. This topography transition could also be observed using the AFM as displayed in Figure 6.6. According to the Z values recorded, incorporation of Triton X-100 into the PDMS matrix decreases its surface roughness slightly. However, the roughness of PDMS surface dramatically increases from about 100 nm to about 1 μm after it is coated with TiO_2. This rough surface promotes adhesion of the plated

Ni-P film (see discussion in Section 6.3.7) but causes a quite rough surface of the Ni-P metal film.

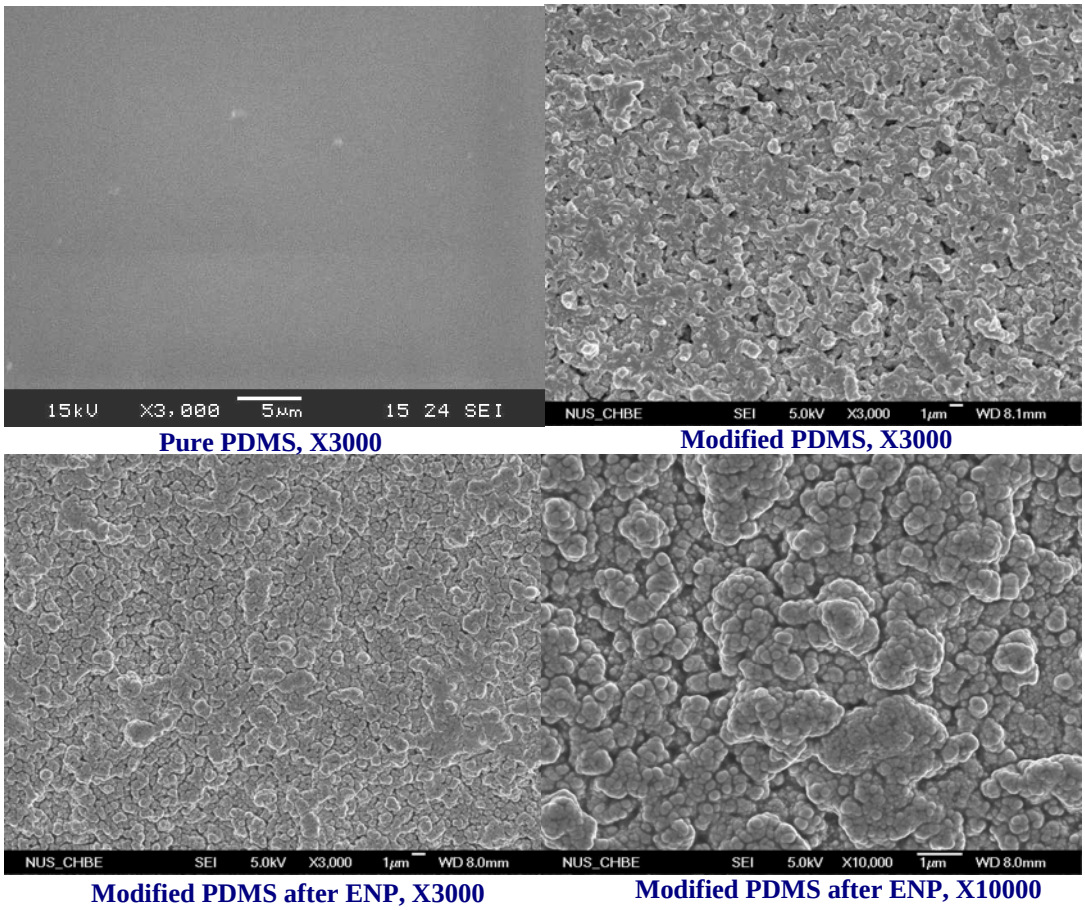

Pure PDMS, X3000 **Modified PDMS, X3000**

Modified PDMS after ENP, X3000 **Modified PDMS after ENP, X10000**

Figure 6.5 Surface morphologies of the pure PDMS, the modified PDMS and the ENP layer developed

This irregular and rough Ni deposit might have potential application in the electromagnetic shielding area.

The composition of the deposited Ni-P film was analyzed by EDX. The phosphorus content in the film reaches 10.4 wt. %, regarded as a typical high-phosphorus ENP layer.

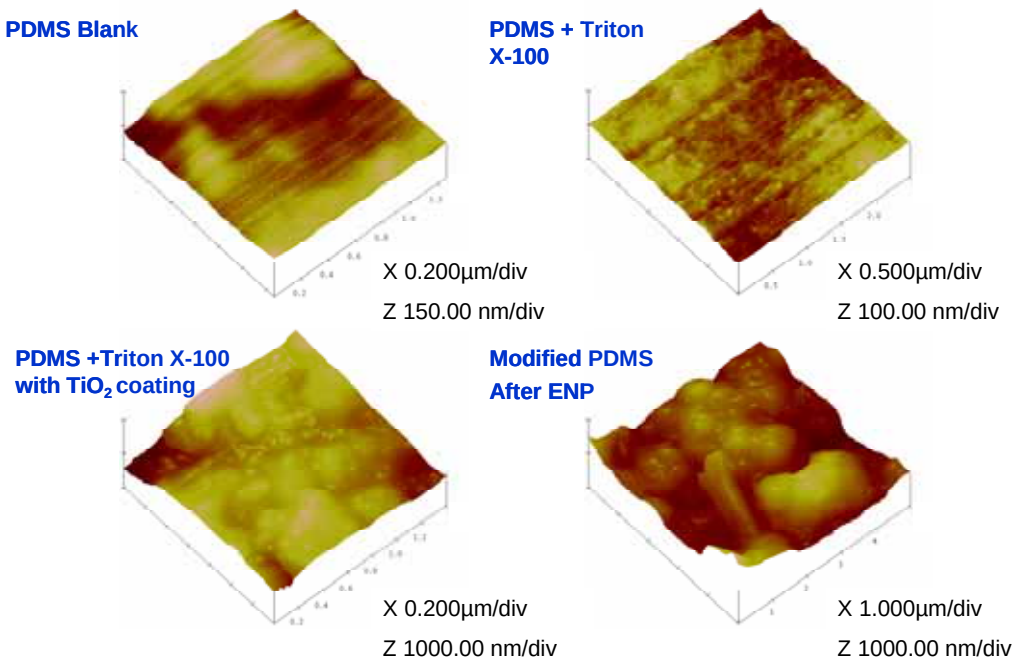

Figure 6.6 AFM images of pure, modified and Ni plated PDMS

The cross-sectional images of the Ni-P deposited PDMS substrate are presented in Figure 6.7. There are no cracks or gaps between the Ni-P film and the PDMS substrate. The non-compatibility between the metallic film and PDMS is successfully overcome through the assistance of the TiO_2 transitional layer.

a)

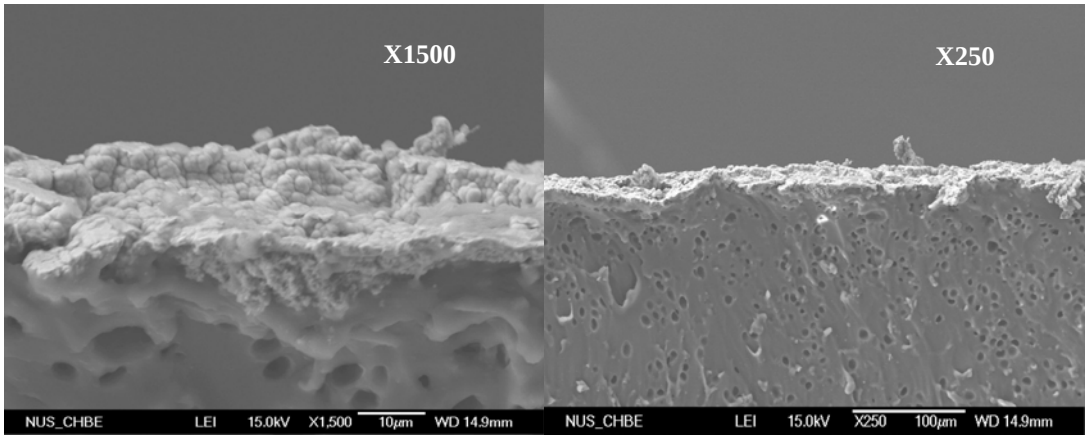

b)

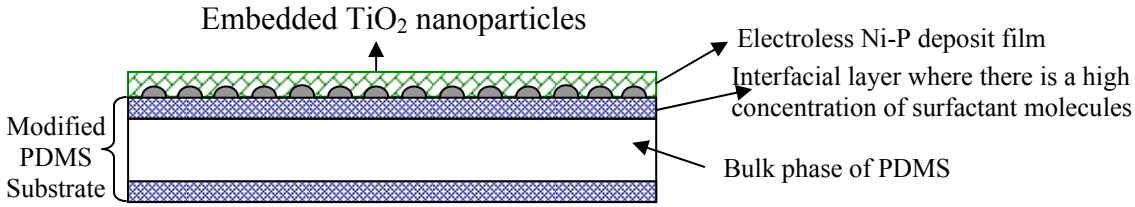

Figure 6.7 a) Cross-sectional image of plated modified PDMS; b) The schematic of the cross section of the ENP plated modified PDMS film

Figure 6.8 shows the results of the XPS elemental analysis of the cross-sectional area of the Ni plated PDMS. Two distinct layers could be recognized: one is the PDMS substrate layer, the other is the plated Ni film. In addition, the thickness of nickel layer is about 11 μm, which resulted from ENP for 20 min.

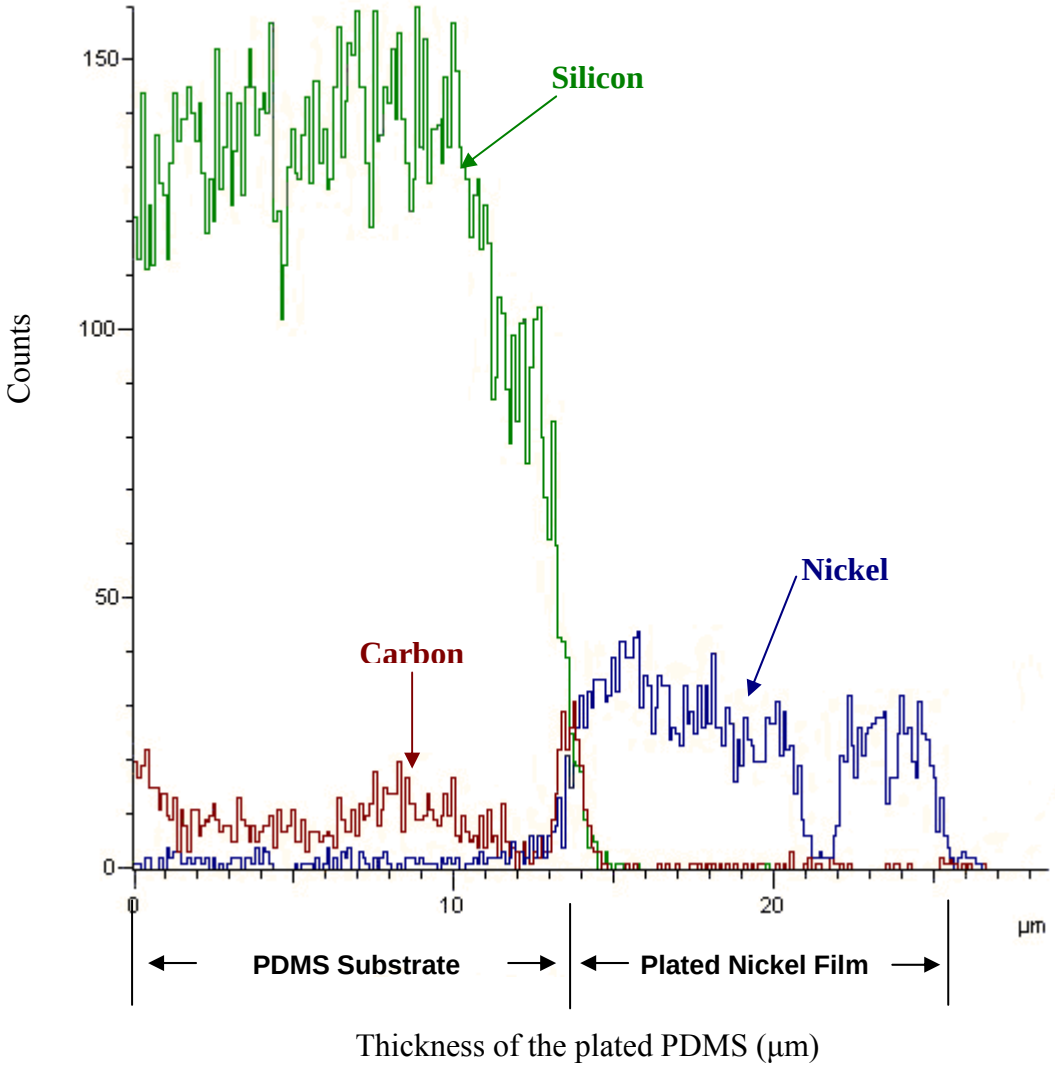

Figure 6.8 Elemental depth profiles of the ENP plated PDMS film

6.3.7 Adhesion between the deposited Ni-P film and the modified PDMS substrate

The adhesion strength of the deposited Ni-P film was evaluated by the tape peel test. The surfaces of the sample before and after tape peel test are compared in Figure 6.9.

The Ni-P deposit film was not significantly removed by peeling off the Scotch tape. In contrast, for samples whose surface was not roughened by TiO_2 nanoparticles, only part of the PDMS surface could be electroless plated and the deposited Ni-P film could be easily wiped off. The result evidences a strong adhesion of Ni-P film to the modified PDMS surface. This good adhesion may be attributed to the rough TiO_2 coating and the high surface concentration of catalyst sites on TiO_2. But more research is needed to understand in detail the great improvement in adhesion between metallic Ni-P film and modified PDMS substrate.

Figure. 6.9 Microscopic views of the Ni plated PDMS surface before and after the peel test

6.3.8 Surface resistivity of EN plated PDMS

Surface resistivity, ρ_s, is determined by the ratio of DC voltage U drop per unit length L to the surface current I_s per unit width D as in Equation 6.2 (Maryniak, 2003).

$$\rho_s = \frac{U/L}{I_s/D} \tag{6.2}$$

The setup for surface resistivity measurement is illustrated in Figure 6.10 (a), where the DC voltage is controlled by a power supplier, and the current is read from an ampere meter. Equation 6.2 can be converted to Equation 6.3 as:

$$\rho_s = \frac{U/L}{I_s/D} = \frac{U/I_s}{L/D} \tag{6.3}$$

where the values L and D are fixed; and the ratio of U/I_s could be read from the slope of the linear line in Figure 6.10 (b). The surface resistivity calculated from Equation 6.3 is 38.7 Ω/sq. PDMS, an insulator, becomes electrically conducting at its surface after being electrolessly Ni plated.

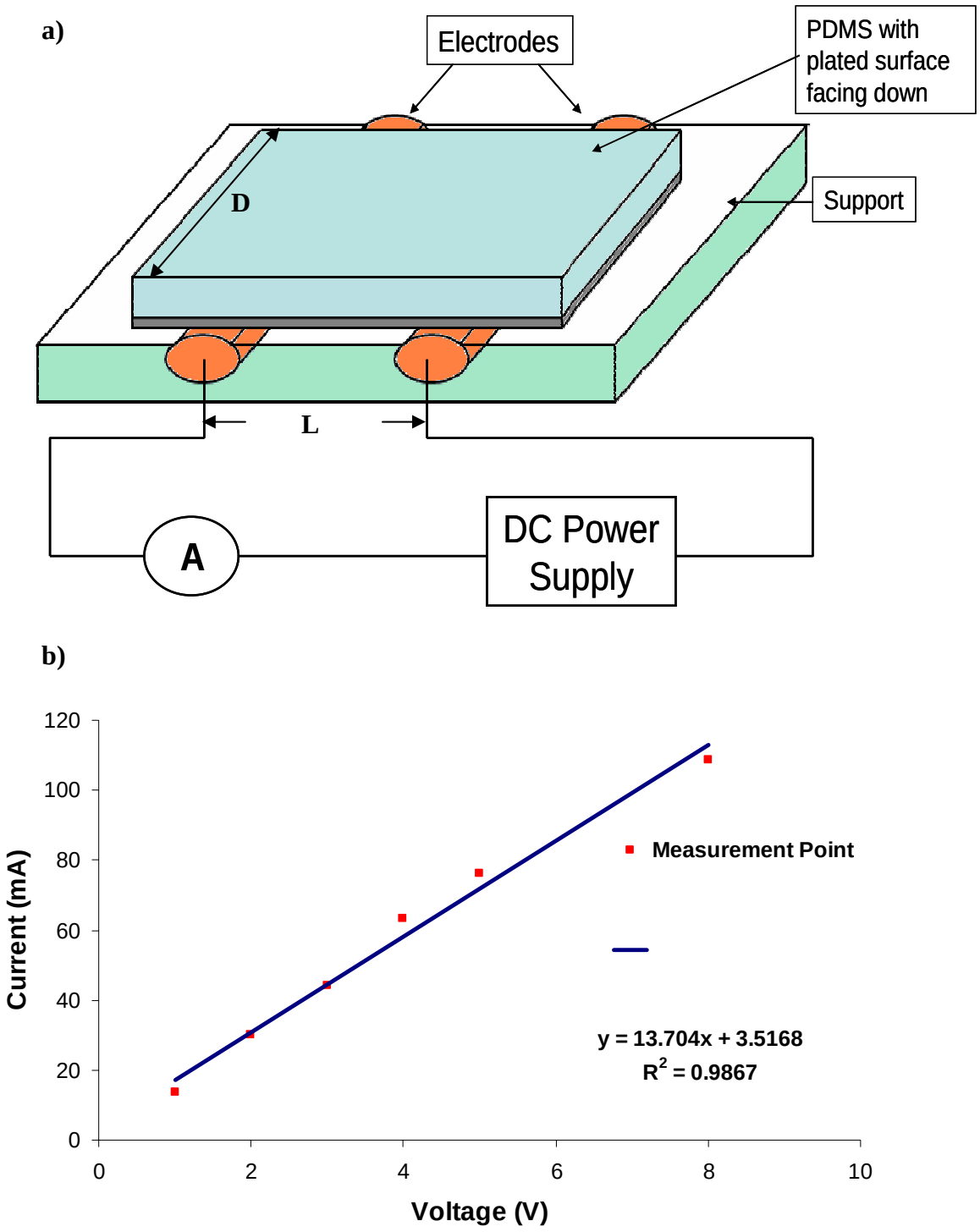

Figure 6.10 a) Schematic presentation of experimental setup for surface resistivity measurement; b) The graph of I against V

6.3.9 Hysteresis loop of EN plated PDMS

The magnetic properties of ENP film on PDMS were studied by the hysteresis loop or the B-H loop, which shows the relationship between the induced magnetic flux density (**B)** and the magnetizing force **(H).** The hysteresis loop for the Ni-P deposit is shown in Figure 6.11, from which it is concluded that the plated Ni-P alloy is a diamagnetic material. It is well known that pure nickel is ferromagnetic because it has unpaired electrons, which give a net magnetic moment. But in the plated Ni-P alloy, these unpaired electrons of nickel are paired with electrons from phosphorus resulting in no permanent net magnetic moment.

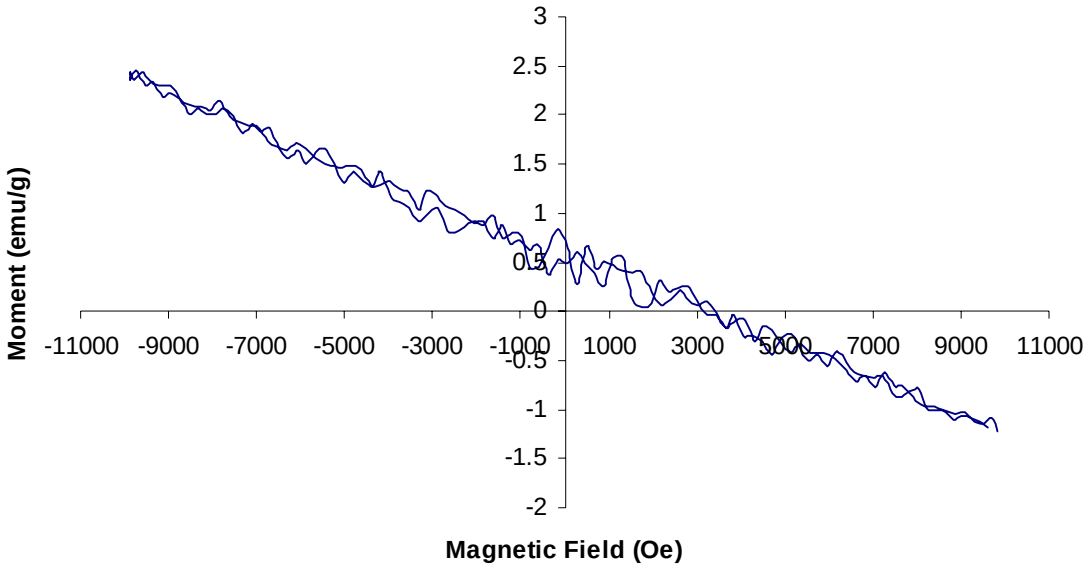

Figure 6.11 B-H loop of ENP deposit on PDMS

6.3.10 Electromagnetic shielding by EN plated PDMS

As mentioned before, the irregular and rough Ni-P deposit might have the capability for electromagnetic shielding, which is of potential application in medical/biomedical area.

The setup to evaluate the electromagnetic shielding property of the EN plated PDMS sheet is shown in Figure 6.12, where the magnetic field is provided by passing an AC current through the wire coil on a PVC tube. Current was induced when the piece of copper foil in the loop was exposed to an electromagnetic field, which caused the temperature increase of the copper foil. The change in temperature is recorded by the thermocouple. In order to eliminate the heat generated by the wire coil that might interfere with the measurement, a water cooler was introduced between the sample and the wire coil.

When the copper foil is sandwiched between two pieces of the EN deposited PDMS, no noticeable heat is induced due to the magnetic shielding property of EN deposit. In contrast, the graph of temperature against time for the sample using unplated PDMS shows a clear rising trend with time (Figure 6.13) due to the generation of induced current in the copper foil in the alternating magnetic field. Each temperature reported here is the average of 3 measurements on the same sample. It can be concluded that the rough and irregular Ni-P metallic deposit on modified PDMS has a great capability for electromagnetic shielding.

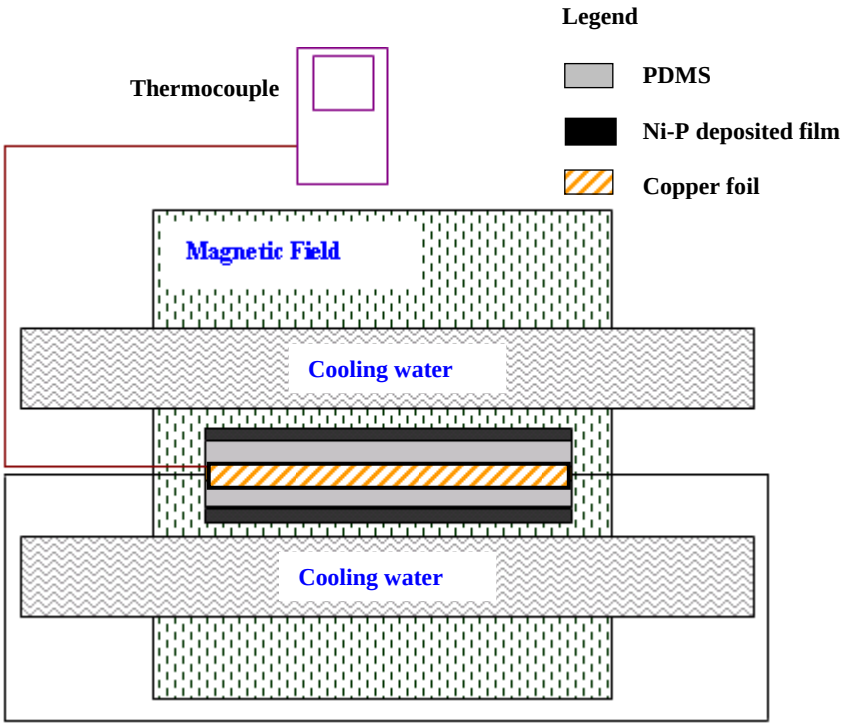

Figure 6.12 Schematic presentation of experimental setup for evaluation of electromagnetic shielding property of the Ni-P layer on the modified PDMS

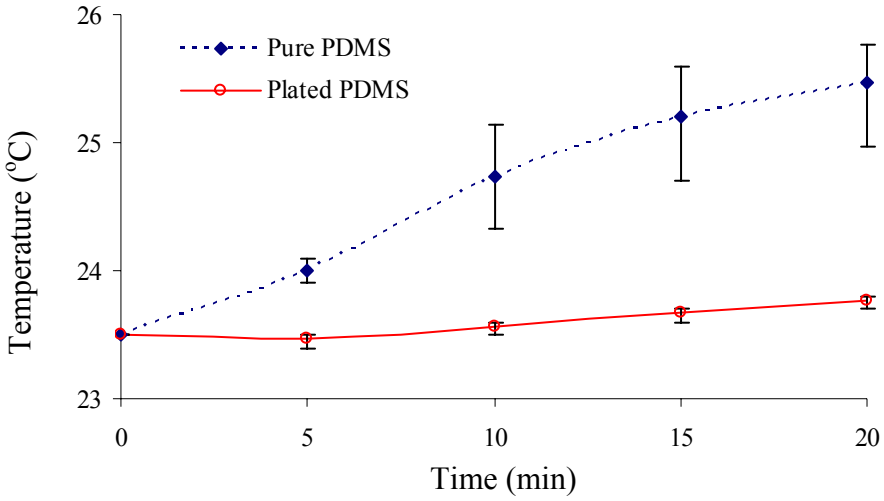

Figure 6.13 Temperature profiles of the copper sheet in the alternating field as shown in Figure 6.12

6.4 Conclusions

In this chapter, a simple and low-cost surface roughening approach is developed to turn the surface property of PDMS from hydrophobic and flat surface to hydrophilic and rough surface. The modified PDMS substrate becomes suitable for the electroless deposition of a Ni-P alloy film on it. The role of surfactant in the modification is investigated from several perspectives. It is found that a non-ionic surfactant, Triton X-100, is the most appropriate for the surface modification of PDMS; this surfactant not only increases PDMS wettability but also improves the TiO_2 embedding quality on its surface. The partially exposed TiO_2 nanoparticles on PDMS surface dramatically increase its roughness. After modification, the PDMS surface shows a great affinity for the adsorption of the catalyst for ENP. Consequently, ENP proceeds successfully on the modified PDMS surface. The resulting Ni-P alloy film has a rough and irregular structure, which has a good adhesion to the PDMS substrate. The Ni-P film on PDMS sheet offers high electrical conductivity and an electromagnetic shielding property. However, it is yet not clear that whether adding surfactant to the PDMS substrate would result in a material that remains acceptable in potential biomedical applications. There is, therefore, an interesting to continue exploring the effects of different components of the modified PDMS in the biomedical environments in future studies.

Chapter 7 Electroless Deposition of Anode Catalyst on Nafion® Membrane – A New Approach for the Fabrication of MEA

This work attempts an alternative approach to prepare membrane electrode assembly (MEA), in which the anode is the electrolessly deposited Pt or Pt-Au bimetallic thin layer on Nafion® membrane. Prior to electroless plating, a defined surface area for the fabrication of anode on a Nafion® membrane was activated using a $Pd/SnCl_2$ colloidal dispersion. The electroless deposition involves optimization of the three parameters: Pt loading (in mg/cm^2), dispersity of metal particles and coverage of the activated area. It was found that the Pt loading of 0.2 mg/cm^2 met the requirements for a full coverage and preservation of the mean particle size smaller than 100 nm as well. In addition, a bimetallic Pt-Au deposition layer was developed via a two-step electroless plating process. The Au loading and the morphology of deposit were manipulated via the variation of plating time so that a minimum loading of Pt was required in the successive plating to entirely cover the existing Au particles and to form an even deposition layer. In this process Au particles and nuclei play a role in affecting the crystal growth of the overlaying Pt phase on them. Consequently, the two anodes, i.e. Pt/Nafion and Pt-Au/Nafion, show satisfactory metal-polymer adhesion strength. Finally, both of them were evaluated in a single stack PEMFC and demonstrated superior performance over a conventional PtRu electrode employed as the benchmark.

7.1 Introduction

Proton exchange membrane fuel cell (PEMFC) is the device that enables automobiles, lap-tops, cell phones, etc. be powered by hydrogen methanol (Alkire, 1997; Liu[a], 2007; Wei, 2007). To operate PEMFC, platinum and its alloys, such as PtRu and PtSn, have been developed as the anode catalyst due to their excellent catalytic activity for the oxidation of fuel, i.e., hydrogen and methanol, under fuel cell operation conditions (Fujiwara, 2002; Koh, 2007; Liu[b], 2007; Mani, 2008; Ramaswamy, 2008; Wei, 2008). To fabricate an anode, nanoparticles of the Pt-based catalyst are, conventionally, loaded on fine carbon particles and the resulting carbon powder is then coated on an electric conducting carbon sheet to form the anode. Regarding the commercialization of PEMFC, high cost of Pt-based catalyst is a major obstacle owing to the scarce resources of precious metals (Vielstich, 2003; Chan, 2004). Therefore, efforts to lower the Pt loading as well as to improve the electrode kinetics and chemical resistance of the catalyst to carbon monoxide represent one of the main trends to advance PEMFC technology (Marino, 2004; Wang, 2005; Park HS, 2007; Wei, 2008).

A great deal of research has been carried out to explore methods that can largely improve power output on the basis of Pt loading (mg/cm^2). In general, there are two methods that are used to prepare the anode and cathode. Besides preparing Pt or Pt alloy nanoparticles separately (Ayyadurai, 2007) as aforementioned, an alternative way is the deposition of the catalyst generated in-situ to the surface of the gas diffusion layer (GDL) or electrolyte membrane (Farhat, 2008). The deposition can

be carried out by means of physical vapor deposition, chemical vapor deposition, sputtering or electrolytic deposition (Lee, 2007; Kim, 2008; Spataru, 2008).

Although electroless plating is a metal deposition method, which offers a number of advantages, such as simple operational process and unaffected by substrate geometry, this technique has seldom used for the preparation of fuel cell catalysts. Fujii and Ito reported the synthesis of high performance Pt catalysts by electrolessly depositing them on carbon black (Fujii, 2006), and pointed out that the output power density was closely related to the sizes of Pt particles. Liu et al. (2002) prepared Pt-based catalysts on carbon nantubes (CNTs) by microwave-aided reduction in a solution. The resultant Pt/CNT cathode catalyst manifested a high electrocatalytic activity for oxygen reduction in a single stack PEMFC. It was also reported that Pt could be directly deposited on polypyrrole modified Nafion composite membranes for the application in direct methanol fuel cell (DMFC) (Li, 2007). However whether the electroless deposition of Pt-based catalysts on pristine Nafion® membrane is viable for the fabrication of a MEA is still unknown. Fascinated by the intimate contact between the catalyst and the electrolyte in such a double-layer design, the present work attempts to realize this structure and to provide a preliminary understanding of its performance.

On the other hand, the electrochemical deposition technique will allow us to hybridize Pt by depositing it on an alien metal particle with the aim of the enhancement of the chemical resistance of Pt to CO, which often exists in the hydrogen stream by about 1 vol.% (Monyanon, 2006). In practice, the preferential oxidation (PROX) of CO may be the simplest and the least expensive method for

CO removing during fuel cell operation (Wei, 2008). Metals like Ru, Rh, Au, are effective for the PROX of CO. But among them, Au has been proven to own the highest catalytic activity for the oxidation of CO at low temperatures (Monyanon, 2006; Russo, 2006). Moreover, the Pt-covered Au nanoparticle was reported to boost the Pt utility in DMFC (Zhao, 2006). In this context, the electroless deposition of Pt/Au bimetallic particles that have Au (core) and Pt (shell or colonies) on Nafion® membrane will be potentially a type of CO-tolerated catalyst. In this work, an electroless plating of Pt or Pt/Au on Nafion® 1135 membrane was performed, so that the metal layer generated consisted of metal nanoparticles but rather than a dense metal thin film. The relations of Pt loading (L_{Pt}) with the metal particle sizes and with the surface morphology were investigated. The similar study was also conducted in the Au/Pt deposition layer. Finally the cell performances of using Pt or Pt/Au as the anode catalyst were evaluated and compared with conventional PtRu alloy anode at same L_{Pt} in a single stack H_2-driven PEMFC.

7.2 Experimental

7.2.1 Materials

All chemicals used were analytical-grade. The perfluorinated polymer electrolyte membrane, Nafion® 1135 (E.I. Dupont de Nemours and Company, 0.09 mm thickness), of size 4×5 cm^2 was used as the substrate for electroless plating in this work. Deionized (DI) water with a resistivity greater than 15 MΩ cm, generated by a

Millipore Elix10 purification system, was used for the preparation of plating solution and samples rinsing.

7.2.2 Electroless Pt and Au plating

The electroless platinum plating (EPP) solution or electroless gold plating (EGP) solution was prepared using the recipes listed in Table 7.1. Before plating, a central rectangular area of 2×3 cm^2 (the same size as the effective electrode area) in one side of a piece of substrate was selectively activated by covering the edge with Scotch tape. The details of this process were as follows: first, let only the selected area contact with the activation solution, an acidic Pd-Sn colloidal suspension that mainly contains 4.0 g of $PdCl_2$/L and 12 g of $SnCl_2$/L for 5 min; and secondly, dipped the activated substrate in a 1 M HCl solution for about 30 sec to remove the outer layer enriched in stannous species. The pH of the plating bath was 12.0 and the plating temperature was maintained at 70 ± 1 °C using the HAAKE DC30/W13 water bath. The pretreated substrate was plated by immersing it in the EPP or EGP solution. Different plating time was set to alter metal loading. After plating, the samples prepared were rinsed thoroughly by DI water.

Table 7.1 Composition of EPP/EGP solution

Chemical	Concentration
Na_2PtCl_6 // $KAu(CN)_2$	3.5 g/L // 0.2g/L
Ethylenediamine	45 ml/L
Rhodanine	60 ppm
Imidazole	15 g/L
KSCN	50 ppm
Styrenesulfonic acid, sodium salt	100 ppm
Sodium Hydroxide	40 g/L

7.2.3 Determination of metal loading

Upon activation, the substrate was placed in a vacuum oven at 60 °C for 2 hr to evaporate the moisture from the membrane. The membrane was then weighed using an analytical balance (A&D GR-200 Goldbell, Singapore). After plating, the plated membrane was dried in vacuum at 60°C for anther 2 hr and then weighted again. The Pt loading was calculated by the following formula:

$$L_{Pt} = \frac{W}{A} \qquad (7.1)$$

where L_{Pt} is the platinum loading in mg/cm^2, W the weight difference before and after plating in mg, A the plating area in cm^2.

7.2.4 Instrumental analyses

The surface morphology of Pt or Au/Pt plating layer was recorded on a FE-SEM instrument (JEOL, JSM-6700F, Japan). The composition of a metal deposit was determined using X-ray photoelectron spectrometer (XPS; Kratos xis HiS System). The binding energy (BE) of a sample was calibrated by the BE of C_{1s} at 284.8 eV. The X-ray diffraction (XRD) patterns of the Nafion® substrate, Pt-Nafion® electrode and Au/Pt-Nafion® electrode were measured on a Bruker GADDS diffractometer with an area detector using the Cu K_α source (λ = 1.54056 Å) operating at 40 kV and 40 mA.

7.2.5 Ion exchange treatment

As the electroless plating was taken in an alkaline solution containing concentrated K^+ and Na^+ ions, the counter ion in the plated Nafion® substrate would be these two alkali metal ions. Therefore before the fuel cell test, each of the plated Nafion® substrates was soaked in 1 M H_2SO_4 at 80 °C for one hour to allow ion exchange between the K^+ (Na^+) ions and proton. After that, the substrates were refluxed in DI water at 80 °C for another one hour to clean up the attached sulfuric acid.

7.2.6 Cell performance

The membrane electrode assembly (MEA) for the PEMFC test cell was made by stacking an anode sheet and a cathode sheet together. The cathode sheet was a carbon paper loaded with a carbon-supported 20 wt.% Pt catalyst layer supplied by E-TEK. The anode was the electrolessly deposited Pt or Au/Pt layer on Nafion® sheet. The catalyst loadings at the anode and cathode were the same as 0.2 mg/cm^2, and the effective electrode area was 6 cm^2. Besides this, a piece of carbon paper (SGL, Germany) with SWCNT and a Vulcan carbon supported PtRu catalyst layer was taken as the benchmark of anode. For the plated anode, hydrogen gas was supplied to anode with a flow rate of 300 cm^3/min, while the oxygen flow purged to cathode was 500 cm^3/min. The cell performance was evaluated at room temperature. DC current was applied to the cell with a current pulse generator (Agilent 6051A System DC Electronic Load).

7.3 Results and Discussion

7.3.1 Deposition of Pd on Nafion® membrane

Similar as what we have discussed about ENP on PDMS in Section 6.3.5 of Chapter 6, implantation of plating initiation sites, which are Pd seeds here, on Nafion® surface is a crucial step for the subsequent electroless plating process, because the adhesion of the catalytic layer to the surface of Nafion® membrane is greatly affected by distribution and binding strength of Pd colloidal particles on the membrane.

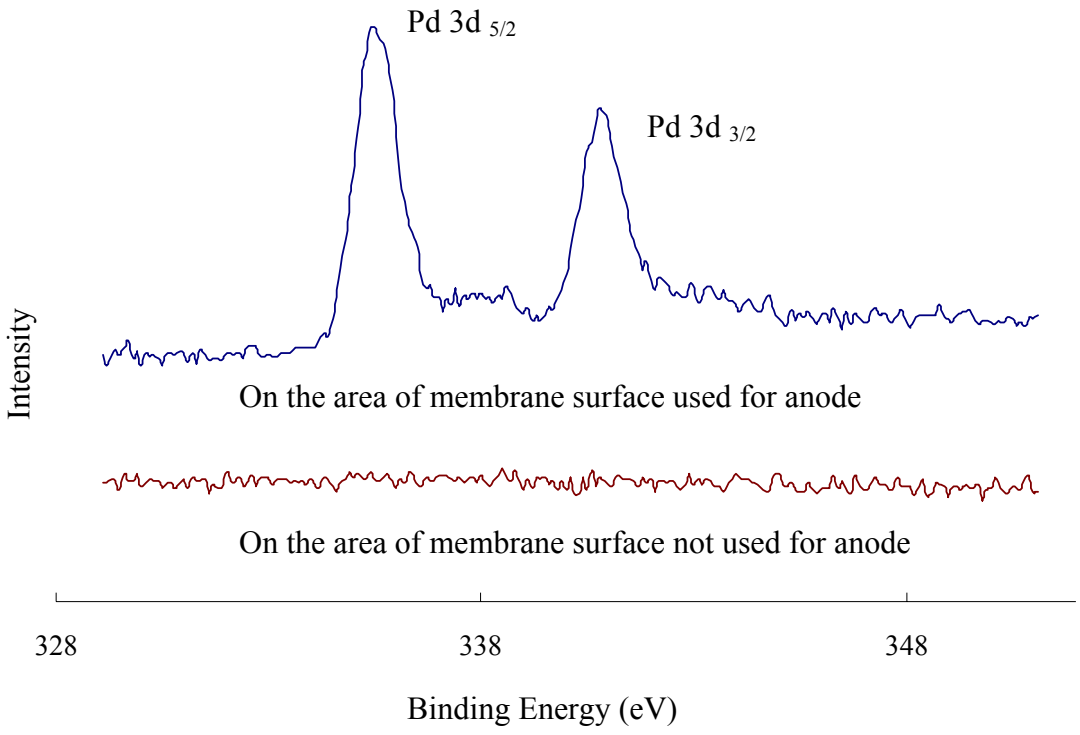

Figure 7.1 XPS spectra of Pd on selectively activated Nafion® substrate

The XPS analysis of the selectively activated Nafion® membrane surface is shown in Figure 7.1. The Pd spectrum on activated surface area, after HCl etching and DI water rinsing, presents a doublet corresponding to Pd $3d_{5/2}$ and Pd $3d_{3/2}$ with a bonding energy difference of approximate 5.3 eV (Moulder, 1992). This result shows the accomplishment of a dense distribution of the anchored Pd seeds, which is necessary to obtain a Pt or Au/Pt layer to the Nafion® substrate with strong adhesion strength.

7.3.2 Electrolessly plated Pt on Nafion® membrane

An electrolessly deposited area on the face side of the Nafion® membrane exhibits a uniform Pt deposition layer (Figure 7.2). The wrinkles of this sheet might be caused by the dehydration of the membrane during the drying process (Section 7.2.3).

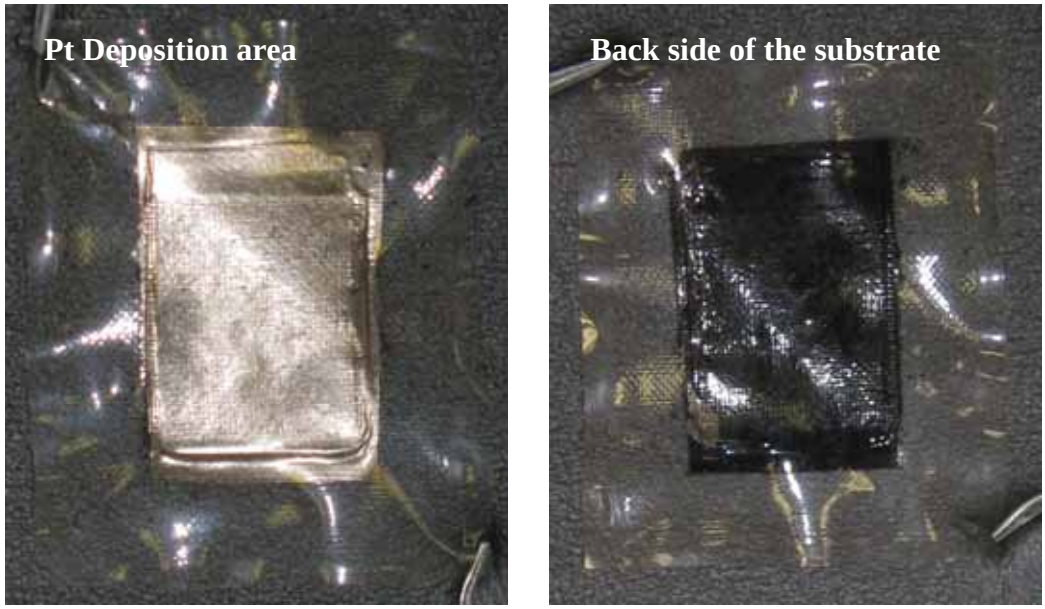

Figure 7.2 Pictures for both face and back sides of electroless Pt plated Nafion® membrane (L_{Pt}=0.2 mg/cm^2)

Figure 7.3 shows the XPS Pt4*f* spectrum of the deposited Pt layer, in which The Pt 4f region shows two doublets from the spin-orbital splitting of the 4f7/2 and 4f5/2 states. The main doublet of 4f7/2 at 71.1eV demonstrates the presence of metallic platinum Pt(0). The smaller doublet of Pt 4f7/2 (at 72.1 eV) indicates the presence of higher oxidation states of Pt, such as Pt(IV) (e.g., PtO2) in the sample (Liu, 2008).

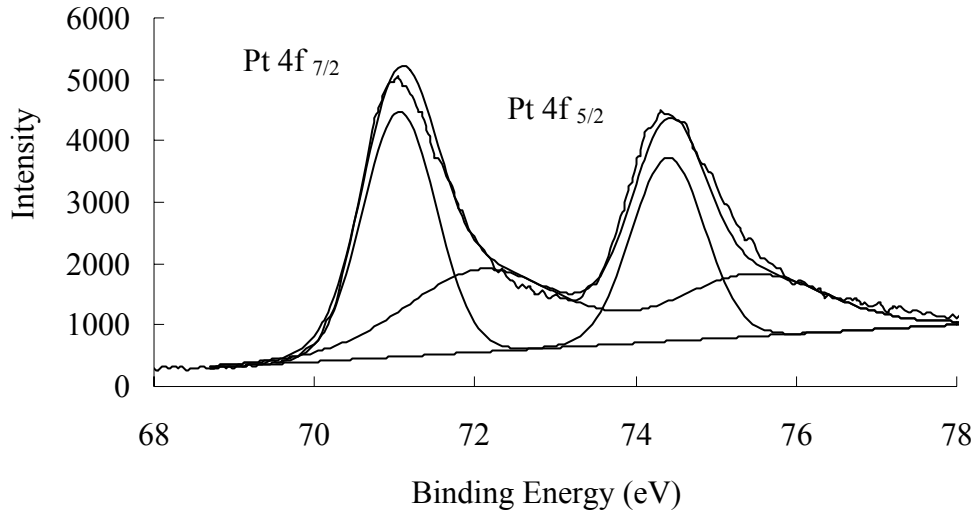

Figure 7.3 XPS spectrum of electrolessly plated Pt4f

The relation of Pt loading on Nafion® membrane with the surface morphology of the deposited Pt layer was also investigated (Figure 7.4). When Pt loading was about 0.1 mg/cm^2 (Sample I), the diameter of Pt particle was around 10-20 nm, but several of these small particles were inclined to cluster together to form a larger particle of a size 50-100 nm. This phenomenon was also found in Sample II (L_{Pt} was about 0.2 mg/cm^2); however, its particle distribution was more uniform than Sample I in which a lot of membrane surface was not covered. When L_{Pt} was increased to about 0.4 mg/cm^2, a dense Pt thin film was formed on membrane surface as seen in

Sample III. After that, further increase of L_{Pt} caused Pt particles to grow irregularly on the Pt layer and form a multi-layer structure as shown in Sample IV. Ostensibly, the ratio of Pt surface area to Pt weight in Sample III and IV was much smaller than that in Sample I and II, which caused a low utilization of Pt. In addition, regarding Sample I, the catalyst coverage on membrane was very insufficient and was expected to lead to a poor anodic catalytic performance. Therefore, L_{Pt} of Sample II offers the maximum surface coverage at the lowest cost of Pt among the four samples.

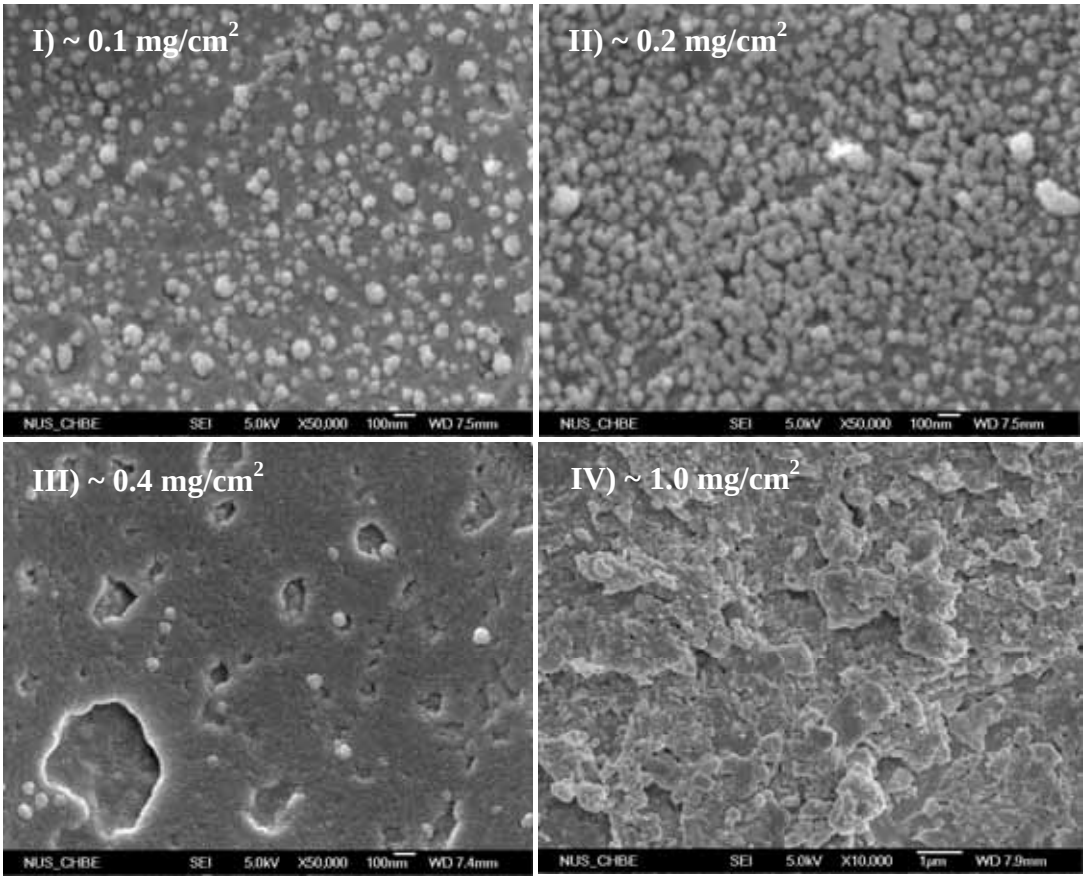

Figure 7.4 Surface morphology of electroless Pt deposits from samples with different L_{Pt}

7.3.3 Electrolessly plated Pt/Au on Nafion® membrane

Development of a Pt/Au dual phase deposition layer that must have a high surface/weight ratio and also uniform in composition on Nafion® membrane is the goal of this design to achieve a bi-metallic anode.

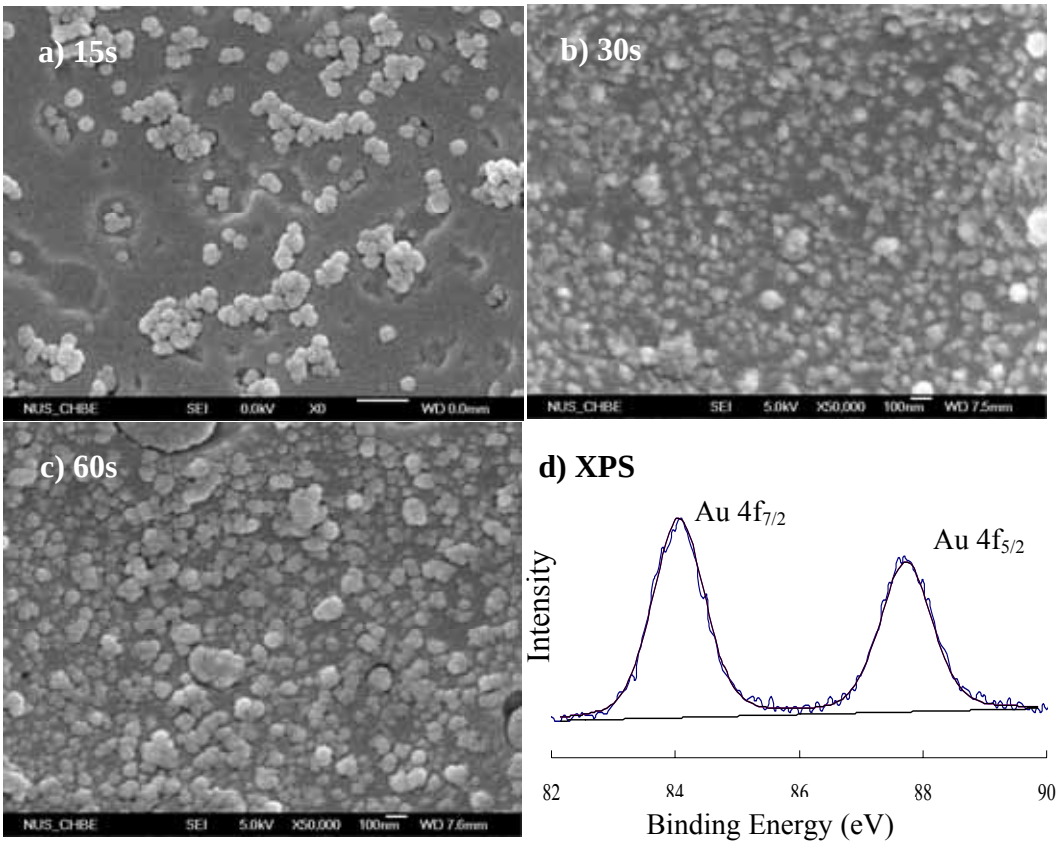

Figure 7.5 Surface morphology of electroless Au deposits from samples with different plating time and XPS spectrum of electrolessly plated Au4f (using sample plated for 30s as an example)

A two-step electroless plating strategy was applied: firstly, electroless Au nanoparticles were deposited on the pre-activated area of Nafion® membrane, and subsequently electroless Pt deposit took place on the tiny Au particles generated in

the first step. According to this arrangement, a high surface coverage of Au particles with small sizes was the desired morphology of this base layer. To realize this design, the plating time of EGP was warily monitored. Sparsely distributed Au particles, 10-20 nm in diameter and a certain extent of clustering, was perceived after 15s (Figure 7.5 a). With the extension of plating time, both Au particle coverage and aggregation increased rapidly (Figure 7.5 b-c). The doublet Au4*f* XPS spectrum was also obtained from the surface of sample 5b as a demo, of which Au4$f_{7/2}$ has BE at 84.0 eV and Au4$f_{5/2}$ at 87.7 eV. The BE values prove that Au prepared is in metallic state (Andreeva, 2009; Patra, 2009).

The electroless Pt was then pursued on the three Au-deposited surfaces (samples a-c in Figure 7.5) by applying the same conditions as those for the deposition of pure Pt with the loading of 0.2 mg/cm^2 as stated above. The resulting deposition layer is named by the symbol Pt-Au(30s), for example. It can be understood that the initial Pt deposition must occur on the Au particles, and hence a particle-to-particle mounding porous structure is solely resulted.

The Pt4*f* spectra of these three samples were therefore basically the same and can be demonstrated by, for instance, the spectrum of Pt-Au(15s) sample in Figure 7.6 (a). The Pt4*f* signal consists of two pairs of doublets. The more intense doublet (BE at 71.07 eV and 74.4 eV) was assigned to metallic Pt. The second set of doublet (BE at 72.4 eV and 75.7 eV), which was at BE that 1.4 eV higher than Pt^0, could be attributed to the Pt(II) chemical state as in PtO or $Pt(OH)_2$ (Liu, 2005).

However, quite different Au4*f* spectra were obtained from these three samples. Au was not found at the surface of Pt-Au(15s), but it can be detected at the surface of the other two deposition layers (Figure 7.6 (b)). The XPS spectra and their fitting results of these two samples show that the peak bonding energy of Au4$f_{7/2}$ and Au4$f_{5/2}$ appears at 84.0 eV and 87.7 eV precisely, which signifies that Au layer deposited underneath remained zero valence and was not totally covered up by the Pt layer.

In light of the catalytic activity and electron conductivity, Au is well behind Pt, it is rational to consider that a full wrapping of Au particles by Pt would attain the maximum anodic catalytic activity. Then again, a sufficiently thin Pt covering layer is required in order to enable the Au phase underneath to affect the catalytic behavior of the overlaying Pt phase. Based on this inference, the Pt-Au(15s) was selected to assess anodic catalytic behavior.

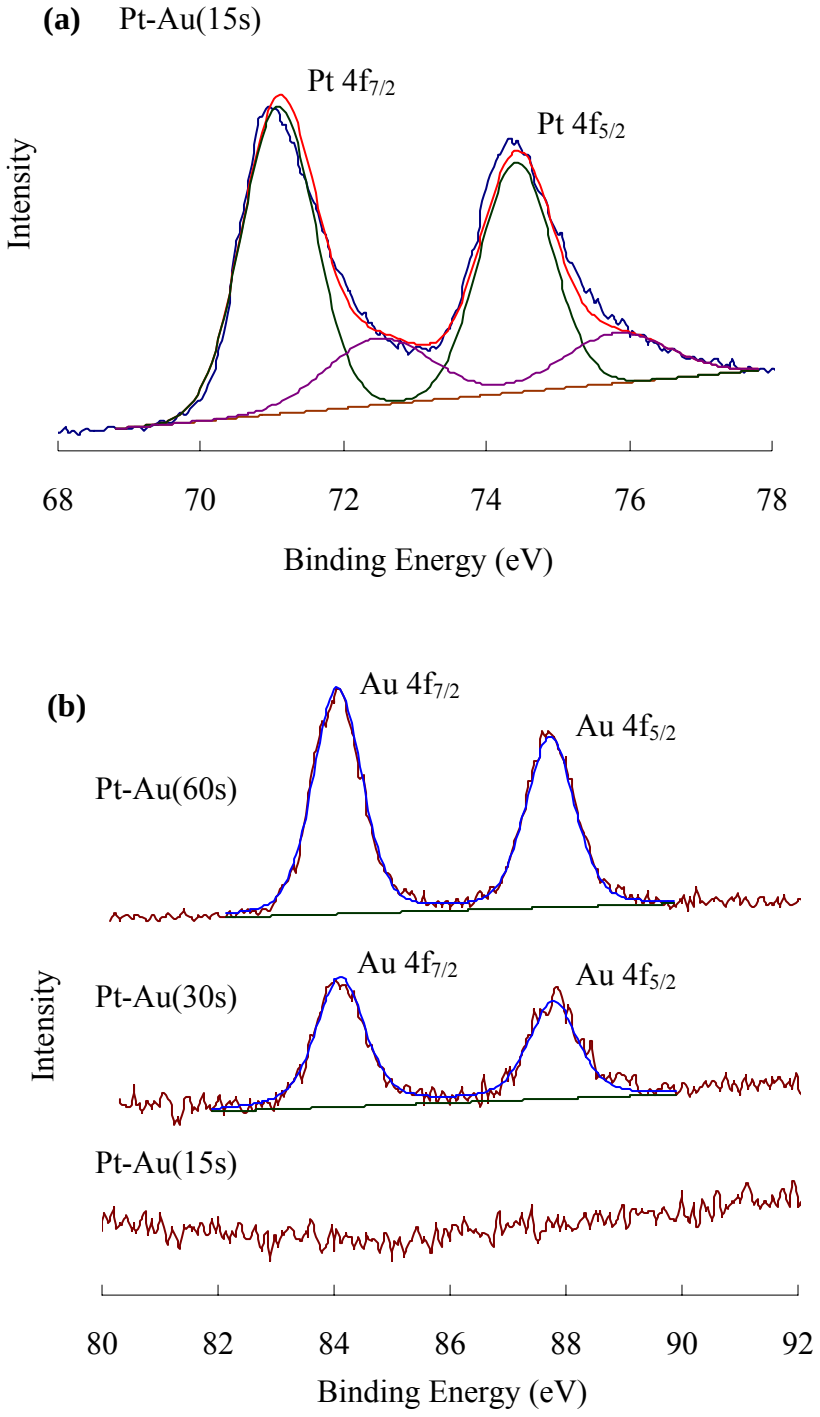

Figure 7.6 XPS spectra of PtAu alloy for different Au plating time (L_{Pt}=0.2 mg/cm^2 for all samples)

Surface morphologies of Pt/Au layers with different Pt loadings on the Au(15s) surface were also compared (Figure 7.7). Particle size of Pt-Au(15s) deposition layer is larger than that of Pt layer with the identical L_{Pt}. Moreover, a complete surface coverage was achieved when L_{Pt} = 0.2 mg/cm^2. For the other two Pt-Au(15s) deposition layers having larger L_{Pt} values, particulate Pt was transformed to a multi-layer Pt. It is now clear, on the basis of surface area/weight ratio, sample II should be the most suitable Au/Pt layer for catalytic assessment.

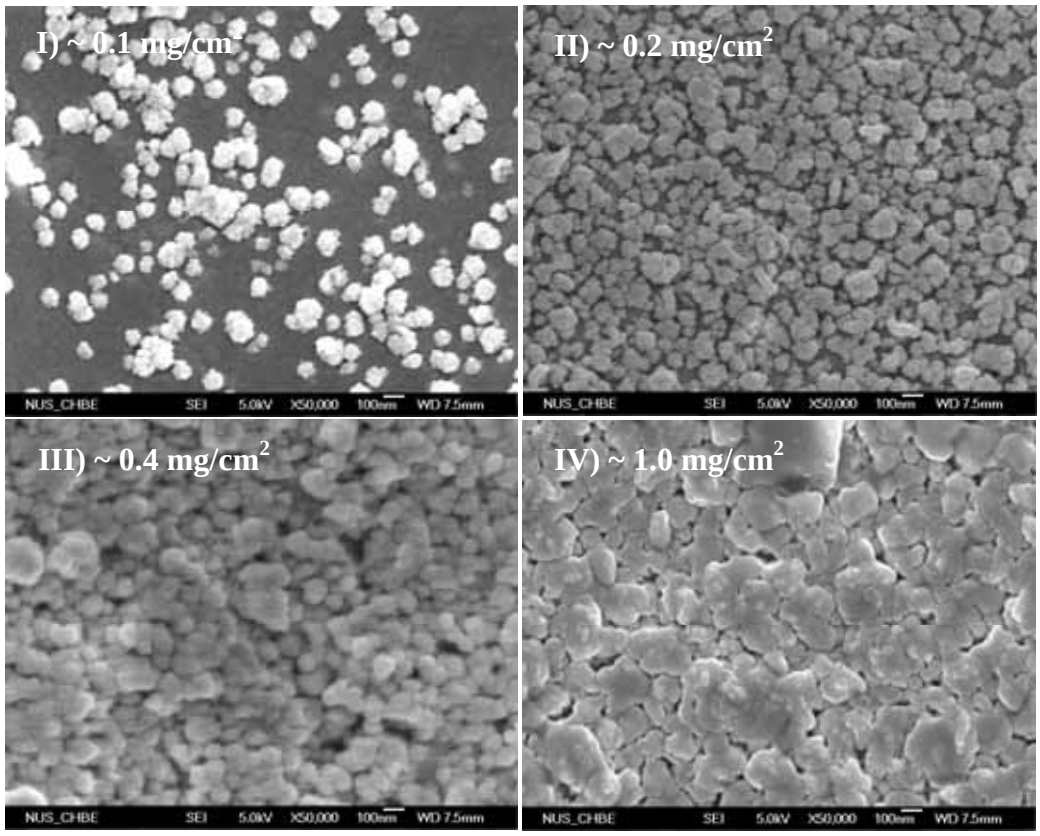

Figure 7.7 Surface morphology of electroless PtAu deposits from samples with different L_{Pt} (plating time for Au: 15s)

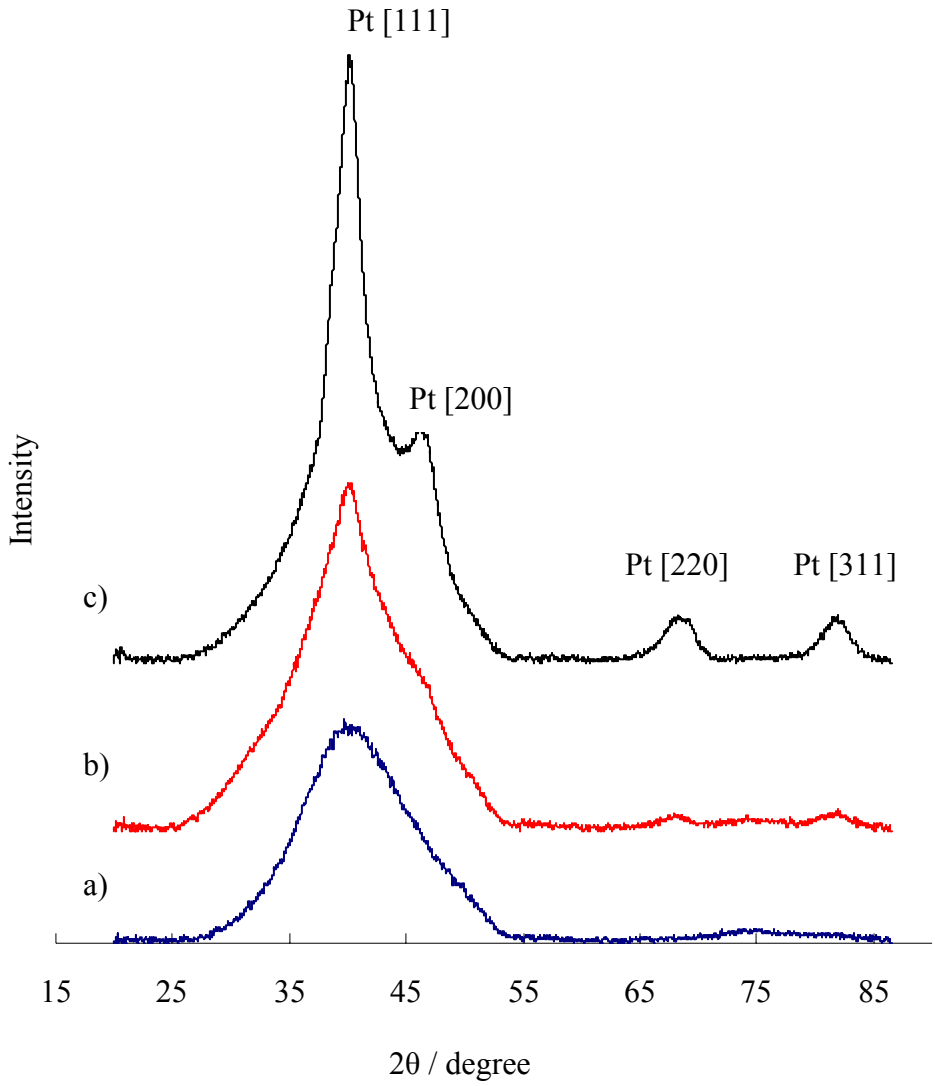

Figure 7.8 XRD patterns of a) Nafion® substrate, b) electroless Pt plated Nafion® substrate and c) electroless PtAu plated Nafion® substrate (L_{Pt}=0.2 mg/cm^2 in samples b and c; Au plating time =15s in sample c)

The Nafion® substrate and its supported catalysts were also characterized by XRD measurement (Figure 7.8). Nafion® substrate showed a broad peak of 2θ values from 27° to 54°, reflecting its amorphous structure. The Pt loading was controlled to be similar (L_{Pt} = 0.2 mg/cm^2) in the other two deposition layers, Pt and Pt-Au(15s). The XRD pattern of Pt (curve b) shows three main characteristic peaks of the FCC

crystalline Pt that has diffraction planes of (111) at 40.3°, of (220) at 69.2° and of (311) at 82.5°, respectively. On the other hand, the XRD pattern of Pt-Au(15s) (curve c) shows a set of clear diffraction peaks at 2θ of 40.3°, 46.8°, 69.2° and 82.5°, these can be attributed to the (111), (200), (220) and (311) facets of Pt crystallites (Liu[a], 2007). Nevertheless, no Au peaks were found in curve c. Compared with curve b, the XRD pattern of curve c was sharper in peak shape and stronger in peak intensity. These indicate that the presence of Au on membrane surface facilitated the growth of crystalline grains of Pt.

7.3.4 Catalytic performance of the fabricated anodes in PEMFC

These two types of deposition layers, Pt and Pt-Au(15s) both with L_{Pt}=0.2 mg/cm^2, were assessed in a single stack PEMFC. The conventional PtRu/Vulcan carbon catalyst with the designated Pt loading was used as benchmark for comparison. The polarization curves obtained from this evaluation (Figure 7.9) show that the PtRu/Vulcan carbon catalyst, offering a maximum power density of 0.31W/cm^2, is behind the two electrolessly deposited catalysts. With using Pt and Pt-Au(15s) anode catalysts, the maximum power density output are 0.44 W/cm^2 and 0.45 W/cm^2, respectively. From this outcome of cell performance, it can be considered that the conversion of the hydrogen to protons and consecutively the injection of protons into Nafion® electrolyte membrane are faster at Pt/Nafion and Pt-Au(15s)/Nafion anodes than at PtRu/Vulcan carbon catalyst/Nafion anode.

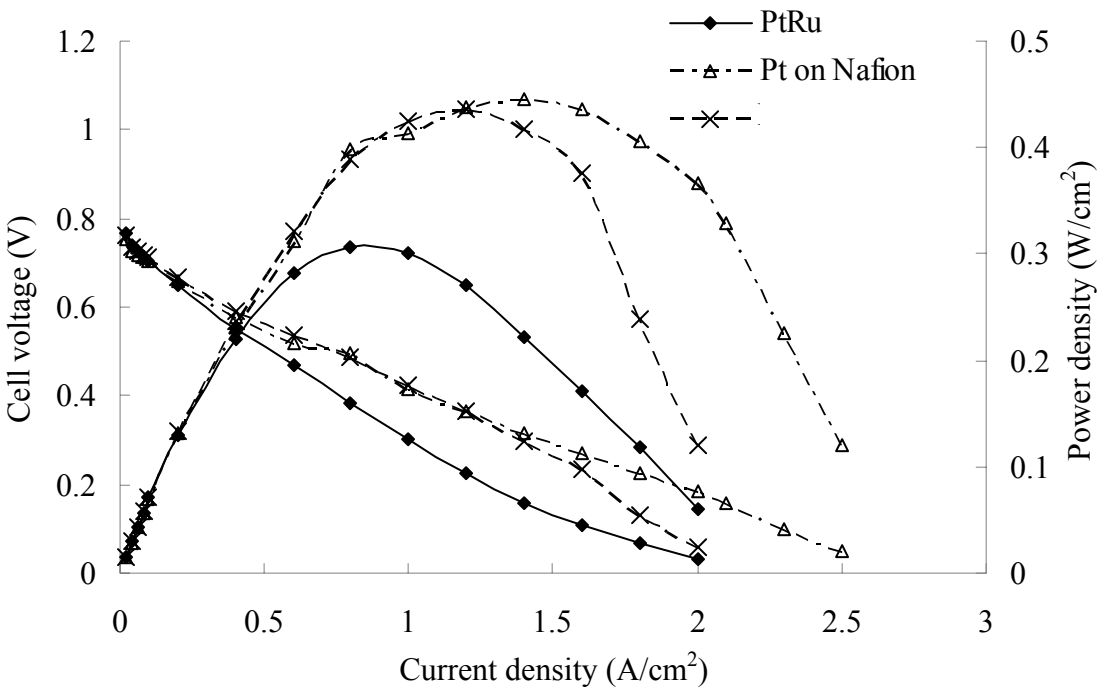

Figure 7.9 I-V & power density curves for three anode catalysts in PEMFC, in which PH_2=1 bar, PO_2=1 bar, L_{Pt}=0.2 mg/cm^2 and T_{cell}=25°C

With respect to the electrochemical polarization behaviors of the Pt/Nafion and Pt-Au(15s)/Nafion anodes, the former electrode exhibited a better capability than the latter one to hold voltage when the current density was above 1.4 A/cm^2. This may be explained by the sizes of crystal grains of Pt. According to XRD, Pt-Au(15s) comprises larger Pt crystal grains than Pt does. The larger size of crystal grains is expected to contain a lower specific surface area and therefore offer a smaller number of catalytic sites primarily located at grain boundary areas. However, the larger crystal grains may have better chemical resistance to catalytic poison species, like CO or carbon residues. The related tests will be performed in a separate study in future.

7.4 Conclusions

This study aims at to the deposition of anode catalyst directly to Nafion® membrane for PEMFC by means of electroless plating. Pt and Pt/Au bimetallic thin layers consisting of highly disperse particles with size smaller than 100 nm were successfully developed on Nafion® membrane, respectively.

The surface morphology of a metal deposition layer as well as the metal loading in mg/cm^2 strongly depended upon the plating time used if the other plating bath conditions were fixed. Too short a plating time led to sparsely distribution of metal particles (10-20 nm); whereas too long a plating time resulted in a full coverage with a scale-like dense multi-layer. For the Pt layer deposited on Nafion membrane, it was confirmed that the loading at ca. 0.2 mg/cm^2 gave rise to the desired surface morphology in terms of coverage and particle size. For the deposition of Pt/Au bimetallic layer, the EGP time was controlled to such an extent that the Au particles deposited on Nafion membrane as well as the unoccupied area can be completely covered with the minimum amount of Pt in the subsequent EPP process. The preferred Pt-Au layer obtained contained a similar loading of Pt to the pristine Pt layer; however, the Pt-Au particles were greater than the pristine Pt particles and the Pt phase in Pt-Au comprised larger crystal grains.

Both Pt/Nafion and Pt-Au/Nafion sheets as prepared were employed as anode respectively in a single stack PEMFC to test their catalytic activities. Both of them displayed better electrode reactivity than the normally used carbon black supported PtRu catalyst. Furhtermore, the pristine electroless Pt layer demonstrated a faster

electrode kinetics than the bimetallic electroless Pt-Au layer. This outcome is ascribed to the greater crystal grains of Pt in Pt-Au.

Chapter 8 Conclusions and Recommendations

8.1 Conclusions

The main theme of this thesis is to explore electroless nickel plating (ENP) solution stabilizers that are environmental-friendly and also as effective as the traditionally used lead(II) salt. Another focus is the development of functional metal deposits on pertinent polymer substrates using the electroless plating methodology.

The effort aiming at exploring green ENP stabilizer has resulted in the finding of three new types of stabilizers, which are sulfur-containing amino acids, Bi^{3+}-complex ions and phosphines. Among them, sulfur-containing amino acids and Bi^{3+}-complex ions stabilize the electroless nickel plating (ENP) bath by regulating the oxidation rate of hypophosphite ion at the plating surface through deactivating those extra fast deposition spots once they are generated; whereas the phosphines act through suppressing the rapid reduction of Ni^{2+} ions at those unusually reactive Ni surface sites. The presence of these stabilizers in ENP bath does not significantly influence the operation of ENP process and characteristics of EN deposit if their concentrations are below the respective critical values. In addition, the phosphines were found to gradually increase the phosphorus-content in the Ni-P deposit with the increasing of their concentrations in the ENP solution. These three types of stabilizers are effective in maintaining steady and continuous operation of ENP bath consisting of 4 MTOs. It is also noted that the sulfur-containing amino acid stabilizer yields a negative impact to the corrosion resistance of ENP deposit, in

particular the effect becomes more severe with an extension of bath operation time, but this is not the case for the other two types of stabilizer. The investigation of how these three types of stabilizers perform in ENP system was evolved along the following four fundamental clues: formation of complex in ENP solution, adsorption of stabilizer on active Ni sites, anodic reaction rate of hypophosphite, and the occurrence of colloidal particles in ENP bath.

Electroless plating chemistry offers a cost-effective and shape/size-independent method for the realization of metal thin films on electrically insulating substrates. This thesis work fathoms two challenging issues in association with the surface metallization of polymeric materials: (a) whether and how can a plastic substrate with non-polar organic structure be electrolessly plated? (b) whether can a metallic thin layer comprising nanoparticles but rather a dense film be attained on a plastic using this method?

Regarding issue (a), ENP on Poly(dimethylsiloxane) (PDMS) is selected. After modified by the reverse surface roughening approach, the hydrophobic PDMS surface becomes hydrophilic according to contact angle measurement and rough. On such a surface a Ni-P thin layer with rough and irregular morphology as well as the desired adhesion strength could therefore be deposited. This Ni-P metallized PDMS offers not only a high electrical conductivity but also an electromagnetic interference (EMI) shielding property.

Regarding issue (b), the anode of proton exchange membrane fuel cell (PEMFC) is fabricated by directly deposition of Pt or Pt-Au bimetallic thin layer, consisting of

highly dispersed particles with size smaller than 100 nm, on patterned Nafion® membrane. Both of Pt and Pt-Au catalysts display better electrode reactivity than the normally used carbon black supported PtRu catalyst, whereas Pt/Nafion® anode shows better cell performance than Pt-Au/ Nafion® anode in high current density range in a single stack PEMFC.

8.2 Suggestions for the future work

In the course of completing this PhD thesis, I also figured out a number of appealing thinkings that are worthy of the further investigations to advance the results achieved from this thesis project. The related suggestions are listed as follows.

8.2.1 Application of environmental-friendly stabilizers in alkaline ENP bath

In my study, all of the three types of stabilizers, namely, sulfur-containing amino acids, Bi^{3+}-complex ions and phosphines, exhibited a great potential to replace Pb^{2+} ion in the acidic ENP solutions in which hypophosphite was used as the reducing agent. However, their performance in alkaline ENP baths has not been investigated yet despite the fact that the alkaline ENP system is far less popular than its acidic counterpart. The reducing agents used in alkaline ENP solutions, generally, are sodium borohydride, dimethylamine borane (DMAB) and hydrazine, which possess stronger reducing power than hypophosphite. Therefore, it will be meaningful to understand whether these environmental-friendly stabilizers can work in an alkaline

ENP bath, what their effects will be on the plating process and deposit, and how they stabilize the bath. In addition, it is a prerequisite to develop suitable methods which allow Bi^{3+} ion and hydrophobic phosphines to be dissolved in the alkaline solution.

8.2.2 Theoretical models for describing working mechanisms of organic stabilizers

Although a modified quantitative theoretical model, based on the electrical double layer theory, has been proposed to describe the stabilizing role of Bi^{3+} ion, this thesis does not tackle the study on corresponding theoretical models for the two types of organic stabilizers due to their complicated interactions with the plating surface. Unlike heavy inorganic ions that inhibit propagation of metal colloidal particles via disprotionation reaction, the organic stabilizers play the same role via chemical or physical adsorptions. An adsorption-based quantitative theoretical model will deal with not only diffusion of stabilizer molecules across the electric double layer but also the definition of active sites and their distribution over the adsorbent (plating surface). Besides these, how the adsorbent (the adsorbed organic species, such as phosphines) retards the cathodic process (reduction of Ni^{2+} to Ni^{0}) through a specific way other than trivial site-blocking effect is the critical issue to be figured out. A simplified picture will be the adsorption of a particular stabilizer (possessing suitable Lewis basicity) on a few individual active sites on a plating surface, and such an adsorption causes a reduction in the work function (or move up) of Fermi level of the plating surface. This will decipher why a substantially dilute stabilizer reveals noticeable effect.

8.2.3 Patterned ENP on plastics

Patterned ENP on plastic substrates is also known as selective ENP. In this process, only the designated surface area of a plastic substrate will be plated. The general patterned ENP process includes the steps of (I) creation of a surface with pendant functional groups at which the initiating seeds (or catalyst) of ENP will be bound; (II) introduction of electroless plating catalyst to the desired surface; (III) surface patterning performed by photolithography, and (IV) forming a metal layer in the pattern form by electroless plating.

According to the above study on Bi^{3+} ion stabilizer, implantation of this ion to the domains where metallization are unwanted will render them passive to electroless plating, and the subsequent plating will not take place over these domains; as a result, a particular pattern of metal coverage will be achieved. This design is schematically illustrated by the flow chart in Figure 8.1. The whole process may involve five steps: (I) formation of a functional polymer overlayer on a substrate; (II) development of a patterned overlayer by photolithographic method or other approaches; (III) implantation of Bi^{3+} ion in the surface layer of the unmasked domains of the substrate, (IV) Removal of the mask from the substrate surface, (V) formation of a metal pattern by immersion of the treated substrate in an ENP bath.

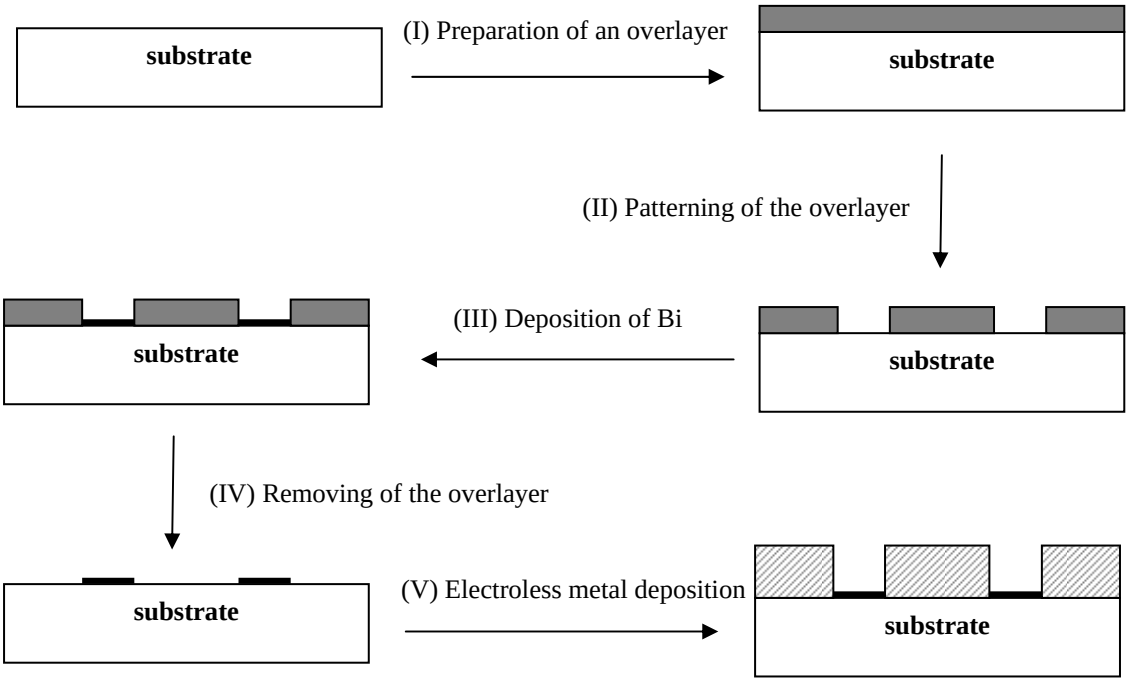

Figure 8.1 Schematic diagram of the selective electroless Ni deposition process using Bi^{3+}-complex ion as the inhibitor

8.2.4 Further investigation of the preparation of anode catalyst on Nafion® membrane by electrroless plating

As discussed in Section 7.3.4 of Chapter 7, the Pt-Au(15s)/Nafion® anode exhibited a lower capability than the Pt/Nafion® anode to hold voltage when the current density was above 1.4 A/cm^2. This may be due to the greater crystal grains of Pt in Pt-Au, and the direct contact of Au and Nafion® substrate which retards the electron transfer. As such, it is considered that the above problems may be resolved if the bimetallic anode catalyst can be prepared using a reversed plating order. In this new process, a thin Pt layer with the desired coverage and particle sizes is initially deposited on Nafion® surface by electroless platinum plating; after that, Au nanoparticles are arranged to grow on Pt particles pre-deposited by controlling

electroless gold plating to ensure most reactive surface area of Pt not to be covered by Au particles. Furthermore, the new location of Au nanoparticles at the outer layer may be beneficial for the preferential oxidation (PROX) of CO in fuel cell operation.

In addition, the chemical resistance of Pt/Nafion® and Pt-Au(15s)/Nafion® anodes to catalytic poison species, like CO or carbon residues, was not studied in my work. Therefore, the performance of the two anodes with the newly proposed Au-Pt/Nafion® anode in the PROX of CO is suggested to perform in detail in the future research.

References

- Abrantes LM, Correia JP. On the mechanism of electroless Ni-P plating, *J. Electrochem. Soc.*, **1994**, 141, 2356-2360.
- Adamson AW, Gast AP. *Physical Chemistry of Surface*, Wiley-Interscience Publication, NY, USA, 1997.
- Alfons H, Heinz-Peter B. Lead-free chemical nickel alloy, US2004007472, 2004-01-15.
- Alkire RC, Gerischer H, Kolb DM, Tobias CW (Editors). *Advances in Electrochemical Science and Engineering, vol. 5*. Weinhein, Germany: Wiley-VCH, 1997.
- Andreeva D, Ivanov I, Ilieva L, Abrashev MV, Zanella R, Sobczak JW, Lisowski W. Gold catalysts supported on ceria doped by rare earth metals for water gas shift reaction: Influence of the preparation method, Appl. Catal., A, **2009**, 357, 159–169.
- Armyanov S, Georgieva J, Tachev D, Valova E, Nyagolova N, Mehta S, Leibman D, Ruffini A. Electroless deposition of Ni-Cu-P alloys in acidic solutions, *Electrochemical and Solid-State Letters*, **1999**, 2, 323-325.
- Ashassi-Sorkhabi H, Rafizadeh SH. Effect of coating time and heat treatment on structure and corrosion characteristics of electroless Ni-P alloy deposits, *Surf. Coat. Technol.*, **2004**, 176, 318-326.
- Auroux PA, Iossifidis D, Reyes DR, Manz A. Micro Total Analysis Systems. 2. Analytical Standard Operations and Applications, *Anal. Chem.*, **2002**, 74, 2637-2652.

- Ayyadurai SM, Choi YS, Ganesan P, Kumaraguru SP, Popov BN. Novel PEMFC cathodes prepared by pulse deposition, *J. Electrochem. Soc.*, **2007**, 154, B1063-B1073.
- Azzaroni O, Zheng Z J, Yang ZQ, Huck WTS. Polyelectrolyte brushes as efficient ultrathin platforms for site-selective copper electroless deposition, *Langmuir*, **2006**, 22, 6730-6733.
- Baird IR, Smith MB, James BR. Nickel(II) and nickel(0) complexes containing 2-pyridylphosphine ligands, including water-soluble species, *Inorg. Chim. Acta*, **1995**, 235, 291-297.
- Baldwin C, Such TE. Plating rates and physical properties of electroless nickel/phosphorus alloy deposits, *Trans. Inst. Met. Finish.*, **1968**, 46(Pt. 2), 73-80.
- Baskaran I, Narayanan TSNS, Stephen A. Effect of accelerators and stabilizers on the formation and characteristics of electroless Ni-P deposits, *Mater. Chem. Phys.*, **2006**, 99, 117-126.
- Baudrand D, Brengston J. Electroless plating process—developing technologies for electroless nickel, palladium and gold, *Met. Finish.*, **1995**, 93, 55-57.
- Berrios JA, Staia MH, Hernandez EC, Hintermann H, Puchi ES. Effect of the thickness of an electroless Ni-P deposit on the mechanical proerties of an AISI 1045 plain carbon steel, *Surf. Coat. Technol.*, **1998**, 108-109, 466-472.
- Bielinski J, Goldon A, Socko B, Bielinska A. Optimization of solutions for electroless nickel coating: Part 2. Additions of transition element compounds, *Metalloberflaeche*, **1983**, 37, 300-305.
- Bindra P, Roldan J. Mechanisms of electroless metal plating III. Mixed potential theory and the independence of partial reactions, *J. Appl. Electrochem., 1987*, 17, 1254-1266.

- Bobrovskaya VP, Sokolov VG, Yurkevich VV. Effect of Bi(III) on electroless nickel plating, *Vestn. Beloruss. Gos. Univ.*, *1993*, 2, 16-18.
- Brandow SL, Chen MS, Wang T, Dulcey CS, Calvert JM, Bohland JF, Calabrese GS, Dressick WJ. Size-controlled colloidal Pd(II) catalyst for electroless Ni deposition in nanolithography applications, *J. Electrochem. Soc.*, **1997**, 144, 3425-3434.
- Brandow, SL, Dressick WJ, Marrian CRK, Chow GM, Calvert JM. The morphology of electroless Ni deposition on a colloidal Pd(II) catalyst, *J. Electrochem. Soc.*, **1995**, 142, 2233-2243.
- Brenner A, Riddell GE. Nickel plating on steel by chemical reduction, *J Res. Nat. Bur. Stand.*, **1946**, 37, 31-34.
- Carbajal JL, White RE. Electrochemical production and corrosion testing of amorphous Ni-P, *J. Electrochem. Soc.*, **1988**, 135, 2952-2956.
- Carlo SR, Perry C, Torres J, Fairbrother DH. Metallization of poly(vinylchloride) by Fe, Ni, Cu, Ag, and Au, *J. Vac. Sci. Technol., A***, 2002,** 20,350-355.
- Castellino N, CastellinoP, Sannolo N (Editors). *Inorganic Lead Exposure: Metabolism and Intoxication*, Lewis Publishers, FL, 1995.
- Caturla F, Molina F, Sabio M, Reinoso FR. Electroless plating of graphite with copper and nickel, *J. Electrochem. Soc.*, **1995**, 142, 4084-4090.
- Cavallotti P, Salvago G. Chemical reduction of nickel and cobalt by hypophosphite: I. Plating of alloys, *Electrochimica Metallorum*, **1968**, 3, 23-41.
- Cavallotti P, Salvago G. Chemical reduction of nickel and cobalt by hypophosphite: II. Characteristics of the process, *Electrochimica Metallorum*, **1968**, 3, 239-66, 338.

- Chan YK, Ding J, Ren JW, Cheng SA, Tsang KY. Supported mixed metal nanoparticles as electrocatalysts in low temperature fuel cells, *J. Mater. Chem.*, **2004**, 14, 505-516.
- Charbonnier M, Goepfert Y, Romand M, Leonard D. Eelectroless plating of glass and silicon substrates through surface pretreatments involving plasma-polymerization and grafting process, *J. adhes.*, **2004**, 80, 1103-1130.
- Charbonnier M, Romand M, Goepfert Y. Ni direct electroless metallization of polymers by a new palladium-free process, *Surf. Coat. Technol.*, **2006**, 200, 5028-5036.
- Charbonnier M, Romand M, Harry E, Alami M. Surface plasma functionalization of polycarbonate: application to electroless nickel and copper plating, *J. Appl. Electrochem.*, **2001**, 31, 57-63.
- Charbonnier M, Romand M. Polymer pretreatments for enhanced adhesion of metals deposited by the electroless process, *Int. J. Adhes. Adhes.*, **2003**, 23, 277-285.
- Chen BH, Hong L, Ma Y, Ko TM. Effects of surfactants in an electroless nickel plating bath on the properties of Ni-P alloy deposits, *Ind. Eng. Chem. Res.*, **2002**, 41, 2668-2678.
- Chen CH, Chen BH, Hong L. Role of Cu^{2+} as an additive in an electroless nickel-phosphorus plating system: A stabilizer or a codeposit? *Chem. Mater.*, **2006**, 18, 2959-2968.
- Chen K, Chen Y. A new low-temperature electroless nickel plating process, *Plat. Surf. Finish.*, **1997**, 84, 80-82.
- Cheng YH, Zou Y, Cheng L, Liu W. Effect of complexing agents on properties of electroless Ni-P deposits, *Mater. Sci. Technol.*, **2008**, 24, 457-460.

- Cheong WJ, Luan BL, Shoesmith DW. The effects of stabilizers on the bath stability of electroless Ni deposition and the deposit, *Appl. Surf. Sci.*, **2004**, 229, 282-300.
- Cheong[a] WJ, Luan BL, Shoesmith, DW. Protective coating on Mg AZ91D alloy - The effect of electroless nickel (EN) bath stabilizers on corrosion behaviour of Ni-P deposit, *Corr. Sci.*, **2007**, 49, 1777-1798.
- Cheong[b] WJ, Luan BL, McIntyre, NS, Shoesmith DW. XPS characterization of the corrosion film formed on the electroless nickel deposit prepared using different stabilizers in NaCl solution, *Surf. Interface Anal.*, **2007**, 39, 405-414.
- Chu SZ, Sakairi M, Takahashi H, Qiu ZX. Local deposition of Ni-P alloy on aluminum by laser irradiation and electroless plating, *J. Electrochem. Soc.*, **1999**, 146, 537-546,.
- Court SW, Barker BD, Walsh FC. Electrochemical measurements of electroless nickel coatings on zincated aluminium substrates, *Trans. Inst. Met. Finish.*, **2000**, 78, 157-162.
- Cui GF, Li N, Li DY, Chi ML Study of optimized complexing agent for low-phosphorus electroless nickel plating bath. *J. Electrochem. Soc.*, **2005**, 152, 10, c C669-C674.
- Cui GF, Li N, Li DY, Zheng J, Wu QL. The physical and electrochemical properties of electroless deposited nickel-phosphorus black coatings, *Surf. Coat. Technol.*, **2006**, 200, 6808-6814.
- Das L, Chin DT. Effect of bath stabilizers on electroless nickel deposition on ferrous substrate, *Plat. Surf. Finish.*, **1996**, 83, 55-61.

- Davidson A, Tempere JF, Che M. Spectroscopic studies of nickel(II) and nickel(III) species generated upon thermal treatments of nickel/ceria-supported materials, *J. Phys. Chem.*, **1996**, 100, 4919 -4929.
- Debe MK, Hartmann JB. *PEM stack component cost reduction*, U.S. Department of Engergy, 2000.
- Debe MK. in *Handbook of fuel cell: Fundamentals, Technology, and Applications;* Vlelstich W, Lamm A, Gasteiger H, (editors). John Wiley & Sons, Chichester, U.K., 2003.
- Delaunois F, Petitjean JP, Lienard P, Jacob-Duliere, M. Autocatalytic electroless nickel-boron plating on light alloys, *Faculte Polytechnique de Mons, Service de Metallurgie physique, Mons, Belg. ATB Metallurgie*, **2001**, 41, 10-13.
- DiBari, GA. Nickel plating, *Plat. Surf. Finish.*, **1997**, 84, 60-61.
- DiBari, GA. Nickel plating, *Plat. Surf. Finish.*, **1998**, 85, 54-56,.
- DiBari, GA. Nickel plating, *Plat. Surf. Finish.*, **1999**, 86, 51-52,.
- Duncan RN. Performance of electroless nickel coated steel in oil-field environments, *Mater. Perform.* **1983**, 22, 28-34.
- Egli A, Heber J. Triazolium stabilizers for Ni-P electroless plating solutions, JP2003183845, 2003.
- El-Rehim SSA, Shaffei M, El-Ibiari N, Halem SA. Effect of additives on plating rate and bath stability of electroless deposition of nickel-phosphorus-boron on aluminum, *Met. Finish.*, **1996**, 94, 29-33.
- EPA: Clean Air Mercury Rule, **2005**.
- EPA: Final Rule To Amend the Final Water Quality Guidance for the Great Lakes System To Prohibit Mixing Zones for Bioaccumulative Chemicals of Concern, Federal Register, **2000**, 65,(219), 67638-67651.

- EPA: National Primary Drinking Water Regulations, **1995**.
- EPA: National Primary Drinking Water Regulations; Arsenic and Clarifications to Compliance and New Source Contaminants Monitoring, Federal Register, 66(14), **2001**, 6975-7066.
- Farhat Z, Alfantazi A. High surface area mechanically alloyed Pt-based catalyst, *Mater. Sci. Eng. A*, **2008**, 476, 169-173.
- Feldstein N, Lancsek TSA. New technique for investigating the electrochemical behavior of electroless plating baths and the mechanism of electroless nickel plating, *J. Electrochem. Soc.*, **1971**, 118, 869-874.
- Fujii T, Ito M. Catalyst preparation by electroless plating and hydrogen direct reduction methods: practical application for a high cell performance PEFC, *Fuel Cell*, **2006**, 5, 356-630.
- Fujiwara N, Yasuda K, Ioroi T, Siroma Z, Miyazaki Y. Preparation of platinum-ruthenium onto solid polymer electrolyte membrane and the application to a DMFC anode, *Electrochim. Acta*, **2002**, 47, 4079-4084.
- Gaevskaya TV, Rakovich EV. Stabilizing action of pyrimidine bases on electroless nickel-plating baths, *Zhurnal Prikladnoi Khimii (Sankt-Peterburg, Russian Federation)*, **1992**, 65, 2700-2706.
- Gafin AH, Orchard SW. Catalytic effects in the initiation of autocatalytic nickel deposition on nickel containing substrates, *J. Electrochem. Soc.*, **1993**, 140, 3458-3462.
- Gawrilov, G.G. *Chemische (stromlose) Vernickelung*. Eugen G. Leuze Verlag, Salugau, 1974. (*Chemical [Electroless] Nickel Plating*, Portcullis Press, Redhill, UK, 1979.)

- Gerischer, H.; Tischer, R. P.: The mechanism of the electrodeposition and solution of solid metals. I. Processes in the stationary solution of silver electrodes and the rate of the phase passage reaction. *Zeitschrift fuer Elektrochemie und Angewandte Physikalische Chemie*, **1957**, 61, 1159-1162.
- Goyer R. Toxic effects of metals. In: Amdur M.O, Doull JD, Klassen CD (Editors). *Casarett and Doull's Toxicology*, *4th ed.* Pergamon Press, New York, 1991, 623-680.
- Gray JE, Norton PR, Griffiths K. Mechanism of adhesion of electroless-deposited silver on poly(ether urethane), *Thin Solid Films*, **2005**, 484, 196-207.
- Grosvenor AP, Biesinger MC, Smart R St.C., McIntyre NS. New interpretations of XPS spectra of nickel metal and oxides, *Surf. Sci.*, 2006, 600, 1771–1779.
- Gulla M, Dutkewych OB. Stabilized baths for electroless nickel and cobalt plating, Ger. Offen. , 23, **1971**.
- Gulla M. Electroless coating with nickel-copper-phosphorus alloys, Ger. Offen., **1972**, 30, Division of Ger. Offen. 2,122,455.
- Guo JZ, Wang ZS. Technology and properties of electroless plated nickel-boron alloy, *Qingdao Huagong Xueyuan Xuebao*, **1996**, 17, 175-179.
- Gutzeit G. Catalytic nickel deposition from aqueous solution. I-IV., *Plating (Paris), 1959*, 46, 1158-1164, 1275-1278, 1377-1378.
- Gyanutene I, Lyankaitene Yu. The effect of nitrogen-containing organic compounds on the autocatalyzed hypophosphite reduction of nickel(II), *Zashchita Metallov*, **1996**, 32, 593-597.
- Haack KJ, Goddard R, Pörschke KR. Applying the macrocyclic effect to smaller ring structures. N,N'-Dimethyl-3,7-diazabicyclo[3.3.1]nonane nickel(0) complexes, *J. Am. Chem. Soc.*, **1997**, 119, 7992 -7999.

- Hampden-Smith MJ, Kodas TT, Powell QH, Skamser DJ, Caruso J, Chandler CD, U.S. Pat. 6,338,809, 2002.
- Han KP, Fang JL. Effect of cysteine on the kinetics of electroless nickel deposition, *J. Appl. Electrochem.*, **1996**, 26, 1273-1277.
- Han KP, Jing LF. Stabilization effict of electroless nickel plating by thiourea, *Met. Finish.*, **1997**, 5, 73-75.
- Haque IU, Ahmad S, Khan A. Electroless nickel plating on ABS plastics from nickel chloride and nickel sulfate baths, *J. Chem. Soc. Pak.*, **2005**, 27, 246-249.
- Hersch, P. *Trans. Inst. Met. Finish.*, **1955-1956**, 33, 417.
- Hessami S, Tobias JL. A mathematical model for anomalous codeposition of nickel-iron on a rotating disk electrode, *J. Electrochem. Soc.*, **1989**, 136, 3611-3616.
- Hillborg H, Ankner JF, Gedde UW, Smith GD, Yasuda HK, Wikstrom K. Crosslinked polydimethylsiloxane exposed to oxygen plasma studied by neutron reflectometry and other surface specific techniques, *Polymer*, **2000**, 41, 6851-6863.
- Hillborg H, Gedde UW. Hydrophobicity recovery of polydimethylsiloxane after exposure to corona discharges, *Polymer*, **1998**, 39, 1991-1998.
- Homma T, Naito K, Takai M, Osaka T. Transmission electron microscopy study of electroless NiP and Cu films at initial deposition stage, *J. Electrochem. Soc.*, **1991**, 138, 1269-1274.
- Hwang BJ, Lin SH. Reaction Mechanism of electroless deposition – observations of morphology evolution during nucleation and growth via tapping mode AFM, *J. Electrochem. Soc.*, **1995**, 142, 3749-3754.

- Iwasaki Y, Takamiya M, Iwata R, Yusa Shin Akiyoshi K. Surface modification with well-defined biocompatible triblock copolymers: Improvement of biointerfacial phenomena on a poly(dimethylsiloxane) surface, *Colloids Surf. B*, **2007**, 57, 226-236.
- Jershow P. *Silicone Elastomers, ChemTec Publishing*, Toronto, 2002.
- Jiang XX, Shen W. *The Fundamentals and Practice of Electroless Plating*, National Defense Industry Press, Beijing, China, 2000.
- Jin Y, Sun DB, Yu JZ, Dong CF, Yang DJ. Effects of complexing agent on the morphology and porosity of electroless nickel deposits, *Trans. Inst. Met. Finish.*, **1999**, 77, 181-184.
- Jolly WL. *Modern Inorganic Chemistry (*2nd edition*)*, McGraw-Hill Inc., New York, 1991.
- Kalantary MR, Holbrook KA, Wells PB. Effects of agitation on conventional electroless plating – implications for production of Ni-P composite coatings, *Plat. Surf. Finish.*, **1992**, 79, 55-62.
- Karuppusamy K, Anantharam R. Pit-free nickel electroplating. *Met. Finish.*, **1992**, 90, 15.
- Keong KG, Sha W, Malinov S. Crystallisation kinetics and phase transformation behaviour of electroless nickel–phosphorus deposits with high phosphorus content, *J. Alloys Compd.*, **2002**, 334, 192-199.
- Keong KG, Sha W, Malinov S. Hardness evolution of electroless nickel-phosphorus deposits with thermal processing, *Surf. Coat. Technol.*, **2003**, 168, 263-274.

- Ketkar SA, Umarji GG, Phatak GJ, Ambekar JD, Rao IC, Mulik UP, Amalnerkar DP. Lead-free photoimageable silver conductor paste formulation for high density electronic packaging, *Mater. Sci. Eng. B.*, **2006**, 132, 215-221.
- Khaldeev GV, Petukhov IV, Shcherban MG. Electrooxidation of the hypophosphite ion on a palladium electrode, *Elektrokhimiya*, **2000**, 36, 934-941.
- Kim DH, Aoki K, Takano O. Soft magnetic films by electroless Ni-Co-P plating, *J. Electrochem. Soc.*, **1995**, 142, 3763-3767.
- Kim HT, Lee JK, Kim J. Platinum-sputtered electrode based on blend of carbon nanotubes and carbon black for polymer electrolyte fuel cell, *J. Power Sources*, **2008**, 180, 191-194.
- Kim KJ, Lee NE, Kim MC, Boo JH. Chemical interaction, adhesion and diffusion properties at the interface of Cu and plasma-treated thiophene-based plasma polymer (ThioPP) films, *Thin Solid Films*, **2001**, 398, 657-662.
- Kim YS, Sohn HJ. Mathematical modeling of electroless nickel deposition at steady state using rotating disk electrode, *J. Electrochem. Soc.*, **1996**, 143, 505-509.
- Kivel J, Sallo JS. The effect of thiourea on alkaline electroless deposition, *J. Electrochem. Soc.*, **1965**, 112, 1021-1023.
- Koh S, Leisch J, Toney MF, Strasser P. Structure-Activity-Stability Relationships of Pt-Co Alloy Electrocatalysts in Gas-Diffusion Electrode Layers, *J. Phys. Chem. C*, **2007**, 111, 3744-3752.
- Krolikowski, A.; Karbownicka, B.; Jaklewicz, O. Anodic dissolution of amorphous Ni-P alloys, *Electrochim. Acta*, **2006**, 51, 6120-6127.

- Kumar A, Welsh DM, Morvant MC, Piroux F, Abboud KA, Reynolds JR. Conducting Poly (3,4-alkylenedioxythiophene) Derivatives as Fast Electrochromics with High-Contrast Ratios, *Chem. Mater.*, **1998**, 103, 896-902.
- Kumar PS, Nair PK. Studies on crystallization of eElectroless Ni-P deposits, *J. Mater. Proc. Tech.*, **1996**, 56, 511-520.
- Kumar PS, Nair PK. X-ray Diffraction studies on the relative proportion and decomposition of smorphous phase in electroless Ni-B deposits, *Nanostructured Mater.*, **1994**, 4, 183-189.
- Kundu PP, Sharma V, Shul YG. Composites of proton-conducting polymer electrolyte membrane in direct methanol fuel cells, Crit. Rev. *Solid State Mater. Sci.*, **2007**, 32, 51-66.
- Kupfer H, Wolf GK. Plasma and ion beam assisted metallization of polymers and their application, *Nucl. Instrum. Methods Phys. Res., Sect. B* **2000**, 166-167, 722-731.
- Lambert MR, Duquette DJ. A study of electroless nickel coatings containing low phosphorus, *Thin Solid Film,* **1989**, 177, 207-223.
- Laptev VA, Pimenov SM, Shafeev GA. Laser-assisted nickel deposition onto synthetic diamonds, *Thin Solid Films*, **1994**, 241, 76-79.
- Lee CY, Chuang CW. A novel integration approach for combining the components to minimize a micro-fuel cell, *J. Power Sources*, **2007**, 172, 115-120.
- Lee KJ, Fosser KA, Nuzzo RG. Fabrication of stable metallic patterns embedded in Poly(dimethylsiloxane) and model application in non-planar electronic and lab-on-a-chip device patterning, *Adv. Funct. Mater.*, **2005**, 15, 557-566.
- Lee WG. 2nd International Congress on Metal Corrosion, NACE, Houston, TX, 1963.

- Lelental M. Catalysis in nickel electroless plating, *J. Electrochem. Soc.*, **1975**, 122, 486-490.
- Li L, Zhang YM, Drillet JF, Dittmeyer R, Juttner KM. Preparation and characterization of Pt direct deposition on polypyrrole modified Nafion composite membranes for direct methanol fuel cell applications, *Chem. Eng. J.*, **2007**, 133, 113-119.
- Lim KS, Chang WJ, Koo YM, Bashir R. Reliable fabrication method of transferable micron scale metal pattern for poly(dimethylsiloxane) metallization, *Lab Chip*, **2006**, 6, 578-580.
- Lin KL, Hwang JW. Effect of thiourea and lead acetate on the deposition of electroless nickel, *Mater. Chem. Phys.*, **2002**, 76, 204-211.
- Lin KL, Liu YC. Manufacturing of Cu/electroless nickel/Sn-Pb flip chip solder bumps, *IEEE Trans. Adv. Packaging*, **1999**, 22, 575-579.
- Lin, KL, Hwang JW. Effect of thiourea and lead acetate on the deposition of electroless nickel, *Mater. Chem. Phys.*, **2002**, 76, 204-211.
- Liu HP, Li N, Bi SF, Li DY, Zuo ZL. Effect of 3-amino-5-mercapto-1,2,4-triazole on electroless nickel deposition, *Chem. Res. Chinese Universities*, **2008**, 24, 101-105.
- Liu ZL, Gan LM, Hong L, Chen WX, Lee JY. Carbon-supported Pt nanoparticles as catalysts for proton exchange membrane fuel cells, *J. Power Sources*, **2005**, 139, 73–78.
- Liu ZL, Guo B, Tay SW, Hong L, Zhang XH, Physical and electrochemical characterizations of PtPb/C catalyst prepared by pyrolysis of platinum(II) and lead(II) acetylacetonate, *J. Power Sources*, **2008**, 184, 16-22.

- Liu ZL, Lin XH, Lee JY, Zhang WD, Han M, Gan LM. Preparation and characterization of platinum-based electrocatalysts on multiwalled carbon nanotubes for proton exchange membrane fuel cell, *Langmuir*, **2002**, 18, 4054-4060.
- Liu[a] ZL, Hong L, Tay SW. Preparation and characterization of carbon-supported Pt, $PtSnO_2$ and PtRu nanoparticles for direct methanol fuel cell, *Mater. Chem. Phys.*, **2007**, 105, 222-228.
- Liu[b] ZL, Ling XY, Guo B, Hong L, Lee JY. Pt and PtRu nanoparticles deposited on single-wall carbon nanotubes for methanol electro-oxidation, *J. Power Sources*, **2007**, 167, 272-280.
- Lo PH, Tsai WT, Lee JT, Hung MP. Role of phosphorus in the electrochemical behavior of electroless Ni-P alloys in 3.5 wt.% NaCl solutions, *Surf. Coat. Technol.*, **1994**, 67, 27-34.
- Lo YL, Hwang BJ. Kinetics of ethanol oxidation on electroless Ni-P/SnO_2/Ti electrodes in KOH solutions, *J. Electrochem. Soc.*, **1995**, 142, 445-450.
- Loos JS, ter Haar BA. Influence of heat treatment on the electrical resistance of thin film copper/electroless nickel microcircuit interconnections, *Thin Solid Films*, **1990**, 188, 247-258.
- Luke DA. Nickel phosphorus electrodeposits, *Trans. Inst. Met. Finish.*, **1986**, 64, 99-104.
- Lukes RM. The mechanism for the autocatalytic reduction of nickel by hypophosphite ion. *Plating (Paris)*, **1964**, 51, 969-71.
- Lyaukonis YY, Yusis ZZ. *Issledovaniya voblasti osazhdeniya metallov, vol.9 (Studies in the Metal Deposition Field)*, Institute of Chemistry and Chemical Technology, Lithuanian Academy of Sciences: Vilnius, 1983.

- M. Kantcheva e, G. Avdeev f, K. Petrov f
- Ma U, Gawne DT. Effect of counterface materials on the wear of electroless nickel-phosphorus coatings, *Trans. Inst. Met. Finish.*, **1986**, 64, 129-162.
- Mai QX, Daniels RD, Harpalani HB, Structural changes induced by heating in electroless nickel-phosphorus alloys, *Thin Solid Films*, **1988**, 166, 235-247.
- Makamba H, Kim JH, Lim K, Park N, Hahn JH. Surface Modification of Poly(dimethylsiloxane) Microchannels, *Electrophoresis*, **2003**, 24, 3607-3619.
- Malecki A, Micek-Ilnicka A. Electroless nickel plating from acid bath, *Surf. Coat. Technol.*, **2000**, 123, 72-77.
- Mallory GO, Haydu JB (Editors). *Electroless Plating-Fundamentals and Applications*, American Electroplaters and Surface Finishers Society, Orlando, FL, 1990.
- Mallory GO. The relationship between stress and adhesion of electroless nickel-phosphorus deposits on zincated aluminum, *Plat. Surf. Finish.*, **1983**, 70, 21-21.
- Mallory Jr., Glenn O. US Patent 6020021 - Method for depositing electroless nickel phosphorus alloys, 1998
- Mani P, Srivastava R, Strasser P. Dealloyed Pt-Cu core-shell nanoparticle electrocatalysts for use in PEM fuel cell cathodes, *J. Phys. Chem. C*, **2008**, 112, 2770-2778.
- Marino F, Descorme C, Duprez D. Noble metal catalysts for the preferential oxidation of carbon monoxide in the presence of hydrogen (PROX), *Appli. Catal. B*, **2004**, 54, 59-66.
- Marshall GW, Lewis DB, Dodds BE. Electroless deposition of Ni-P alloys with and without the use of superimposed pulsed current, *Surf. Coat. Technol.*, **1992**, 53, 223-230.

- Martyak NM, McCaskie JE. Electrochemistry of solutions for electroless nickel plating, *Galvanotechnik*, **1997**, 88, 2222-2228.
- Martyak NM. Characterization of thin electroless nickel coatings, *Chem. Mater.*, **1994**, 6, 1667-1674.
- Maryniak MA, Uehara T, Noras MA. Surface resistivity and surface resistance measurements using a concentric ring probe technique, *Trek Application Note, No. 1005*, **2003**, Trek, Inc.
- Matsubara H, Toda M, Sakuma T, Homma T, Osaka T, Yamazaki Y, Namikawa T. Structural control of electroless plated magnetic recording media by underlayers, *J. Electrochem. Soc.*, **1989**, 136 (3), 753-756.
- Matsubara H, Yamada A. Control of magnetic properties of chemically deposited cobalt nickel phosphorus films by electrolysis, *J. Electrochem. Soc.*, **1994**, 141, 2386-2390.
- Metz S, Holzer R, Renaud P. Polyimide-based microfluidic devices, *Lab on A Chip*, **2001**, 1, 29-34.
- Miedaner A, Noll BC, DuBois DL. Synthesis and characterization of palladium and nickel complexes with positively charged triphosphine ligands and their use as electrochemical CO_2-reduction catalysts, *Organometallics*, **1997**, 16, 5779-5791.
- Mimani T, Mayanna SM. The effect of microstructure on the corrosion behavior of electroless Ni-P alloys in acidic media, *Surf. Coat. Technol.*, **1996**, 79, 246-251.
- Mittal KL (Editor). Metallized Plastics 5&6: Fundamental and Applied Aspects, VSP, Utrecht, 1998.
- Mittal KL (Editor). Metallized Plastics 7: Fundamental and Applied Aspects, VSP, Utrecht, 2001.

- Mittal KL, Susko JR. (editors) *Metallized Plastics I: Fundamental and Applied Aspects*, Plenum Press, NY, USA, 1989.
- Monyanon S, Pongstabodee S, Luengnaruemitchai A. Catalytic activity of Pt-Au/CeO_2 catalyst for the preferential oxidation of CO in H_2-rich stream, *J. Power Sources*, **2006**, 163, 547-554.
- Moulder JF, Stickle WF, Sobol PE, Bomben KD. *Handbook of X-ray Photoelectron Spectroscopy*, Perkin-Elmer Cooperation Physical Electronics Division: Boston, M.A., 1992.
- Nicolas-Debarnot D, Pascu M, Vasile C, Poncin-Epaillard F. Influence of the polymer pre-treatment before its electroless metallization, *Surf. Coat. Technol.*, **2006**, 200, 4257-4265.
- Nihei K, Ohsaka, T, Asa, F. Studies on electroless nickel plating--Part 1. Effects of stabilizers on electroless nickel plating with sodium borohydride, *Denki Kagaku oyobi Kogyo Butsuri Kagaku*, **1975**, 43, 721-728.
- Norris CM, Schreiner S. Chemistry in environmentally benign media: Synthesis and characterization of water-soluble nickel-phosphine complexes, *Abstr. Pap. Am. Chem. Soc.*, **1999**, 217, U1012-U1012 227-INOR Part 1.
- Ohno I, Wakabayashi O, Haruyama S. Anodic oxidation of reductants in electroless plating, *J.Electrochem. Soc.*, **1985**, 132, 2323-2330.
- Osaka T, Homma T, Inoue K. Effect of heat treatment on the magnetic and structural properties of perpendicular magnetic anisotropy CoNiReP films produced by electroless deposition, *J. Electrochem. Soc.*, **1991**, 138, 538-541.
- Palaniappa M, Seshadri SK. Friction and wear behavior of electroless Ni-P and Ni-W-P alloy coatings, *Wear*, **2008**, 265, 735-740.

- Park HJ, Shin HJ, Jung HS, Kim C, Sung MM, Lee CM, Soh HS, Lee JG. Iodine-catalyzed chemical vapor deposition of Cu on MPTMS monolayer surface in a low deposition temperature regime, *Surf. Coat. Technol.*, **2007**, 201, 9432-9436.
- Park HS, Cho YH, Cho YH, Jung CR, Jang JH, Sung YE. Performance enhancement of PEMFC through temperature control in catalyst layer fabrication, *Eelectrochimica Acta*, **2007**, 53: 763-767.
- Parker K. Effects of heat-treatment on the properties of electroless nickel depositions, *Plat. Surf. Finish.*, **1981**, 68, 71.
- Parker K. *The properties of electrodeposited metals and alloys, 2nd edition*, Safranek WH (editor), American Electroplaters and Surface Finishers Society, Orlando, FL , 1986.
- Patra S, Das J, Yang H. Selective deposition of Pt on Au nanoparticles using hydrogen presorbed into Au nanoparticles during $NaBH_4$ treatment, Electrochim. Acta, **2009**, 54, 3441–3445.
- Paunovic M, Schlesinger M. *Fundamentals of Electrochemical Deposition, 2nd edition*, The Electrochemical Society Series, A John Wiley & Sons, Inc., Publication, Pennington, NJ, 2006.
- Prokopcikas A, Butkevicius J, Levickas E. Effect of thiosulfate ion the chemical nickel plating process, *Lietuvos TSR Mokslu Akademijos Darbai, Serija B: Chemija, Technika, Fizine Geografija*, **1971**, 4, 17-26.
- Qi RB, Wang YJ, Chen J, Li JD, Zhu SL. Removing thiophenes from n-octane using PDMS–AgY zeolite mixed matrix membranes, *J. Membrance Sci.*, **2007**, 295, 114-120.

- Rajam KS, Rajagopal I, Rajagopalan SR. Phosphorus content and heat treatment effects on the corrosion resistance of electroless nickel, *Plat. Surf. Finish.*, **1990**, 77, 63-66.
- Ramaswamy N, Hakim N, Mukerjee S. Degradation mechanism study of perfluorinated proton exchange membrane under fuel cell operation conditions, *Electrochim. Acta*, **2008**, 53, 3279-3295.
- Randin JP, Hintermann HE. J. Electrochem. Soc., 1970, 117, 160.
- Raub E. Fundamentals of Metal Deposition, Galvanotechnik, 1980, 71, 214-221.
- Reda M, El-Magd A. Additives for electroless nickel alloy coating process, *Met. Finish.*, **2001**, 2, 77-82.
- Reksc W, Idziak A. Plating plastics with electroless nickel in a bath containing boron hydride hydrazine, *Plat. Surf. Finish.*, **1990**, 77, 56-59.
- Riedel W. *Electroless Nickel Plating*, ASM International, Stevenage, Herts. Finishing Publications, 1991.
- Roman GT, Culbertson CT. Surface Engineering of poly(dimethylsiloxane) Microfluidic Devices Using Transition Metal Sol-Gel Chemistry, *Langmuir*, **2006**, 22, 4445-4451.
- Russo N, Fino D, Saracco G, Specchia V. Supported gold catalysts for CO oxidation. *Catal. Today*, **2006**, 117, 214-219.
- Ryabinina EI, Sotskaya NV, Shikhaliev KS, Kravchenko TA. Heterocyclic analogs of thiourea and urea as stabilizers of electroless nickel-plating electrolyte, *Russ. J. Appl. Chem.*, **1999**, 72, 1932-1935.
- Sadeghi M, Longfield PD, Beer CF. Effects of heat treatment on the structure, corrosion resistance and stripping of electroless nickel coating. *Trans. Inst. Met. Finish.*, **1983**, 61, 141-146.

- Saito T, Sato E, Matsuoka M, Iwakura C. Effect of heat treatment on magnetic properties of electroless Ni-B films, *Plat. Surf. Finish.*, **1999**, 82, 53-57.
- Sano[a] Y, Satoh H, Chiba M, Shinohara A, Okamoto M, Serizawa K, Nakashima H, Omae K. Oral toxicity of bismuth in rat: Single and 28-day repeated administration studies., *J Occup Health.*, **2005**, 47, 293-298.
- Sano[b] Y, Satoh H, Chiba M, Shinohara A, Okamoto M, Serizawa K, Nakashima H, Omae K. A 13-week toxicity study of bismuth in rats by intratracheal intermittent administration, *J Occup Health.*, **2005**, 47, 242-248.
- Sawai H, Kanamori T, Koiwa I, Shibata S, Nihei K. A study on the low energy consumption thermal head using electroless Ni-W-P alloy films as heating resistors, *J. Electrochem. Soc.*, **1990**, 137, 3653-3660.
- Schenzel HG, Kreye H. Improved corrosion resistance of electroless nickel phosphorus coatings, *Plat. Surf. Finish.*, **1990**, 77, 50-54.
- Schilling ML, Katz HE, Houlihan SM, Stein SM, Hutton RS, Taylor GN. Selective electroless nickel deposition on patterned phosphonate and carboxylate polymer films, *J. Electrochem. Soc.*, **1996**, 143, 691-695.
- Schlesinger M, Paunovic M (Editors). *Modern Electroplating, 4th edition*, John & Sons, Inc., New York, 2000.
- Seita M, Kusaka M, Nawafune H, Mizumoto S. Direct metallization using Ni-Co alloy on surface modified polyimide film, *Plat. Surf. Finish.*, **1999**, 86, 62-64.
- Seo J, Lee LP. Effects on wettability by surfactant accumulation/depletion in bulk polydimethylsiloxane (PDMS), *Sens. Actuators, B*, **2006**, 119, 192-198.
- Serfontein WJ, Mekel R, Bank S, Barbezat G, Novis B. Bismuth toxicity in man - I. Bismuth blood and urine levels in patients after administration of a bismuth

protein complex (Bicitropeptide), *Res Commun Chem Pathol Pharmacol.*, **1979**, 26, 383-839.

- Sevugan K Selvam M, Srinivasan KN, Vasudevan T, Manisankar P. Effect of agitation in elecrtroless nickel plating, *Plat. Surf. Finish.*, **1993**, 80, 56-58.
- Singh BK, Chatterjee A, Daw AN, Mitra RN. Study of the contact resistance of electroless Ni-B doped silicon using sodium borohydride as reducing agent, *J. Electrochem. Soc.*, **1989**, 136, 785-787.
- Singh D, Balasubramaniam R, Dube RK. Effect of coating time and coating time on corrosion behavior of electrolesss nickel-phosphorus coated powder-metallurgy iron specimens, *Corros.*, **1995**, 51, 581-585.
- Singh DDN, Ghosh Rita. Electroless nickel-phosphorus coatings to proctect steel reinforcement bars from chloride induced corrosion, *Surf. Coat. Technol.*, **2006**, 201, 90-101.
- Sipaut CS, Ibrahim MNM, Izat ME. Electroless plating of moisture-curable polyurethane undercoating films, *J. Appl. Polym. Sci.*, **2007**, 103, 1554-1565.
- Sotskaya NV, Goncharova LG, Kravchenko TA, Zhivotova EV. Effect of phosphite ions on the kinetics of nickel deposition by hypophosphite, *Elektrokhimiya*, **1997**, 33, 485-489.
- Sotskaya[a] NV, Ryabinina EI, Kravchenko TA, Shikhaliev KS. Kenetics of electroless plating of Ni-P alloys with organic additives containing –S-S- fragments, *Zashchita Metallov*, **2003**, 39, 281–285.
- Sotskaya[b] NV, Kravchenko TA, Ryabinina EI, Bocharova OV. Anodic oxidation of hypophosphite on a nickel-phosphorus electrode in the presence of some organic compounds, *Elektrokhimiya*, **2003**, 39, 1074-1081.

- Spataru N, Zhang XT, Spataru T, Tryk DA, Fujishima A. Platinum electrodeposition on conductive diamond powder and its application to methanol oxidation in acidic media, *J. Electrochem. Soc.*, **2008**, 155, B264-B269.
- Stevanovic R, Stevanovic J, Despic A. Electrochemical activation of the electroless deposition of Ni-P alloy and phase structure characterization of the deposit, *J. Appl. Electrochem.*, **1999**, 29, 747-752.
- Suezer S, Ertase N, Ataman OY. XPS Characterization of Bi and Mn collected on atom-trapping silica for AAS, *Applied Spectroscopy*, **1999**, 53, 479-482.
- Sugita K, Ueno N. Composition and crystallinity of electroless nickel, *J. Electrochem. Soc.*, **1984**, 131, 111-114.
- Tabandeh H, Crowston JG, Thompson GM. Ophthalmologic features of thallium poisoning, *Am. J. Ophthal.*, **1994**, 117, 243-245.
- Taheri R, Oguocha NA, Yannacopoulos S. Effect of heat treatment on age hardening behaviour of electroless nickel-phosphorus coatings, *Mater. Sci. Technol.*, **2001**, 17, 278-284.
- Tamao K. Discovery of the cross-coupling reaction between grignard reagents and C(sp^2) halides catalyzed by nickel-phosphine complexes, *J. Organomet. Chem.*, **2002**, 653, 23-26.
- Tarozaite R, Luneckas A. Effect of copper (II) in nickel deposition by hypophosphite. *Lietuvos TSR Mokslu Akademijos Darbai, Serija B: Chemija, Technika, Fizine Geografija*, **1986**, 4, 3-8.
- Tarozaite R, Luneckas A. Effect of stabilizing additives on electroless nickel plating, *Lietuvos TSR Mokslu Akademijos Darbai, Serija B: Chemija, Technika, Fizine Geografija*, **1981**, 5, 19-26.

- Tarozaite R, Luneckas A. Solution for electroless nickel plating, U.S.S.R., 1980, SU1110818.
- Tarozaite R, Selskis A. Electroless nickel plating with Cu^{2+} and dicarboxylic acids additives, *Trans. Inst. Met. Finish.*, **2006**, 84, 105-112.
- Touir R, Larhzil H, Ebntouhami M, Cherkaoui M, Chassaing E. Electroless deposition of copper in acidic solutions using hypophosphite reducing agent, *J. Appl. Electrochem.*, **2006**, 36, 69-75.
- Tulsi SS. Properties of electroless nickel, *Trans. Inst. Met. Finish.*, **1986**, 64, 73-79.
- Tzeng GS. Effect of halide ions on electroless nickel plating, *J. Appl. Electrochem.*, **1996**, 26, 969-975.
- Van der Meeraker JEAM. On the mechanism of electroless plating: II. One mechanism for different reductants, *J. Appl. Electrochem.*, **1981**, 11, 395-400.
- Van der Putten AMT, de Bakker JWG. Anisotropic deposition of electroless nickel, *J. Electrochem. Soc.*, **1993**, 140, 2229-2235,.
- Vickers JA, Caulum MM, Henry CS. Generation of hydrophilic poly(dimethylsiloxane) for high-performance microchip electrophoresis, *Anal. Chem.*, **2006**, 78, 7446-7452.
- Vielstich W, Gasteiger H, Lamm A (Editors). *Handbook of Fuel Cell – Fundamentals, Technology and Applications*. New York: John Wiley & Sons, 2003.
- Wang B, Eberhardt W, Kuck H. Plasma pre-treatment of liquid crystal polymer and subsequent metallization by PVD, *Vacuum*, **2006**, 81, 325-328.

- Wang SL, Sun GQ, Wang GX, Zhou ZH, Zhao XS, Sun H, Fan XY, Yi BL, Xin Q. Improve of direct methanol fuel cell performance by modifying catalyst coated membrane structure, *Electrochem. Commun.*, **2005**, 7, 1007-1012.
- Wang XC, Cai WB, Wang WJ, Liu HT, Yu ZZ. Effects of ligands on electroless Ni-P alloy plating from alkaline citrate-ammonia solution, *Surf. Coat. Technol.*, **2003**, 168, 300-306.
- Wei ZD, Chen SG, Liu Y, Sun CX, Shao ZG, Shen PK. Electrodepositing Pt by modulated pulse current on a Nafion-bonded carbon substrate as an electrode for PEMFC, *J. Phys. Chem. C*, **2007**, 111, 15456-15463.
- Wei ZD, Feng YC, Li L, Liao MJ, Fu Y, Sun CX, Shao ZG, Shen PK. Electrochemically synthesized Cu/Pt core-shell catalysts on a porous carbon electrode for polymer electrolyte membrane fuel cell, *J. Power Sources*, **2008**, 180, 84-91.
- Xiang YH, Hu WB, Liu XK, Zhao CZ, Ding WJ. A study on surface state during the pretreatment of electroless nickel plating on magnesium alloys, *Trans. Inst. Met. Finish.*, **2001**, 79, 27-29
- Wing LM. The use of electroless nickel on automotive components, *Trans. Inst. Met. Finish.*, **1997**, 75, B11-B14
- Wu FC, Wan CC, Wang YY, Tsai LD, Hsueh KL. Improvement of Pt-catalyst dispersion and utilization for direct methanol fuel cell using silane coupling agent, *J. Electrochem. Soc.*, **2007**, 154: B528-B532.
- Wu SH, Chen DH. Synthesis and characterization of nickel nanoparticles by hydrazine reduction in ethylene glycol, *J. Colloid Interface Sci.*, **2003**, 259, 282-286.

- Wu Y, Xiang Y, Hu W, Zhao C, Ding W. Study on the process of electroless nickel plating on magnesium alloys. *Trans. Inst. Met. Finish.*, **2005**, 83, 2, 91-94.
- Xu HW, Brito J, Sadik OA. Mechanism of stabilizer acceleration in electroless nickel at wirebond substrates, *J. Electrochem. Soc.*, **2003**, 150, C816-C822.
- Yagi S, Matsumura K, Nakano Y, Ikenaga E, Sardar SA, Syed JA, Soda K, Hashimoto E, Tanaka K, Taniguchi M. Adsorption behavior of sulfur-containing amino acid molecule on transition metal surface studied by S K-edge NEXAFS, *Nucl. Instrum. Methods Phys. Res.: Sect. B*, **2003**, 199, 244 – 248.
- Yagi S, Takenaka S, Yokoyama T, Kitajima Y, Imanishi A, Ohta T. Asymmetric adsorption of CS2 on Cu (100) studied by S K-edge X-ray absorption fine structure spectroscopy, *Surf. Sci.*, **1995**, 325, 68.
- Yamasaki T, Izumi H, Sunada H. Scripta Metal, 1981, 15, 177.
- Yan YH, Chan-Park MB, Chew CP, Yue CY, Electroless Nickel Deposition on Silicone-Rich Polyester Surface, *J. Electrochem. Soc.*, **2004**, 151, C685-C693.
- Ye HK, Gu ZY, Gracias DH. Kinetics of ultraviolet and plasma surface modification of poly(dimethylsiloxane) probed by sum frequency vibrational spectroscopy, *Langmuir*, **2006**, 22, 1863-1868.
- Yin X, Hong L, Chen BH, Ko TM. Modeling the stability of electroless plating bath – diffusion of nickel colloidal particles from the plating frontier, *J. Colloid Interface Sci.*, **2003**, 262, 89-96.
- Yin X, Hong L, Chen BH. Role of a Pb^{2+} stabilizer in the electroless nickel plating system: A theoretical exploration, *J. Phys. Chem. B*, **2004**, 108, 10919-10929.
- Yu LG, Zhang XS. Study of the friction and wear behaviour of electroless Ni-P coating, *Thin Solid Films*, **1993**, 229, 76-82.

- Zeis R, Mathur A, Fritz G, Lee J, Erlebacher J. Platinum-plated nanoporous gold: an efficient, low Pt loading electrocatalyst for PEM fuel cell, *J. Power Sources*, **2007**, 165, 65-72.
- Zhang S, Kang ET, Neoh KG, Tan KL. Electroless plating of copper and nickel on surface-modified poly(tetrafluoroethylene) films, *J. Electrochem. Soc.*, **2001**, 148, C71-C80.
- Zhao D, Xu BQ. Platinum covering of gold nanoparticles for utilization enhancement of Pt in electrocatalysts, *Phsy. Chem. Chem. Phys.*, **2006**, 8, 5106-5114.
- Zhong, H. M.; Huang, L. Z.; Chen, R. Y.; Zheng, X.; Chen, Z. Electroless nickel plating technique by using ultrasonic wave. *Fujian Shifan Daxue Xuebao, Ziran Kexueban*, **2006**, 22, 56-59.
- Zylberberg J, Belik AA, Takayama-Muromachi E, Ye ZG. Bismuth aluminate: A new high-T-c lead-free piezo-/ferroelectric, *Chem. Mater.*, **2007**, 19, 6385-6390.